Assessment of tibial fracture healing with dual energy X-ray absorptiometry: influence of metallic implants at the fracture site

Cattermole, Howard Charles

ASSESSMENT OF TIBIAL FRACTURE HEALING WITH DUAL-ENERGY X-RAY ABSORPTIOMETRY: INFLUENCE OF METALLIC IMPLANTS AT THE FRACTURE SITE

A Thesis submitted for the Degree of M.Sc.

by

Howard Charles Cattermole

School of Engineering

University of Durham

1995

I declare that all material in this thesis which is not my own work has been acknowledged and that no material is included which has previously been submitted for a degree in this or any other university.

Howard Cattermole

Howard Charles Cattermole

CONTENTS

FIGURES

TABLES

Acknowledgements

Primarily I must thank my supervisor, Dr Jimmy Cunningham, for his continuing encouragement and interest in this work.

At South Cleveland Hospital in Middlesbrough, the following deserve thanks for their various essential contributions: Olwyne Pitcher and Jackie Bates of the Bone Densitometry Unit, Dr J.N. Fordham of the Department of Rheumatology and Mr D.S. Muckle of the Department of Orthopaedic Surgery. I must also thank Juliette Cook of the School of Engineering, University of Exeter for permission to use a slightly adapted form of one of her diagrams as Appendix 3.

Abstract

ASSESSMENT OF TIBIAL FRACTURE HEALING WITH DUAL-ENERGY X-RAY ABSORPTIOMETRY: INFLUENCE OF METALLIC IMPLANTS AT THE FRACTURE SITE

Evaluation of the progress of fracture healing traditionally combines manual fracture manipulation with a visual radiographic assessment. This approach can lead to satisfactory healing, but trouble can ensue when the type of fixation compromises the healing assessment, and in fractures of long bones such as the tibia, where a high incidence of delayed union is still a problem. Dual-energy X-ray absorptiometry (DXA) offers a safe, accurate, repeatable and non-invasive method of measuring bone mineral density (BMD), a quantity which is directly related to the mechanical properties of bone. DXA has been successfully used to monitor BMD changes around fractures treated by external fixation. Nine patients with fractures stabilized in this way have been scanned at monthly intervals, and two distinct patterns of healing have been identified.

Before this technique could be extended to fractures treated by internal fixation, the effect of large areas of radio-dense material in scans had to be established. To judge the effect of steel implants on scanning and image analysis, tests were conducted on steel and aluminium phantoms in three geometries - parallel rectangular blocks, a square rod in a square case, and a circular rod in a circular case. A perspex base was used in all scans. ANOVA (analysis of variance) performed on the BMD data from scans with and without steel indicated that steel had no effect on scanning (5% significance level). These results implied that steel implants would not affect the reliability of DXA scanning, and that this method of monitoring healing could be used with fractures stabilized by internal fixation. On this basis several patients with nailed tibial shaft fractures have been scanned and their scan images analyzed.

CHAPTER 1 - INTRODUCTION

The prediction of the healing potential of fractures of any of the bones in the human skeleton remains an essentially qualitative activity. In the majority of cases the assessment of the state of healing involves a combination of manual manipulation of the fractured bone to measure the mechanical strength, and radiographic examination to gauge the extent of callus formation. Whilst these techniques are usually helpful, they are certainly not foolproof, and manipulation of the fracture can sometimes induce loss of stability. A more quantitative method of assessment would therefore be of considerable benefit. Additionally, under certain treatment regimes, for instance where external fixation is used, the form of fracture fixation may jeopardize the reliability of this type of examination by interfering with its outcome. In such cases there is even greater advantage to be secured by improving the way in which fracture healing is assessed.

1.1 Bone - Structure

One of the peculiar features of all mammalian bone is that its macromolecular composition is remarkably constant. At this scale bone is always a two-phase anisotropic composite structure. The two phases of the composite are an organic matrix made up primarily of collagen fibres, and an inorganic matrix consisting mainly of hydroxyapatite, a salt of calcium. Collagen accounts for around 40% of the mass of solid bone and 60% of its volume, while hydroxyapatite, the so-called bone mineral, takes up 40% of the volume and about 60% of the mass (Cameron and Skofronick, 1978). The organic fraction of bone gives it its flexibility, elasticity and tensile strength, whereas the inorganic component confers a degree of rigidity, hardness and compressive strength. Currey (1962) commented that one of the fundamental reasons for the success of vertebrates is likely to be the indisputable superiority of bone over other skeletal materials.

1.1.1 Gross Structure

At a higher organizational level, bone can be divided into two broad categories which have distinct features and appearance. Compact or cortical bone is a dense form of bone with few pores or spaces - it is found in the shafts of long bones and in the skull and is characterized by comparatively high strength and rigidity. Trabecular (sometimes known as cancellous or spongy) bone is a less dense structure which is found in the vertebrae and in the epiphyses of long bones - it is more flexible and elastic than cortical bone. The lower density is due to the structure, which consists of a network of small bars of bone known as trabeculae. In living bone, the spaces between the trabeculae are filled with haemopoietic tissue.

Some authors also distinguish a third gross type of tissue, subchondral bone, which occurs in certain joints beneath the articular cartilage, whereas other classifications include this under the general heading of cortical bone. Choi *et al.* (1990) have shown that subchondral bone has a significantly lower elastic modulus than cortical bone (1.15 GPa as against 5.44 GPa), which does indeed suggest the need for this third division. There are usually 206 bones in the human skeleton, each of which has evolved as a specialized compromise between the greater strength and rigidity of compact bone and the reduced mass and greater flexibility of trabecular bone. A common example of this compromise evident in many bones has a thin outer shell of compact bone encasing an internal network of trabeculae.

1.1.2 Microscopic Structure

Under the microscope, there are no longer obvious differences between the three gross bone types discussed above - at the same stage of maturity, all distinctions disappear. The differences at the microscopic level are related to the bone's age, and its speed and manner of deposition. Woven bone, so called because of the random pattern of

collagen fibres and lacunae (the small compartments inhabited by osteocytes), is associated in adult life with pathologic processes. Its most common manifestation is as fracture callus, but it is also laid down during the initial development of the foetal skeleton. Woven bone is unique amongst the various microscopic types of bone in that it can be deposited without the presence of a cartilaginous or hard tissue base. Its main function is as a structure which gives temporary strength and forms a foundation for the subsequent deposition of mature lamellar bone.

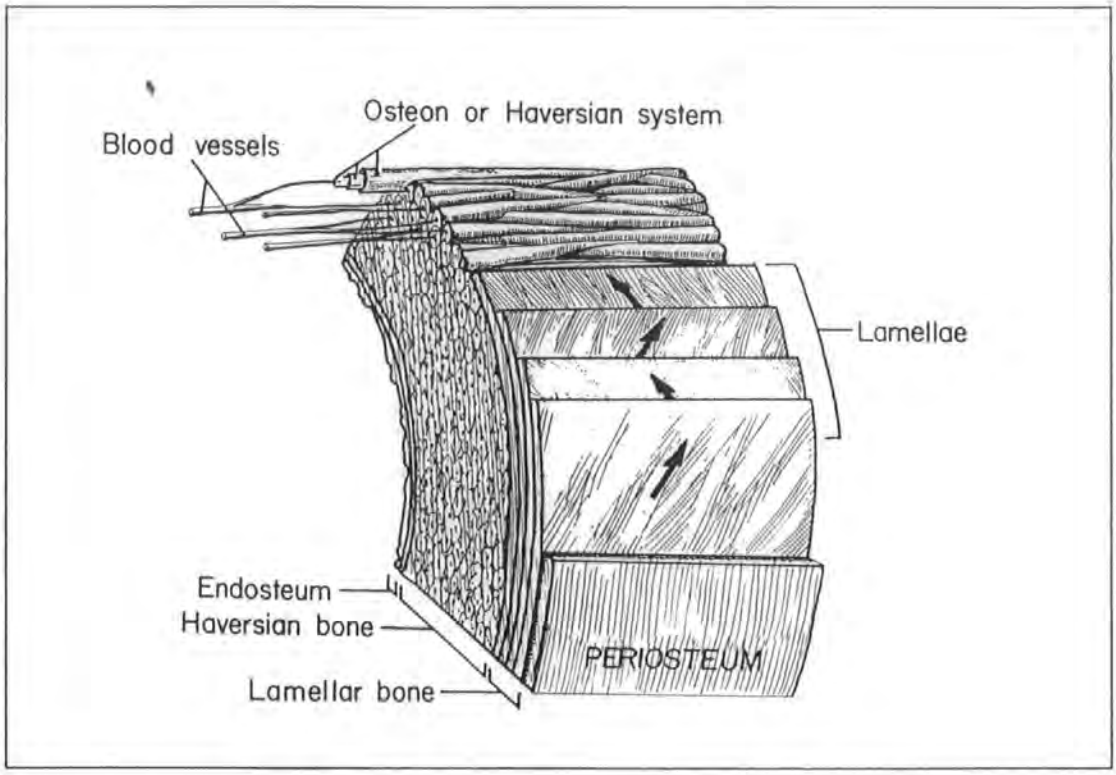

Figure 1.1 Mature bone, showing the two types of lamellar structure. Haversian bone is made up of osteons, each composed of 15-20 lamellae organized concentrically around a blood vessel. The second arrangement occurs in the periosteum and endosteum of long bones, where circumferential lamellae encircle the bone (from Shipman *et al.* 1985).

Mature bone of any type is arranged in thin sheets of parallel collagen fibres called lamellae. For additional strength it is usual for adjacent lamellae to be orientated in different directions. The lamellae are organized in one of two ways depending on their position (see Figure 1.1). In the interior of a bone, sets of 15-20 lamellae are

arranged concentrically around a central vascular opening, a unit known as an osteon. Individual osteons are in turn surrounded by cement lines which separate them from their immediate neighbours. The canals in the centres of osteons form a part of the Haversian system which is the vascularized network that supplies bone with nutrients. Within this network, the Haversian canals run in general longitudinally and within osteons, whereas Volkmann's canals are not surrounded by lamellae and tend to cut through the osteonal structure. The other lamellar arrangement occurs at the inner and outer surfaces of the long bones. Instead of being organized into osteons, the lamellae here encircle the circumference of the bone.

1.2 Bone - Function

Bone seems, superficially at least, to be distinct from the other tissues of the body because at the macroscopic level it retains the same appearance regardless of whether its constituent cells are living or dead. This initial impression is of course misleading as, just like other tissues, bone is a vital, dynamic structure continuously engaged in a whole variety of activities. Above all, there are endless pressures on the skeleton to remodel to take account of changing patterns of activity whilst retaining metabolic efficiency of form and function (Rubin *et al.* 1990). There are four main groups into which the functions performed by bone fall, and these are mechanical support, protection, haemopoiesis and mineral homeostasis. The last two of these are both the least well documented and the least important as far as this study is concerned, and so will be dealt with first.

1.2.1 Haemopoiesis

The production of red blood cells, or haemopoiesis, occurs in adults in the bone marrow situated in the central cavities of the major long bones and the cancellous layers of the skull, ribs and sternum. There is an intimate relationship between bone

and blood in terms of both development and function. At the embryonic stage, blood vessels and bony tissue find their common origin in the connective tissue mesenchyme, which then differentiates as the bone precursor is invaded by capillaries. In adult life, these same capillary networks function as a transport system, bringing the different types of bone cell to their required sites.

1.2.2 Mineral Homeostasis

Mineral homeostasis is a broad term for a collection of interrelated processes which happen within each bone. The skeleton is in this sense a reservoir of minerals which can be tapped as necessary by the body. The principal mineral constituent of bone is calcium, 99% of the body's supply being stored in this way, and phosphorus is also found in large quantities. Calcium is concentrated particularly in the dense cortical bone, although the most labile volume is located in cancellous bone. It is interesting to note in this context that areas with largely trabecular content are the most rapidly formed and destroyed in animals with a variable seasonal requirement for calcium.

1.2.3 Protection

The protective function of bone falls into two categories. Firstly, many bones serve as shields for important soft tissues, the two obvious examples here being the rib-cage and the skull which protect, respectively, the heart and lungs, and the brain and sensory organs. The second method of protection applies to the joints and spongy bone which absorb shocks due to movement, again in order to shield soft tissues.

1.2.4 Support

The most self-evident function of the skeleton is undoubtedly support, and this is also the best understood. The vast majority of bones (excepting the bones of the ear) serve

this purpose to some greater or lesser extent. Different combinations of compact and trabecular bone will have different sets of properties. As well as giving strength and rigidity, most bone is adapted to withstand fatigue or stress fracture, i.e. fracture within the so-called physiologic loading range. In resisting fatigue failure, which is caused by catastrophic crack propagation, the ability of bone to slow crack growth is more important than its capacity for inhibiting crack initiation, since cracks can be repaired through remodelling (Martin and Burr 1989). Osteonal bone is well adapted to limit crack growth, as the discontinuities between osteons act to arrest propagation (Currey 1975). In every case structure is closely related to function, and this is exemplified by the fact that the same bone in different animals will have an alterred microscopic structure specific to the usual scope of activity of the animal in question.

1.3 Fracture

Fracture of a bone can occur either as a result of direct injury, or after repeated loading of the bone, in which case the term stress fracture is used and the fracture is analogous to a fatigue failure of an engineering component. The former type is likely to have a much more obvious manifestation - traumatic fracture is very sudden, a film speed of about ten thousand frames per second being necessary to record it (Perren 1992). Stress fractures may not be noticed at all until or unless further injury precipitates catastrophic failure of the bone. The type and severity of fracture will affect the healing process. In particular, an undisturbed stress fracture will have a very small (or even non-existent) gap between the two fracture surfaces; conversely, a traumatic fracture will usually involve some degree of displacement of these surfaces, making direct healing impossible.

1.3.1 Fracture Healing

Bone has the notable property of being able to regenerate itself completely when wounded, unlike other tissues, which form a scar. The efficiency of this mechanism is such that, under ideal healing conditions, all evidence of a fracture may have disappeared a year after injury (Halstead 1974). In biochemical terms, many of the events which occur while a fracture heals closely parallel the processes which take place during the initial growth of a bone. The difference between the two is that in a healing fracture the progress of events is consecutive in time, whereas in a developing bone several processes can be observed simultaneously at spatially separated points of the growth plate (Pan and Einhorn 1992).

Fracture healing involving bone which has suffered trauma will almost invariably be indirect. Direct (or primary) healing can occur only when there is a negligible and stable fracture gap, which then allows the reparative phases of healing to be bypassed and remodelling to begin immediately. The fracture gap is bridged directly by so-called cutting cones, with osteoclasts in front removing bone, and behind them osteoblasts laying down new bone. This type of healing is marked by the absence of extensive callus formation, but it is not necessarily faster than indirect healing. Otherwise indirect healing takes place, a series of events which is typically broken down into four phases (see Figure 1.2): (1) the inflammatory stage, characterized by formation of a haematoma and death of bony tissue, (2) the soft callus or cartilaginous stage, (3) the mineralization (or hard callus) stage, and (4) remodelling.

The endpoint of healing is defined as that time at which the original integrity of the bone has been restored. Various attempts at quantitative interpretation of this definition have been made. Richardson *et al.* (1992, 1993), for example, have suggested that healing has occurred in fractures of the tibia when the fracture bending stiffness reaches 15 $Nmdeg^{-1}$. Some surgeons, on the other hand, might prefer to rely

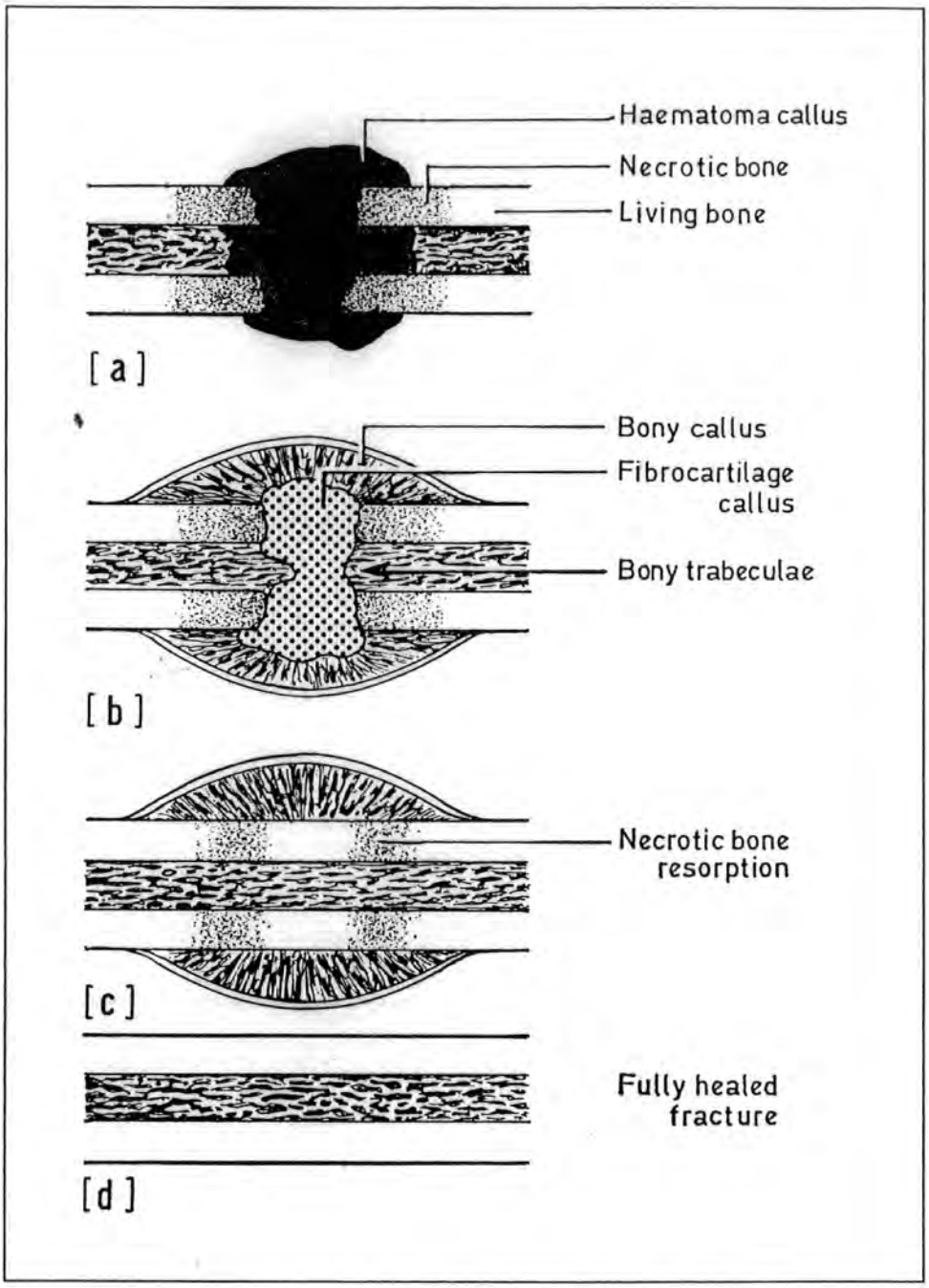

Figure 1.2 Diagram of the four stages of fracture healing. (a) The inflammatory phase, (b) the cartilaginous phase, (c) mineralization of the repair tissue, and (d) the endpoint of healing when remodelling is complete (from Halstead 1974).

upon radiographic evidence of union of the fracture surfaces. It is certainly not helpful that the clinical classification of healing relies so heavily on radiographic criteria, and it has been proposed that an alternative biomechanical pattern of healing would be more appropriate. There would again be four stages, based on the failure properties of the healing bone: (1) failure through the existing fracture site with a low stiffness, rubbery pattern, (2) failure through the original site with a high stiffness pattern, (3) failure partially through the original site, and (4) failure unrelated to the original fracture (Simon *et al.* 1986).

1.3.1.1 Inflammatory Phase

The first event after traumatic fracture is the formation of a haematoma around the fracture site. Within hours vasodilation becomes marked and inflammatory cells have begun to amass around the fracture surfaces, a response which is little different to the initial reaction to sepsis, except for the absence of a self-perpetuating stimulus (Brand and Rubin 1987). Coagulation of the ends of ruptured blood vessels is usually complete after about 24 hours, and as a consequence osteocytes die, leaving an area of necrotic bone. Over a period of days or weeks, depending on the severity of injury, monocytes and phagocytes from the inflammatory exudate clean up the fracture fragments by digesting necrotic cells and other debris.

1.3.1.2 Cartilaginous Phase

Overlapping with the inflammatory phase is this first stage in the repair of the traumatized bone. Repair begins with the formation of callus, which gradually envelops the injured part of the tissue. This callus is derived from two sources, cells from the periosteum and cells from the bone marrow. A proliferation of cells from the periosteum, usually seen within a day of fracture, will over a period of weeks encase the whole of the damaged area in a bony collar. Most of the collar is composed of

cartilaginous callus, with only an outer shell of initially stiffer fibrous material, but it is subsequently invaded by capillary networks bringing the cells required to build new bony tissue.

The cells from the marrow play a distinct part in the healing process by invading the fracture haematoma and constructing a bridge of trabeculae which ultimately links the separated fracture surfaces. This development is referred to as the internal callus - as distinct from the bony or external periosteal callus. In combination, the internal and external calluses form a natural fixation of the fracture which allows the onset of the further phases of healing.

1.3.1.3 Mineralization Phase

Mineralization of the cartilaginous callus tissue is generally the next stage in healing, but after callus formation it becomes harder to predict the temporal progression of events (Brand and Rubin 1987). The usual order from this point is ossification of callus, followed by the formation of pockets of woven trabecular bone, and the restoration of blood supplies. Once the mineralization of fresh osteoid has begun, the healing process becomes radiographically observable. A few weeks after fracture, all that are visible are radiodense patches dotted throughout the callus. Later on, these patches appear to coalesce into larger areas of feathery white callus and the edges of this tissue improve in definition. The end of mineralization (somewhat arbitrary, as there is again overlap with the next phase of healing) is heralded by the completion of a network of bony trabeculae, with individual trabeculae visible across the fracture line. Repair can take anything from a matter of weeks to several months to complete, the length of this period depending on the location of the fracture, both within the skeleton and within each bone, as well as on the severity of fracture and the imposed treatment strategy.

1.3.1.4 Remodelling Phase

Whilst it may be difficult to predict the rate of healing through the reparative phases, it is the remodelling phase which is hardest to distinguish from the routine behaviour of the body - in this case the parallel processes of bone resorption and deposition that occur throughout the life of the skeleton. Remodelling at the fracture site is required because deposition of trabeculae during reparative healing creates an architecture which does not share the same orientation as existing bone. Thus, at the same time as new trabecular bone is being deposited, the trabeculae which served to immobilize the fracture at an earlier stage are resorbed. Overall, more resorption than deposition takes place in this phase of healing, as the bulging callus formed to increase the stiffness of the fracture is gradually removed and the bone regains a more conventional appearance.

1.3.2 Post-Traumatic Osteoporosis

It has been recognized for many years that traumatic fractures are accompanied by an increased rate of remodelling activity, on balance resorptive, which is not restricted to the area immediately surrounding the injury. The newer non-invasive mineral content measurement techniques have been used to confirm this received wisdom. A study on twenty-seven tibial shaft fractures used photon absorptiometry to monitor changes in bone mineral content (BMC) at the upper end of the tibia and fibula (Andersson and Nilsson 1979). Continuous decrease in BMC in the fractured leg during the first five months after fracture was followed by a brief steady state and then a slow increase. The gain stopped at around a year after injury, when the mineral content was at about 25% of its original level, having risen from a minimum of close to 45%. Ulivieri *et al.* (1990) studied BMD distal to tibial shaft fractures, again with photon absorptiometry, using the healthy contralateral tibia as a control for each of the seven patients. They found a steady but slowing decrease in BMD over the four months of observation - in

none of the patients had recovery in mineral content begun within the period of the study.

Smith *et al.* (1993) were interested more specifically in post-traumatic osteoporosis in patients with externally fixated diaphyseal tibial fractures. Radiographs were taken at two to four weekly intervals and inspected for signs of bone thinning. A surprisingly high incidence of acute localized osteoporosis of the ankle (14 out of 20 patients) was observed, compared with 6 out of 20 in two control groups treated by internal plate fixation and external cast respectively. Acute localized osteoporosis is a severe form of osteoporosis - the milder regional osteoporosis had a lower rate of occurrence in all but the plastered group. For both types of osteoporosis, replacement of the lost bone took several months and was often incomplete six months after fracture. Complementary behaviour has been noted in the femur (Van der Wiel *et al.* 1994). Sixteen patients with unstable fractures of the ankle or tibia were scanned at the femoral head and trochanter by dual-energy X-ray absorptiometry shortly after fracture, and then at around 8, 16, 29 and 57 weeks later. The second scan was done at the end of immobilization, after which weight-bearing was allowed to 50% of body weight, increasing to 100% over the next month. The lack of weightbearing during the first two months of healing appeared to induce a significant loss of bone mineral of around 9% in the femoral trochanter, increasing to 15% a year after fracture, at which time no signs of recovery were evident. Losses from the head of the femur were lesser, but significant nonetheless. This result confirms that post-traumatic osteoporosis can have a pronounced effect on regions isolated from the immediate area of the fracture.

1.3.3 Influences on Healing

It has already been noted that the size and severity of fracture will establish whether repair is effected by direct or indirect healing. Beyond this straightforward

classification, the various factors that may influence the speed and success of healing are less easy to quantify. In general, it could be said that the greater the energy involved in a fracture, the greater the likelihood is that healing will not proceed without complication. Healing cannot go ahead at all if there is a lack of living pluripotent cells local to the fracture (Müller *et al.* 1991); this is an absolutely fundamental requirement.

1.3.3.1 Blood Supply

One important factor in this respect is the extent of disruption of the blood supply around the fracture site. An intact blood supply is necessary for cell nutrition and support. It has further been suggested that osteoclasts and osteoblasts are actually derived from the blood cells which invade the haematoma after fracture (Trueta 1963). Whether or not this is true, it is certain that vascularization is crucial for healing. There are particular problems associated with the healing of tibial shaft fractures, as the tibia has only a thin covering of soft tissue from which the essential extraosseous blood supply must be obtained (Rhinelander 1974). One study on open tibial fractures has found a significantly greater incidence of delayed union or non-union in patients with arterial occlusion (Dickson *et al.* 1994). The various treatment techniques have therefore been adapted to encourage as far as possible the successful establishment of efficient circulation in the area of the fracture.

1.3.3.2 Mechanical Environment

There is now a substantial body of evidence available which demonstrates the dependence of efficient fracture healing on the mechanical environment. Much emphasis has been placed recently on this determinant as it has become increasingly easy for the surgeon to control the loading applied to a fracture during the course of healing. It is conversely very difficult to regulate directly determinants such as

vascularization and the bioelectrical environment. However work by, for instance, Wallace *et al.* (1993, 1994) on the vascular response to micromovement, and by Goodship *et al.* (1993a) on prostaglandin synthesis stimulation, again by micromotion, has shown that regulation of the mechanical environment will have an attendant effect on these other factors.

It is generally accepted that strain can be useful at all stages of healing, i.e. that complete immobilization of a fracture is not necessarily advisable. Also, there is some agreement that a low level of strain is a genuine requirement in the early stages of healing (Goodship and Kenwright 1985, Kershaw *et al.* 1993) in order to promote effective callus growth. Despite these results, it is still not clear exactly how much strain is the optimum. Work by White *et al.* (1977) on experimental rabbit tibial osteotomies showed that 20 N cyclical loading at 55 cpm for four hours a day in combination with 20 N of compression was not an improvement on compression alone. Subsequent studies on the tibia have tended towards the definition of an optimum in terms of induced displacement. Around 1 mm axial displacement at 0.5 Hz for 30 minutes per day has been shown to have a beneficial effect without increasing the rate of complications (Goodship *et al.* 1993b, Kenwright *et al.* 1986).

Early weight-bearing of the fractured leg is encouraged by some authors (Dolder 1991, Van der Wiel *et al.* 1994) whereas others (Riggins *et al.* 1985, Goodship *et al.* 1993b) have found that it has no noticeable effect on the progress of healing. One problem, commented on by Kershaw *et al.* (1993), is that even if early weight-bearing is beneficial, patients will usually be uneasy about loading their fractures until several weeks into healing. Most attention has been devoted to the action of compression on fracture healing. This is largely because it has been known for some time that torsional instability, and by implication shear, is deleterious to healing. Mabuchi *et al.* (1992) gave an elegant demonstration of this fact using robotic control of the mechanical environment in experimental rabbit tibial osteotomies. Clinical

confirmation is provided by May (1989) in a study of patients treated for unstable tibial shaft fractures by single plane and bi-planar external fixation, which showed that biplanar fixation halved the time to unaided walking. Biplanar fixation cuts down considerably on shear by increasing torsional rigidity, but at the same time maintains compressive elasticity.

1.3.4 Delayed Union and Non-union

In any sizeable group of tibial shaft fractures, there will be some in which progress to union is noticeably slower than for the majority. Fractures of this type fall into two categories. Delayed union describes healing which simply takes longer than usual, but which does eventually reach completion without further intervention. A non-union is diagnosed when a fracture has failed to heal within a normal period and exhibits no sign of doing so at all. There is no straightforward generalization to be made about the cause of delayed or non-union. The following, though, are common agents involved in complicated healing: extensive soft tissue damage, bone loss, infection, inadequate immobilization, and interrupted blood supply.

Few studies have been conducted on complicated healing in smaller animals, as it is rare to find non-unions occurring naturally and requires fairly extreme surgical efforts to produce them experimentally (Brand and Rubin 1987). This has unfortunately hampered attempts at understanding the biological reasons for delayed union, although it has recently been proposed that delayed healing in tibial diaphyseal fractures is related to an early increase in the turnover of types I and III collagen (Joerring *et al.* 1994). Other reports indicate that non-union is not related to a low rate of mineralization or to reduced biochemical activity. The fact therefore remains that most delayed unions are due to an inappropriate biomechanical environment or unsuitable surgical intervention. They should consequently be avoidable if prompt corrective action can be taken.

1.3.5 Prediction of Healing

If delayed unions are to be excluded, means must exist for distinguishing between normal and abnormal patterns of healing. Since, as has become clear from the above discussion, healing is an umbrella term for a rather complex collection of spatio-temporally interacting processes, there is no single reliable measure of the state of repair of a fracture. In reality, a number of complementary approaches have been proposed. The details of the individual assessments will be given in Section 1.5, but some overall comments can be made here about what constitutes the basis of any appraisal of healing.

All healing assessments, whether mechanical, radiographic, or ultrasonic, aim to say something about the state of the tissue which occupies the gap between the fracture surfaces. There is as yet no reliable way of acquiring data about this tissue indirectly. In consequence, prediction of healing potential for all but the most stable fractures (where repair is by primary healing) involves techniques which essentially comment on the condition of the callus.

It is commonly accepted that the mechanical strength and stiffness of fracture tissue are useful indicators of its healing status (Chakkalakal *et al.* 1990). Ultimate strength is clearly an unacceptable parameter to measure *in vivo*. Stiffness can in certain cases be measured as a fracture heals without interfering with the outcome of repair, and a number of techniques for achieving this have been investigated. These protocols tend however to rely on the fracture fixation being of a particular type, and so are not of universal application. Fortunately, bulk mechanical properties have been shown to depend upon other properties of the healing fracture.

One of the earliest enquiries into the interrelationship of bone properties was conducted by Currey (1969), who correlated a number of mechanical attributes with

the ash (or bone mineral) content of rabbit metatarsals, and found a linear increase of both static strength and elasticity with mineral content over the mineral range explored. Whilst it is not until the last few years that the characteristics of callus itself have been studied, the results from earlier studies are nevertheless applicable because the repair tissue has the same ultrastructural components as mature bone. Subsequently the same author (Currey 1988, 1990) has confirmed a strong positive relationship between mechanical properties of bone in a diversity of species of bird, mammal and reptile, and volume fraction and mineral content. These observations have been backed up in more specific instances by a now extensive literature (see, for example, Williams and Lewis 1982; Ashman and Rho 1988; Schaffler and Burr 1988; Chakkalakal *et al.* 1990). One of the most promising consequences of the work summarized above is the reliance of mechanical properties on BMC. In the last few decades, there has also been a small explosion of sophisticated non-invasive methods for measuring this and so the prospects for healing prediction are very promising.

1.4 Fracture Fixation Techniques

There are now around four distinct techniques available and in common use for fixation of tibial fractures. Although it is common for the fibula to be fractured at the same time as the tibia, it is highly unusual for fixation to be provided to both bones. Shen and Shen (1993) surveyed 335 extraarticular tibio-fibular fractures, and found non-union of the fibula in 15 cases (4.5%), of which 11 were asymptomatic and only 2 required further surgical intervention. The method of fixation chosen will depend primarily on the severity of fracture and the extent of soft tissue injury. As a general guide, the stiffer the fixation, the less movement will be induced at the fracture site, the less callus will form and the lower is the stress on healing tissues - depending on the particular injury, different proportions and magnitudes of these variables will be appropriate (Latta and Zych 1991). It is worth bearing in mind that most fractures are

splinted not to ensure union but instead to minimize pain and to hold the fragments together accurately (Apley and Solomon 1982).

1.4.1 Casts and Functional Bracing

Until the last twenty or so years, the accepted method of treatment for fractures of the lower extremites involved application of a cast followed by a period of traction of the limb. The emphasis on rest inherent in this treatment regime has since been largely discredited as detrimental to the healing process (Mooney 1982). Plaster casts and functional braces are still used in the stabilization of some fractures, but in such a way as to allow movement of the adjacent joints and reasonable use of the affected limb.

Functional bracing, so called because it permits movement of the limb, is a refinement of the basic plastering in which (for a tibial fracture) the knee and ankle tend to be included in the cast to control rotation. This latter approach can be satisfactory so long as the limb does not swell and the joints do not stiffen due to lack of exercise. Since complete immobilization is certainly not needed for healing, bracing with a functional cast is an improvement on straightforward plaster casting, allowing early weightbearing (Bowker *et al.* 1978, Apley and Solomon 1982). Nevertheless, both plaster casts and braces control the fracture fragments only through support of the soft tissues and are therefore better at regulating angulation than rotation, and maintain length unreliably.

1.4.2 Screw and Plate Fixations

With both screw and plate fixations primary healing dominates and there is very little callus formation. Screws may be used independently of or in conjunction with plating as a method of fixing fracture fragments. In the former case the screws are known as lag screws - these are the most effective means of realising direct interfragmentary

compression (Müller *et al.* 1991). A lag screw has a purchase only in the far cortex - this is accomplished either by the shank of the screw being unthreaded or by overdrilling the near cortex to a diameter greater than or equal to that of the screw thread. The interfragmental compression generated in this way is known as static because of its minimal variation with load. Whilst the stability developed is good, lag screwing does not provide much strength. Typical applications are in fractures of the metaphyses of long bones and in uncomminuted shaft fractures, in which case two or more screws are applied.

There is now a very large variety of plates available to the orthopaedic surgeon, some of which have been designed to perform very specific jobs, and others which can be contoured to fit different local anatomies. Plates which are used in combination with lag screws to protect the screw fixation and allow earlier weightbearing through the fracture are labelled neutralization plates. Neutralization plates are therefore not responsible for the fracture stabilization. Other types of plate which do contribute to stabilization are the buttress, compression and tension band designs.

Buttress plates act to supplement the compressive effect of lag screws, normally to prevent axial deformity from shear or bending in cases of comminution in the metaphyseal cortex. Compression plates, on the other hand, are put into use when lag screw fixation is not feasible, for instance in transverse and flat oblique fractures (Müller *et al.* 1991). The ideal use of a plate is as a tension band, on the tension side of the bone. Although there are weaknesses at the stress concentrating screw holes and plate ends, under this condition plate fixation gives improved bending rigidity and early functional use is possible.

The main problems associated with plate and screw fixations are related to the stress-protecting effect of the plate during remodelling and the stress concentrations at the screw holes, and for this reason the period immediately after removal of the plate must

be carefully monitored to avoid refracture (Latta and Zych 1991). Recent developments have attempted to reduce the area of the bone-plate interface so as to ensure minimal disruption of the blood supply near the fracture, which should in turn lead to less disturbed healing and lower incidence of complications (Gautier *et al.* 1992).

1.4.3 Intramedullary Nailing

Küntscher outlined the principles of intramedullary splinting in the early 1940's. This original technique was the precursor to present day unlocked nailing, which uses the nail as a load-sharing device. The main improvement on the original procedure has been the introduction of reaming before nail insertion, which enables a closer fit between the nail and the medullary canal and therefore leads to a more secure fixation. Subsequently interlocking nails have been developed, which can act as load bearers rather than sharers and are consequently of wider application in less stable fractures.

The advantages of the secure fixation offered by intramedullary nailing are that it may stabilize the fracture to the extent that primary healing takes place, and it allows early weightbearing through the injured limb and prompt mobilization of the associated soft tissues (Mooney 1982). There are also considerable pitfalls to be avoided if inappropriate use of nailing is made. In particular, reaming of the medullary canal can cause severe obliteration of the endosteal blood supply. Whilst Rhinelander (1974) has shown that this is not necessarily a significant problem in the tibia as regeneration occurs quite rapidly, being obvious at four weeks post fracture, Gautier *et al.* (1992) point out that extensive necrosis results if the periosteal circulation has also been damaged. When reaming is not used, for the smaller diameter solid interlocking nails, the danger of long term weakening of the bone due to stress concentration at the locking screws and stress protection is unfortunately amplified (Latta and Zych 1991).

1.4.4 External Fixation

Such a profusion of designs of external fixator is now in current use that it will only be possible here to outline the differences between this and other forms of fixation. On the whole, external fixation is considered as an option in cases of severe soft tissue damage, for fractures which are one aspect of polytraumatic injury, or more generally when a rigid stabilization, with rapid application, is important (Kenwright 1992). One property common to all external fixators is the possibility of varying frame stiffness. In some cases this is effected very simply, whereas other fixation systems have sophisticated inbuilt arrangements for dynamization of the frame, allowing precise amounts of micromovement at the fracture site.

There are two standard frame geometries - unilateral and circular. In addition, unilateral frames can be combined in bilateral, triangular and right-angled configurations for greater rigidity. A circular frame is the preferred option for complex leg-lengthening operations, but due to its complex structural nature it is applied to fractures solely in exceptional circumstances. The various arrangements of unilateral fixators have become increasingly popular for long bone fractures due largely to their versatile nature. This versatility is made apparent by listing the variables which can affect the stiffness of a typical frame - pin diameter, number of pins, separation between pins, separation between pin clamps, clamp assembly type, offset from bar to leg, number of bars, and bar size (Latta and Zych 1991).

1.5 Assessment of Fracture Healing

The traditional way of monitoring healing progress is qualitative. It involves a combination of manual manipulation of the fractured bone and X-ray examination. Manipulation of a fracture may cause destabilization, and conventional radiographic examination has been shown to be largely inconclusive as an assessment of healing

(Hammer *et al.* 1985). Thus much could be gained from translating this qualitative, subjective assessment into a quantitative, objective measurement. Two obvious routes to investigate would be quantification of image analysis or stiffness testing (Van der Perre 1993).

Quantification of image analysis has been considered from two complementary angles. The first is as an approach to reviewing the biological processes of healing, whereas the second blends quantitative image analysis with a mechanical model to gauge stiffness or strength. The more straightforward technique is quantitative stiffness testing, whereby the actual response of the fracture to an applied load is measured, either dynamically or statically.

1.5.1 Fracture Stiffness Measurement

Static testing of the stiffness of a fracture to give some measure of the state of repair of the injured bone has been proposed by a number of authors over the past two or so decades. The strategy in studies of this type has almost invariably involved fixing strain or dial gauges to the frames of fractures treated by external fixation, although the use of instrumented plates *in vivo* has been reported (Burny *et al.* 1985, 1990, Schneider *et al.* 1990). Since no-one has as yet described a technique with wider application, even to the whole range of external fixation devices, the regular use of stiffness measurement in the clinical environment has been restricted to a small number of specialist centres. An Oxford group has had notable success with routine fracture stiffness measurement (Harris *et al.* 1985), defining a combination of bending and axial stiffnesses which allows the removal of fixation with a very low incidence of refracture (Cunningham *et al.* 1987). Bending stiffness may be a valuable measure of healing during the later stages, but it is not useful earlier on because of the unquantified effect of muscle activity (Richardson et al. 1993).

An *in vitro* inquiry by Beaupré *et al.* (1983) used a dial gauge to measure pin displacements in an externally fixated fracture model under controlled axial loading. Five neoprene disks of varying mechanical properties modelled the healing fracture, and strong agreement was found between directly measured properties and those derived from a combination of finite element modelling and the displacement test results. Theoretical analysis of bilateral and unilateral fixation frames (An *et al.* 1988), again by a finite element method, demonstrated that recovery of rigidity up to around 25% of that of intact bone could be accurately determined by measuring pin displacement and side bar strain. These experimental and theoretical results back up the experience gained from the clinical trials discussed above.

1.5.2 Vibration Analysis

For a uniform slender beam, vibrating by bending, the resonant frequency of the beam is proportional to the square root of its bending stiffness. By approximating a tibia under forced vibration as a straight beam with constant properties, and locating the resonant frequency an effective stiffness can therefore be calculated for the fractured bone and compared with the contralateral value. Another approach looks at the response of a fractured bone to an instantaneous impulse, producing free vibration, in which case the free vibration modes are analyzed and compared with those for the unfractured contralateral tibia.

Using modal analysis on excised tibiae (dry and fresh), and tibiae in an amputated leg and *in vivo*, it has been shown that two single bending modes exist, one for each of the planes of maximum and minimum flexural rigidity, with good agreement between the four cases (Van der Perre *et al.* 1983). Subsequently, monitoring of fracture healing has been successfully accomplished using modal analysis (Taktak *et al.* 1993) and by bone resonance analysis (Van der Perre and Borgwardt-Christensen 1985). In both of these techniques there is an upward trend in natural or resonant frequency as normal

healing progresses. Other less well proven procedures which show promise for fracture healing monitoring include phase delay and amplitude analyses (Collier *et al.* 1993). The main disadvantage of all of these methods is that they can only be used in conjunction with external fixation (if the fixator column is removed prior to testing) or cast-bracing, as long as it is safe for the cast to be taken off for each test.

1.5.3 Ultrasound Techniques

The velocity of ultrasound across a discontinuity in a structure will be lower than if the structure were intact. In the case of a fracture the ultrasonic velocity will increase as healing progresses, and by comparison with the velocity through the unfractured contralateral bone it can be used as a measure of the state of healing. As long as the measurement points on the control and fractured bones are the same distance apart it is also possible to use transmission time as the measure of healing (Cunningham and Kershaw 1991). The standard method of application of the ultrasonic pulse is by means of ultrasound transducers mounted on the skin.

Problems encountered with this technique include the fact that even when a fracture has been clinically defined as consolidated, the ultrasound velocities in the fractured and control bones do not agree (Lowet *et al.* 1991). This is probably because ultrasonic velocity is proportional to density and elastic modulus rather than stiffness, so coincidence of the velocities would not be expected until significant remodelling of the fracture had taken place (Cunningham and Kershaw 1991). Another disadvantage is that measurement of ultrasound velocity is not helpful when the fixation is internal and, as with the various vibration analysis methods, plaster casts would need to be removed before testing.

1.5.4 Scintigraphy

The application of scintigraphy to fracture healing assessment is a relatively new departure. Scintigraphy is defined as the imaging of an organ (in this case a fractured bone) by the introduction of some radioactive material which can be detected by a scintillation detector. Bone scintigraphy involves intravenous injection with ^{99m}technetium methylene diphosphonate (^{99m}Tc-MDP). Scintigrams fall into two categories - dynamic imaging entails acquisition of consecutive frames immediately after injection so that an activity *vs* time curve can be constructed, whereas static scintigrams are single images taken during the static activity phase when most of the ^{99m}Tc-MDP has been cleared from the soft tissues surrounding the fracture but the activity in the bone itself is still significant.

Much of the evidence so far amassed is conflicting, but some recent studies on tibial fractures suggest that there may be a place for scintigraphy in the prediction of healing. The notion that scintigraphy may be useful at all is based on the assumption that radionuclide uptake is related to new bone formation. Oni *et al.* (1989) carried out dynamic and static scintigraphy on fifty closed adult tibial shaft fractures, at zero, six and twelve weeks after fracture. Nine fractures showed delayed union. Apart from significant overall differences in uptake ratios, mean net counts and an osteogenesis index between the two healing groups, the ratio of uptake over the fracture to an adjacent site in the same bone at six weeks was found to be an especially strong predictor, with a value above 2 indicating the potential for normal healing. Wallace *et al.* (1992), on the contrary, had no success in proving a relationship between early phase uptake at the fracture site and at a corresponding site in the contralateral tibia. In summary, more data are required before scintigraphy can play a routine role in fracture management.

1.5.5 Photon Absorptiometry (PA)

Photon absorptiometry was the first commercially available technique for quantitative measurement of bone mineral. There are now two kinds of PA, single and dual, the former using a monoenergetic γ-ray source and the latter two sources of different energies. SPA is applicable only to the peripheral skeleton, where a constant thickness can be obtained - the amount of bone mineral in the scanned tissue is derived from the attenuation through soft tissue relative to that through bone and soft tissue. DPA was developed to eliminate this shortcoming and is used primarily for axial measurements, where a constant overall thickness is impossible to attain. It is not feasible, for instance, to allow for the volume of gas in the intestines when scanning the spine. A dual-energy system gets around this problem by comparing the absorption of the two energies. In both cases the measurement is an areal density, with units of gcm^{-2}.

The most common measurement site for SPA is the distal third of the radius, which has a useful predictive value for appendicular fractures. Since the distal third is about 95% cortical bone, however, response to therapy is better monitored by scanning the ultradistal radius or the os calcis, which have greater percentages of trabecular bone (Genant *et al.* 1991). In any case, precision and accuracy are high, and the effective dose is very low (<1 μSv). SPA has been used with some success to observe changes in BMC following tibial shaft fractures (Aro *et al.* 1988), but the requirement for a constant tissue thickness means that the method is not ideal in this province (Andersson and Nilsson 1979). DPA is used mainly for spine, hip and total body scans. Precision and accuracy are not quite so high as with SPA (Johnston et al. 1991), and spinal scans especially tend to be unreliable in older patients because of artefacts such as disc degeneration, endplate hypertrophy and stress fractures (Alhava 1991). Nevertheless, effective use has been made of DPA in monitoring changes in bone mineral density (BMD) after tibial fracture (Ulivieri *et al.* 1990). One mutual drawback of SPA and DPA is that their photon sources need regular replacement -

^{153}Gd, an ideal source for DPA in other respects, has a half-life ($T^{1/2}$) of only 240 days and ^{125}I, widely employed in SPA, has a very short $T^{1/2}$ of sixty days.

1.5.6 Dual-Energy X-Ray Absorptiometry (DXA)

Dual-energy X-ray absorptiometry shares the advantages of DPA without suffering from the undesirable aspects, and is proving to be applicable in a wide variety of situations. There is still some argument over the appropriate acronym for this technique, but the consensus is with DXA as being analogous to DPA. Important benefits of X-ray sources, all due to a higher radiation flux than with DPA, include improved spatial resolution, higher precision and lower scan times (Alhava 1991). In addition, the X-ray tube does not need replacement - the consequence is that all previous manufacturers of DPA equipment have now switched their attention to DXA scanners (Genant *et al.* 1991).

A comparative study by Markel *et al.* (1990) considered the three commonly used bone mineral measurement methodologies, SPA, DXA and QCT, as well as magnetic resonance imaging. In each case, the correlations between non-invasive measurements, and invasive tests of gross torsional properties and local stiffness and calcium content were investigated for osteotomized dog tibiae at various stages of healing. DXA had good associations with most of the properties measured, and never came out the worst of the four techniques. DXA has been taken up quickly as a clinical tool. The effect of reduced weightbearing on femoral BMD was evaluated in sixteen patients with unstable fractures of the tibia and ankle (Van der Wiel *et al.* 1994). The femoral neck and trochanter of the fractured and contralateral legs were scanned immediately after fracture and then at three month intervals for a year. The time of unloading ranged from five to eleven weeks. Significant reductions in BMD at both sites were recorded for all patients, and there were no signs of recovery at the end of the study. Another application which shows promise is in leg-lengthening.

Eyres *et al.* (1993a) found that DXA provides an objective quantitative method of assessing new bone formation during femoral and tibial distractions. Particular advantages of DXA in this situation are that the high quality of the scan image permits accurate measurements of the osteotomy gap size and angulation to be made.

1.5.7 Quantitative Computed Tomography (QCT)

QCT is unique amongst the methods of measuring BMD in that a true volumetric density can be derived. An additional advantage is that the cross-sectional nature of the image offers the possibility of examining the properties of adjacent trabecular and cortical bone independently (Tothill, 1989). Research into the use of X-ray CT machines for BMD measurement has been concentrated in two areas - vertebral bone mineral density can be assessed using standard apparatus installed for general radiological purposes, whereas distal forearm measurement would be better served by the development of a dedicated system.

An *in vitro* investigation by Bentzen *et al.* (1987) established a strong correlation between the results of X-ray CT and six mechanical properties for tibial trabecular bone. Their conclusion was that CT would provide an immediately clinically applicable way of reliably predicting mechanical properties. The work by Markel *et al.* (1990) on tibial osteotomy healing in dogs has shown equally strong correlations between QCT results and both gross mechanical properties and local BMD values. QCT was also shown to perform at least as well as photon absorptiometry and DXA in these circumstances. There are unfortunately a number of disadvantages associated with X-ray CT: radiation dosage is comparatively high (roughly 60 μSv effective dose equivalent, slightly higher than that from a chest radiograph), the method can be prohibitively expensive, and clinical precision is highly dependent on fat content (Genant *et al.* 1991).

1.5.8 Other Methods

Image analysis can be quantified simply by using ordinary radiographs in conjunction with a digital photometer. This technique depends on the measurement of optical density, and so is reliant for its success on parameters such as voltage variation, and film and processing characteristics, but it can be used profitably for fracture healing assessment (Tiedeman *et al.* 1990). At the other end of the scale of sophistication is magnetic resonance imaging (MRI), the clinical elaboration of chemical analysis by nuclear magnetic resonance. This is a remarkably powerful technique in its regular usage for the diagnosis of brain abnormalities, cancers and vascular diseases. It is based upon the absorption of radio frequencies by atomic nuclei and allows any part of the body to be imaged in any plane required without any known risk to the patient. The few data that have been collected on the use of MRI in orthopaedic applications unfortunately suggest that there is not much to be gained from further research. Markel *et al.* (1990) compared the correlation of MRI, SPA, DXA and QCT results with invasively determined torsional and local properties of osteotomized dog tibiae at different stages of healing. With the exception of localized indentation stiffness, MRI had the poorest association with all properties examined. In any case, the use of MRI would require specially designed non-ferrous fixation implants (Lewallen *et al.* 1988), and it would be unlikely to be adopted for this reason alone.

CHAPTER 2 - DUAL-ENERGY X-RAY ABSORPTIOMETRY

The impetus for the commercial development of dual-energy X-ray absorptiometry came from dissatisfaction with the existing techniques for osteoporosis screening (Sartoris *et al.* 1990). Osteoporosis is now a major problem - in the UK it causes in the region of two hundred thousand fractures per year, which in 1993 cost the NHS over £640 million (National Osteoporosis Society 1993). Thus a cost-effective screening technique is an important goal. SPA has been in use for many years now, but queries have been raised over how well measurements of radial BMC correlate with values at the spine and hip, which are much more important osteopenic fracture sites. DPA is less than ideal in terms of precision, examination time and image resolution, and the need for periodic source replacement is a persistent irritation. QCT, as already mentioned, uses a comparatively expensive piece of apparatus in strong demand for other duties and involves a high radiation dose. DXA manages to surmount most of these problems, whilst retaining the benefits of a dual-energy system.

2.1 Advantages of DXA

The technique of dual-energy X-ray absorptiometry is very similar in concept to dual photon absorptiometry except that the radio-isotopic source is replaced by an X-ray tube. This change brings with it a number of important advantages, which are clear from the comparison of some key features of DPA and DXA in Table 2.1. Perhaps best of all, the precision (or repeatability) of measurements of BMC and BMD is improved from upwards of 1.5% to 0.5% for spine scans. Specific benefits of an X-ray tube are greater speed of scan and higher resolution, the latter translating simply into a cleaner scan image. From the patient's point of view, probably the most meaningful change is in radiation dose, which is lower than for any comparable technique.

	DPA	DXA
Radiation source	^{153}Gd	X-ray
Beam energies (keV)	44/100	40/70 or 43/110
Source renewal (months)	12-18	N/A
Dose equivalent (μSv)	3–5[1]	1-5[1]
Examination time (min)		
Spine	30[1]	5[1]
Total body	40[1]	10–20[1]
In vivo precision (%)	2–4[2]	0.5–2[2]
Accuracy (%)	4–10[2]	3–5[2]

Table 2.1 Comparison of bone mineral measurement by DPA and DXA. [1]Genant *et al.* (1991). [2]Johnston *et al.* (1991).

Most of the practical clinical advantages of DXA over single or dual PA follow directly from the large increase in beam intensity possible with an X-ray tube. The photon flux available from an X-ray source with an average tube current of 1 mA is 500-1000 times more than that from a typical ^{153}Gd DPA source (Sartoris *et al.* 1990). Despite the unarguable evidence in favour of DXA as a bone mineral measurement system, it was more than 20 years between the first reported use of a dual-energy X-ray methodology in Scandinavia in 1964 and the first commercial package, which came onto the market in 1987.

2.2 Commercial DXA Bone Densitometers

There are now three established manufacturers of DXA bone densitometry equipment - Hologic (Hologic Inc, Waltham, MA), Lunar (Lunar Radiation Corporation, Madison, WI) and Norland (Norland Corporation, Fort Atkinson, WI). The three systems are alike in using an X-ray source to generate two energies of photon, and in having a computer interface for imaging, calculations of BMC and BMD, and comparisons with reference populations, but there are important differences which are more than cosmetic. The essential distinction is in the method of X-ray energy

separation. There are two basic methods - the Hologic QDR systems use an X-ray tube pulsed at two voltage peaks to produce two X-ray energies, whereas Lunar and Norland use K-edge filtration to give the same effect but at different beam energies.

More specifically, the Hologic QDR-1000 utilizes a self-contained X-ray source mounted beneath the patient which is pulsed alternately at 70 and 140 kV, giving effective beam energies of 43 and 110 keV. Unlike the Lunar and Norland systems, the QDR-1000 includes a rotating calibration disk consisting of two sections of epoxy-resin-based materials, with similar densities to bone and soft tissue, and one section of air. This arrangement compensates for beam-hardening by making the ratio of patient to calibration material attenuations independent of variations in the source or detectors. Beam-hardening arises because the incident X-ray beam is not monochromatic - as the beam passes through tissue, low-energy photons are preferentially absorbed, leaving a greater percentage of high-energy photons in the transmitted beam. The thicker the tissue, the more pronounced is this 'hardening', thus X-rays which pass through the periphery of the scanned object are hardened less than those which take a more central route, and the scan image is distorted (Webster 1988).

Lunar, whose DPX-L system has been used in this study, have adopted the K-edge filtration approach to the production of dual-energetic photons. A constant potential is applied to a highly stable, low-scatter X-ray tube photon source and the filtration is applied to give two effective beam energies of 40 and 70 keV. 'K-edge' refers to the attenuative properties of the filtering element (in this case cerium), which has an edge in its absorption spectrum corresponding to a k-shell electron transition. In the Lunar system the filter has been selected so that this edge is just above the 40 keV level. Thus an incident broadband photon spectrum will be modified into two relatively narrow transmitted energy bands. The source ensures uniform exposure of pixels to both energies with negligible tissue thickness and composition effects, and photons are counted by an integral-line scintillation detector and photomultiplier tube.

The Norland densitometer works on a slightly different basis, although K-edge filtration is again the photon energy separation method used. Samarium is used to filter a broad spectrum photon beam to give a dual-energetic beam, with the degree of filtration depending on patient thickness. The difference is in detection, as Norland use two sodium iodide (NaI) crystals instead of the integral-line approach. A thin NaI crystal detects low-energy photons; high-energy photons pass through this and are detected by a thicker second crystal.

2.3 Accuracy and Reliability

There are three common statistical indices used for assessing measurement reliability. Short-term and long-term repeatability, or precision, give a relative indication of measurement stability, usually expressed as a percentage coefficient of variation (CV). In the case of DXA, this is done both *in vitro* (with suitable phantom materials) and *in vivo* (short-term only). Accuracy gauges the absolute extent to which a DXA measurement reflects the true level of bone mineral in the scanned substance and is expressed as a mean percentage difference. Phantoms of known BMC and BMD or sometimes excised cadaver vertebrae of known volume and ash weight are used for this purpose.

Early findings with a prototype Lunar DPX system (Mazess *et al.* 1988) suggested from ten scans of one subject that short-term precision would be about 1%. Johnson and Dawson-Hughes (1991), in a comparative study of DPA and DXA, assessed short-term precision of the Lunar DPX system in six subjects who were scanned six times each with repositioning between scans, initially and after nine months. The mean CV was 1.04% for spinal and 2.13% for femoral neck BMD; whole body BMD precision, determined in five subjects, was 0.64%. Long-term precision was measured over nine months with aluminium phantoms in water - mean CV's were 0.89% in 15.2 cm, 0.88% in 20.3 cm and 1.42% in 27.9 cm. Sartoris *et al.* (1990) reported similar

findings from scans of two phantom geometries, one cylindrical and the other a realistic model of four lumbar vertebrae. Short-term precision was 0.88% and long-term 0.97% (CV's). DXA was three times more precise in the long-term ($p < 0.01$) than DPA. Accuracy of repetitive scanning of known concentrations of K_2HPO_4 was high ($r = 0.99$, constant = –0.003).

Some doubt has been thrown on the value of DXA areal BMD measurements compared to the volumetric information provided by QCT (Börner and Schneider 1992), because changes in follow-up measurements could be due to alterations in bone size or the composition of surrounding tissues. This comment is not important in the context of the monthly scans taken in this study, however, as such unpredictable alterations would need longer periods before becoming problematic. Additionally, as Kellie (1992) points out, in the more standard applications for which DXA is used radiation exposure should preferably be kept to a minimum; exposures from QCT scans are over 100 times greater than those from DXA. The areal nature of DXA BMD also means that care must be taken when comparing measurements from individual subjects. Carter *et al.* (1992) note that a 20% increase in patient height would result in a 20% increase in both thickness and BMD of any bone, assuming a constant volumetric bone density and proportional increases in bone linear dimensions with height. Again this is not relevant as far as monitoring of healing is concerned, where inter-patient comparisons of absolute values are not especially meaningful.

An attractive investigation into the theoretical validity of DXA measurements was recently presented by Heymsfield *et al.* (1994). The soft tissue model assumption upon which Lunar DXA is founded is that the ratio of fat to fat-free soft tissue attenuation coefficients (Rst) is 1.20 at 40 keV and 1.40 at 70 keV. This assumption was tested by scans of fat (beef-lard mixtures and *in vivo* tissues) and ethanol/sugar/salt/protein solutions. The former gave an Rst of 1.18 at 100% fat in both cases, and the latter showed that measured values were within 2% of theoretical

Rst values. A final calculation from measured elements of Rst for lean soft tissue in men gave a value of 1.399 ± 0.02. These experiments provide useful assurance of the authenticity of the theory behind the Lunar DPX system.

2.4 Osteoporosis Screening

DXA was developed to improve on dual photon absorptiometry as a technique for osteoporosis screening. This is still by far its most widespread clinical use, while other applications remain as yet at the research stage. Osteoporosis is a progressive demineralization of the skeleton which is estimated to affect 1 in 3 women over the age of 50 and 1 in 20 men (National Osteoporosis Society 1993). Most osteoporosis in women is postmenopausal, at which stage bone loss begins at about the rate of 2% of trabecular bone mass per year, regardless of age at onset (Simon *et al.* 1986). Various factors are thought to be involved in its development - these include low activity, calcium-deficient diet, alcoholism and steroid use. The main culprit, though, is the reduction in the level of oestrogen production suffered after a natural menopause, or after an artificial one caused by a hysterectomy. Screening of perimenopausal women has been shown to be cost-effective (Tosteson *et al.* 1990), and once those at risk have been identified there is a range of more or less effective treatments available, such as hormone replacement therapy to counterbalance the natural oestrogen loss (Lindsay *et al.* 1976), increased dietary intake of calcium, and exercise. Without screening, osteoporosis is left to take its course, and the danger of vertebral and hip fractures grows.

Diagnosis of osteoporosis after the menopause is complicated by the fact that an age-matched control population is not available, as all women lose bone to some extent (Overgaard *et al.* 1992). Before this change, the difficulty does not exist, but then premenopausal osteoporosis is not so prevalent. There has so far been limited longitudinal data generated relating directly to DXA's predictive power, although it is

possible to infer from the considerable literature on SPA and DPA as predictors of fracture risk that DXA, with its higher precision and accuracy, is likely to be at least as good (Kellie 1992). At any rate, DXA is well established in this application.

2.5 Monitoring Fracture Healing and Limb-Lengthening

Now that DXA scanners have become more widely available and their advantages over other methodologies, particularly in terms of precision, accuracy and convenience, have been spread to a broader audience, applications beyond osteoporosis screening are being investigated. Research has so far been concentrated in three areas: measurement of bone formation during leg-lengthening, monitoring of BMD changes around orthopaedic implants, and assessment of fracture healing. Further use for DXA has been found in predicting iliac bone graft strength (An *et al.* 1994), with a high correlation existing between BMD as measured by DXA, and load to failure and compressive stress.

With the experience amassed over the last few decades in designing and adapting complex external fixations for specific functions, leg-lengthening operations have progressed towards greater sophistication and reliability. Nevertheless, treatment is not without pain and possible complication, especially if the correction is acute or rapid (Simpson and Kenwright 1993), and the most appropriate approach to distraction has yet to be verified (Figueiredo *et al.* 1993). The need for lengthening is usually due to achondroplasia, an inherited disorder in which the limb bones fail to reach normal size because of defects in bone and cartilage, but a discrepancy may also be acquired. Operative limb lengthening is often partly a cosmetic correction, and so it is important that the distraction can be monitored effectively with respect to angulation, gap size and mineralization. DXA has been demonstrated to be an appropriate monitoring technique because of its good precision, even in small areas with low BMC (Trémollieres *et al.* 1993, Markel and Bogdanske 1994a), and the high

resolution of scan images, allowing adequate assessment of alignment and distraction length (Eyres *et al.* 1993). DXA has also been used to study the effect of transplanting bone marrow cells into the primitive callus in experimentally lengthened rabbit tibiae. Defective callus formation during distraction is a troublesome complication, which means either that further lengthening should be postponed or that some augmentative procedure must be instated. Hamanishi *et al.* (1994) have shown that in such circumstances osteogenesis can be enhanced by transplantation of fresh autologous marrow cells.

In the realm of orthopaedic implants, work has been conducted by Fenner *et al.* (1993), who used a Lunar DPX densitometer to monitor changes in BMD following cemented total hip replacement (THR). Precision error was small (2-4%) compared to the magnitude of BMD changes (10-20%), and the technique is therefore suited to this usage. Valuable reference is made, however, to the fact that for satisfactory precision, easily reproducible positioning of the patient may be crucial - this issue is related to BMD being an areal measure of density (see Section 3.2 for further consideration). A similar study, this time comparing measurements of BMD around uncemented THR's from Lunar and Norland DXA systems, found that whilst correlation between results from the two devices was high, Lunar BMD's were on average 11% greater, and the instruments should not be used interchangeably (Cohen and Rushton 1994). On a different note, Markel *et al.* (1993) studied the effect of press-fit and cemented THR's on the determination of BMD by DXA in a canine model. Press-fitting of the endoprosthesis caused a mean increase in BMD of 11.2%, but with negligible change in precision error (1.1% before implantation; 1.8% afterwards). Cementing, on the other hand, increased the mean precision error to 7.2% - the effect on BMD was variable, with a decrease distal to the implant and an increase elsewhere. The remarkable precision possible with DXA is underlined by Mosheiff *et al.* (1992), who discovered that bone ingrowth into hydroxyapatite implants in rats could be accurately monitored despite the presence of the dense inorganic background.

The use of DXA for monitoring fracture healing is clearly the main concern of this thesis and it is discussed in a variety of contexts elsewhere. It remains here to summarize previous relevant work. Cook and Cunningham (1995) and Cook (1993) discuss a feasibility study using aluminium and hydroxyapatite phantoms to examine the sensitivity of Lunar DPX-L scans to small fracture gaps (transverse and oblique) and to low mineral densities. Gaps in an aluminium phantom could be detected, regardless of orientation, down to a size of 0.05 mm, and low BMC's and BMD's could be measured precisely. Reproducibility of results was good, with a CV of less than 1.5% in all cases. Already discussed is a study by Markel *et al.* (1990), which compared the ability of QCT, SPA, MRI and DXA to quantify bone healing in bilateral tibial osteotomies in dogs. Osteotomies were stabilized at a separation of 2 mm with unilateral external fixation, and the dogs were anaesthetized, imaged and killed at 2-12 weeks after fracture. Associations of the four methodologies with calcium content and with invasively determined torsional and local stiffness properties were determined. In general, DXA and SPA came close behind QCT, with MRI coming a poor fourth. Cook (1993) also reported on the use of DXA for monitoring tibial fractures treated by external fixation, and concluded that it was a promising technique which could be used to follow accurately changes in mineralization at the fracture site, with the potential for identifying abnormal patterns of healing.

CHAPTER 3 - PHANTOM STUDIES

All scans of fractured bones treated by external or internal fixation include some visible metal from the fixation device. For fractures treated externally the amount of obstruction is minimal due to the peripheral nature of this material, and this contributes to the ease of analysis in two ways. Firstly, the fracture and surrounding bone are not obscured, thus making it a simple matter to fit ROI's to the whole width of the fractured tibia along a significant proportion of its length. Secondly, it had not been clear to what extent the presence of highly attenuating metal in a scan might affect the accuracy or repeatability of analyses, and so the absence of significant volumes of such material in scans made this consideration less pressing. However, it would widen the applicability of this method of assessing fracture healing if other forms of fixation involving more obtrusive metalwork could also be scanned and analyzed successfully. Another common form of fracture fixation is the intramedullary nail, but this method of treatment introduces a considerable volume of metal (usually stainless steel) into the area of the scan. Since some clinical evidence existed to suggest that large volumes of metal might well affect the scanning process (Cook 1993), phantom tests were conducted to quantify the effect of metal on scan analysis, before reliable analysis of *in vivo* scans could be undertaken.

3.1 DXA Scans with Metal

There are two ways in which metal might affect scan analysis. The first of these obtains in a situation where metal simply obscures the area of bone near the fracture site. This would be the case where complex external fixation has been applied around a fracture. In these circumstances, if much of a scan is rendered useless because of metal superimposed on large areas of bone, there is nothing that can be done to redeem the situation. The second way in which metal might affect scans would be by somehow interfering with the X-ray absorptiometry process. This effect would

become relevant in situations where the amount of metal was not sufficient to render a scan useless due to obscuration of the bone but where nevertheless there was a considerable volume of metal present, probably in more intimate contact with the bone or soft tissue. In the case of intramedullary nailing, it is only the central portion of the tibia (the area corresponding to the location of the medullary canal) which is obscured by steel, whereas the greater part of the cortex is free from obstruction. As long as the effect of metal on scans could be shown to be predictable or negligible, it should therefore be possible to analyze scans of fractured tibiae treated by intramedullary nailing. The experiments conducted to assess the effect of metal on scans are described in the following sections.

3.1.1 Aluminium on Perspex Scans

As a preliminary test, scans were conducted with aluminium phantoms alone. Aluminium should exhibit very similar radiological behaviour to cortical bone, as the mass attenuation coefficients, μ, are close in magnitude at the two X-ray energies used by the DXA scanner - at 40 keV, μ_{bone} is 0.6400 cm^2g^{-1} and μ_{Al} 0.5630 cm^2g^{-1}, whilst at 70 keV μ_{bone} is 0.2651 cm^2g^{-1} and μ_{Al} 0.2389 cm^2g^{-1} (Hubbell 1982). Firstly, two aluminium blocks of width 25 mm and length 150 mm but of thickness 10 mm and 20 mm respectively were scanned on a 39 mm thick perspex block resting on a plastic base (Figure 3.1). Full reasons for the selection of this arrangement are given by Cook (1993). In brief, it was found after investigation of a range of soft-tissue substitutes, including water, that aluminium on perspex gave a good coefficient of variation (1.1% as against 0.9% for aluminium in water, the best recorded value). In addition, it was found that there was very little

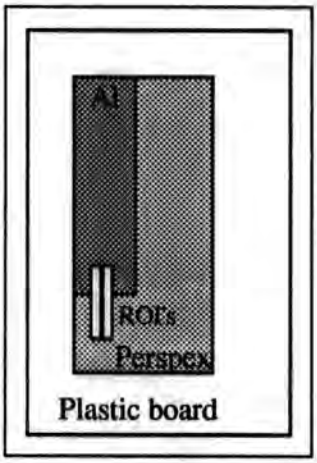

Figure 3.1 Analysis method for first series of phantom tests using aluminium blocks. Not to scale.

difference in the magnitude of results whichever phantom combination was used. Thus the standard phantom settled upon was aluminium on perspex due to the advantages over aluminium in water of simplicity and consistency in size, which balanced the very slight shortfall in coefficient of variation.

To assess the linearity of behaviour when these blocks were analyzed, two adjacent regions of interest each of size 8 by 30 pixels were orientated vertically and moved pixel by pixel onto the phantom. Readings of BMC and BMD were recorded at each step, and as a check for internal consistency in the results, each value of BMC was divided by the area of the region of interest (1.728 cm^2) and the result compared with the respective value of BMD obtained from the computerized analysis (one pixel equals 1.2 mm vertically, 0.6 mm horizontally). This experiment is summarized graphically in Figure 3.2.

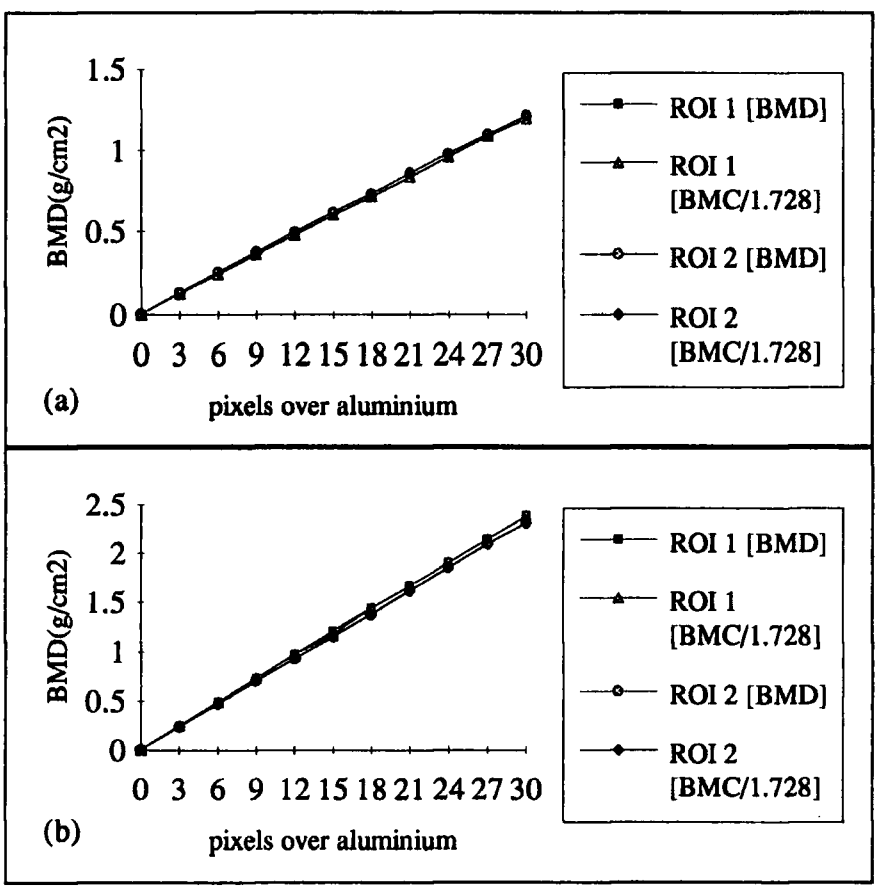

Figure 3.2. Two adjacent ROI's of size 8 by 30 pixels were moved 3 pixels at a time onto an Al block, (a) 10 mm thick and (b) 20 mm thick, which had been scanned by DXA. BMC and BMD were recorded at each increment and are plotted here.

As can be seen from Figure 3.2, the behaviour of the readings of bone mineral content and density was highly predictable. There was a linear variation of BMD with volume of aluminium analyzed, which suggests that aluminium is a satisfactory phantom material for this application. There is also strong agreement between values of BMD and BMC/1.728 in all four cases, so it can be assumed that the Forearm software converts reliably between BMC and BMD. Finally, there are no significant differences evident in the plots for the two adjacently positioned ROI's; the slight differences that are seen can be put down to inhomogeneity of the aluminium and to the pixelation of the computerized analysis. Since the scan image is composed of pixels, it is only possible to place regions of interest in specific locations, and so it is unlikely that an ROI will cover exactly the same region of aluminium in different scans. As a corroborative test of the success of these initial phantom experiments, it should be the case that the following equations hold true at each position of the ROI's:

$$\rho_{TOT} = (\rho_a A_a + \rho_p A_p)/A_{TOT} = (\rho_a P_a + \rho_p P_p)/P_{TOT}$$

where $\rho_{a,p}$ are areal densities of aluminium and perspex

$A_{a,p}$ are percentage areas of the ROI over aluminium and over perspex

$P_{a,p}$ are numbers of (vertical) pixels over aluminium and perspex ($\propto A_{a,p}$)

ρ, A, P_{TOT} are total areal density, ROI area (1.728 cm^2) and vertical pixels (30)

Since the plots are linear, it can be assumed that the equation is satisfied at all positions of the ROI's as long as it is satisfied at one position. This is true, and so the results of these first scans provide a firm basis for more realistic phantom trials.

3.1.1.1 The Effect of the Plastic Board

The plastic board on which the perspex and aluminium phantom rested during the scans of Section 3.1.1 has been used by the radiographers in the Bone Densitometry

Unit at South Cleveland Hospital to improve the quality of the scan image. For phantom tests involving the perspex block, use of this board had two disadvantages. Firstly, the plastic does not provide an absolutely flat surface on which the perspex can rest, and secondly, it is not possible to use the lines on the scan table for positioning the phantom as the plastic is opaque. In these circumstances, a simple comparative test was done to check whether the presence of the plastic board was quantitatively beneficial. Using the aluminium on perspex phantom discussed above, two scans were carried out, one with the plastic board and one without. Values of BMC and BMD were recorded for twenty adjacent ROI's on each phantom and these data were assessed by ANOVA (analysis of variance) using the Minitab™ statistical package. The results showed conclusively that there is no discernible difference between data from scans with and without the plastic board ($p = 0.627$). There is an improvement in coefficient of variation with the plastic board present, perhaps because the combined thickness of plastic and perspex is closer to a realistic soft-tissue thickness than the perspex thickness alone, but this is only moderate (from 1.8% to 1.08%). In subsequent phantom scans the plastic board was therefore abandoned.

3.1.2 Aluminium and Steel on Perspex

The next set of phantom scans and analyses was conducted using three thicknesses of aluminium block (10 and 20 mm as before, and with an extra 30 mm block) with three identically dimensioned steel blocks. Blocks were 25 mm wide by 150 mm long, and all possible combinations of Al and steel were scanned, giving a total of nine arrangements. The Al blocks were also scanned alone to enable control analyses to be carried out. When the scans came to be analyzed it was clear that those including 30 mm thick Al blocks would be of no use, since there is already impairment of the scan image due to high attenuation at this thickness. Consequently, only two series of four scans yielded useful results (10 and 20 mm of Al alone and alongside 10, 20 and 30

mm of steel). The purpose of these tests was to model in a simple fashion the effect of a steel intramedullary nail (steel blocks) next to bone (Al blocks) on the DXA results.

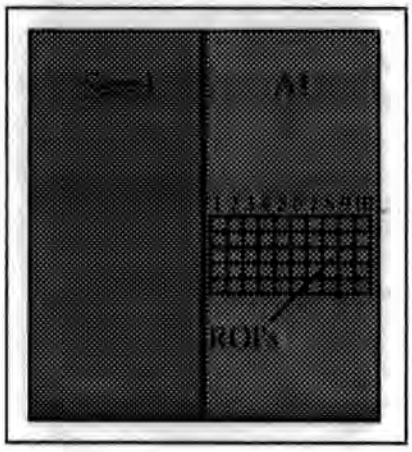

Figure 3.3 Method of analysis of scans of steel and Al blocks. Fifty ROI's, each 2.4 mm by 4.8 mm, in a grid 10 by 5 were analyzed on each of the available scans. Not to scale.

The analysis method adopted for this second series of phantom experiments is sketched in Figure 3.3. For each of the available scans, a block of forty ROI's, ten columns wide by five rows deep, was analyzed on the aluminium phantom in each of the eight cases described above. Each ROI was 2.4 mm vertically by 4.8 mm horizontally (4 by 4 pixels). The top lefthand corner of the grid was positioned one pixel in from the steel and fifty pixels down from the top edge of the aluminium. Comparison between the scans was then possible by consideration of BMC and BMD values. These two measures of bone mineral were compared by looking at both individual ROI's and average values from each of the ten columns. As an initial check on the accuracy of the Forearm software's conversion, an overall ratio of BMC/BMD for all ROI's was calculated and found to be 0.1152 cm^2 (exactly the area of an ROI, as it should be) with coefficient of variation 0.01%. Thus from this point forward it will be necessary to examine the BMD data only. Figure 3.4 summarizes the results of these tests.

The most striking aspect of these graphs is the fall-off at either end of the plots. On the other hand, there seem superficially to be fairly insignificant differences between the four plots within each set. In order to be sure that the presence of steel had not had any statistically significant effect on the results of scanning, and to investigate further the apparent column effect, ANOVA tests were conducted on the two sets of data.

The scheme used was a two factor (steel and column) crossed analysis of variance at the 5% significance level. The factor 'steel' has four levels - 0, 10, 20 and 30 mm; the factor 'column' has ten, for there are ten columns of ROI's. Additionally, the five rows of ten ROI's each are treated as replica measurements - it is this replication which allows the ANOVA model to be crossed, *i.e.* to test for an effect on BMD due to an interaction between the two factors.

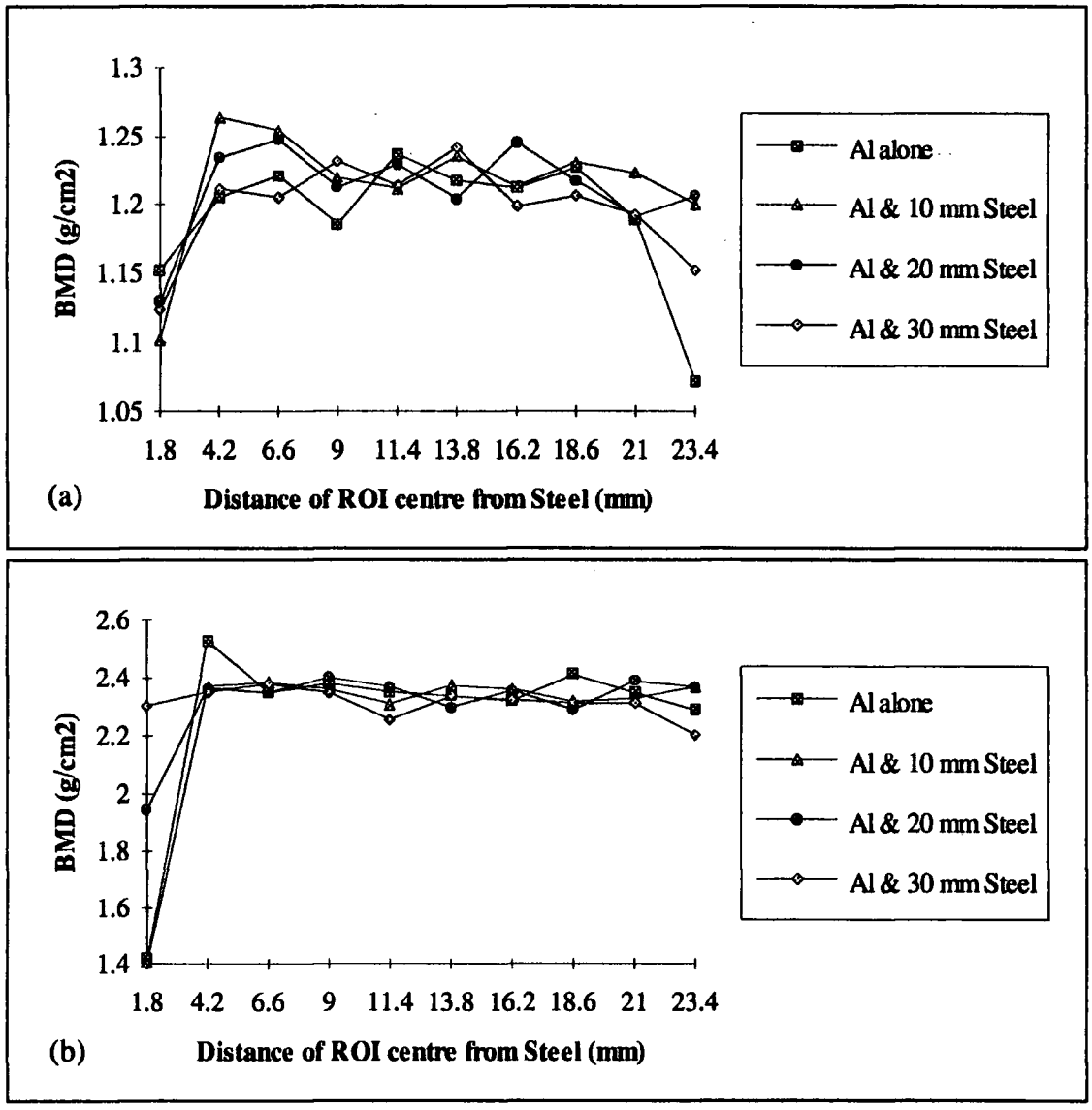

Figure 3.4 A grid of ROI's each 2.4 mm wide by 4.8 mm deep was analyzed on the scan image of an aluminium bar of thickness (a) 10 mm and (b) 20 mm. These graphs show the variation of BMD in the aluminium with thickness of and distance from a parallel steel bar.

P-values from this analysis are summarized in Table 3.1. The column headed 'Column*Steel' refers to the interaction effect. The cells that need careful consideration are those with a p-value below 0.05 (the significance threshold), so a steel effect can be discounted for both Al thicknesses, but there is definitely some effect due to position.

Al (mm)	Columns	Column	Steel	Column*Steel
10	1-10	0.002	0.640	0.391
	2-9	0.800	0.872	0.697
20	1-10	0.000	0.111	0.000
	2-9	0.164	0.136	0.537

Table 3.1 Results from ANOVA's of BMD data from DXA scans of steel and aluminium bars in parallel. Numbers in the body of the table are p-values to 3 significant figures.

One feature of the Lunar Forearm software allows the user to inspect BMD cross-sectional profiles. By doing this for each of the scans being discussed, it becomes obvious that step changes in density are not picked up exactly by the software - instead, a finite distance of around 1 mm is required before a new plateau value is reached. This confirms what Figure 3.4 had already suggested, and so a further pair of ANOVA tests was conducted with columns 1 and 10 omitted from the calculations, which gives 2 mm or so clearance from the step change in density on either side of the Al bar. As Table 3.1 shows, removing the outermost columns also removes any suspicion of a column effect and of any interaction effect (this was artefactual and caused by the constraint of pixelation mentioned above).

3.1.3 Concentric Aluminium and Steel - Square Cross-Section

The simplest symmetrical geometry to model the case of an intramedullary nail within a tibia is a block of aluminium, square in cross-section, with a square steel rod running down the centre. This phantom was made up, with an aluminium cross-section of 24 mm by 24 mm and an 8 mm square steel rod in its centre, and then scanned on a perspex base with and without the steel in place. Three scans of each configuration were analyzed and the results compared, again using the Minitab™ statistical package. The analysis method, shown in Figure 3.5 and similar to that used before, involved a grid of ROI's five wide by five deep, with each ROI 1.2 by 2.4 mm (2 by 2 pixels). The upper lefthand corner of the grid was positioned 12 pixels in from the righthand edge of the aluminium and 40 pixels down from the top for all six scans. A smaller ROI size than before was required so that a reasonable number of ROI's could be fitted in across the width of the aluminium.

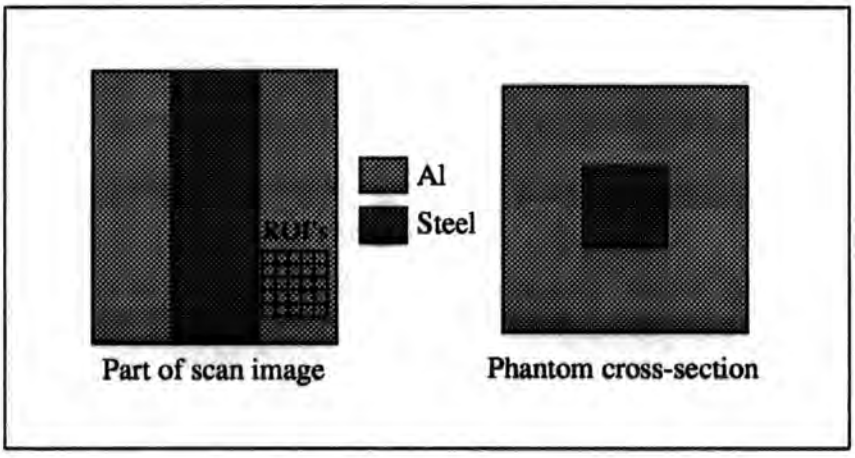

Figure 3.5 Analysis method for the third series of phantom tests. Not to scale.

Plots of the variation in volumetric BMD (for straightforward comparison with Figure 3.9 below) with ROI position and presence or absence of steel - the latter case including an air space instead - again show a fall-off at the edges of the aluminium (Figure 3.6). On this occasion the effect is noticeable only at the lefthand end of the curves, the rightmost ROI being inset by more than 1 mm. Table 3.2 displays the

results of a two-way crossed analysis of variance conducted on the data summarized in Figure 3.6. As for the flat geometry discussed in Section 3.1.2, removing the lefthand column from the analysis eliminates the column effect. Since this is a very similar geometry to that discussed in the previous section, it would be expected that the presence of steel would not have any effect on values of BMD, and this is the case as Table 3.2 shows.

Columns	Column	Steel	Column*Steel
1-5	0.008	0.311	0.616
2-5	0.229	0.276	0.480

Table 3.2 ANOVA results from analysis of BMD data from the third series of phantom scans. P-values are quoted to 3 significant figures.

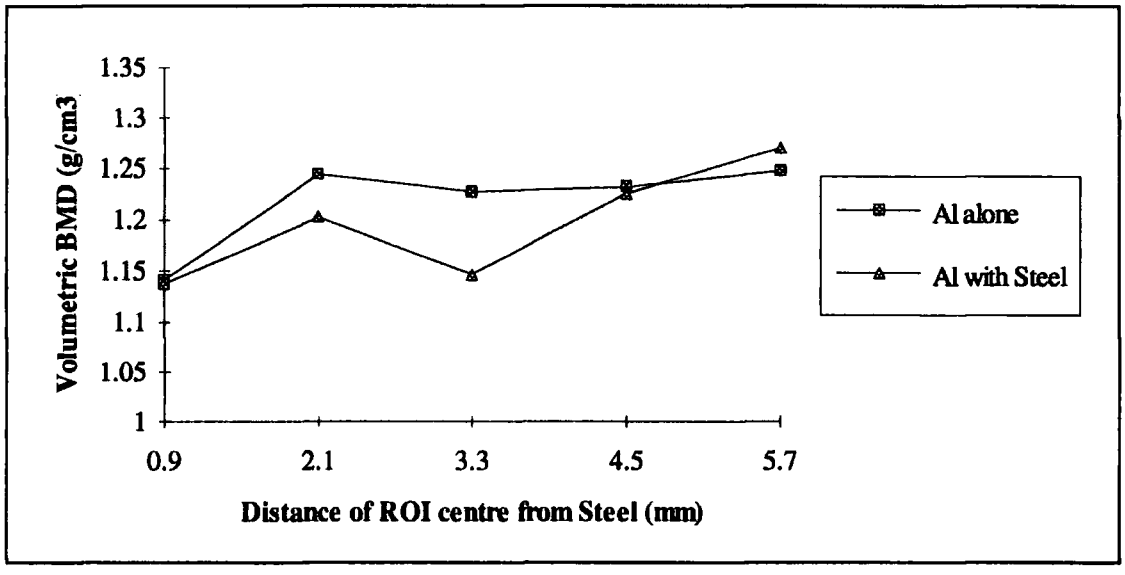

Figure 3.6 Graph showing the variation of volumetric BMD across a square aluminium phantom with and without a square steel rod in its centre.

3.1.4 Concentric Aluminium and Steel - Circular Cross-Section

The final series of aluminium and steel analyses used scans of a geometry which makes a further improvement on the square geometry of Section 3.1.3 in terms of realism, namely an aluminium tube with a solid steel rod running through it. The tube represents the tibia with its medullary canal, and the steel rod acts as a simple model of an intramedullary nail. A diagram of this arrangement, showing the steel rod in place, is given below (Figure 3.7). Scans of the configurations with and without steel were analyzed in a similar manner to those already discussed, except that due to the circular cross-section BMC and BMD values from ROI's at different distances from the steel rod were not directly comparable. For this reason, beyond the straightforward computerized analysis procedure, both BMC and BMD were converted into volumetric densities to allow for a more straightforward comparison.

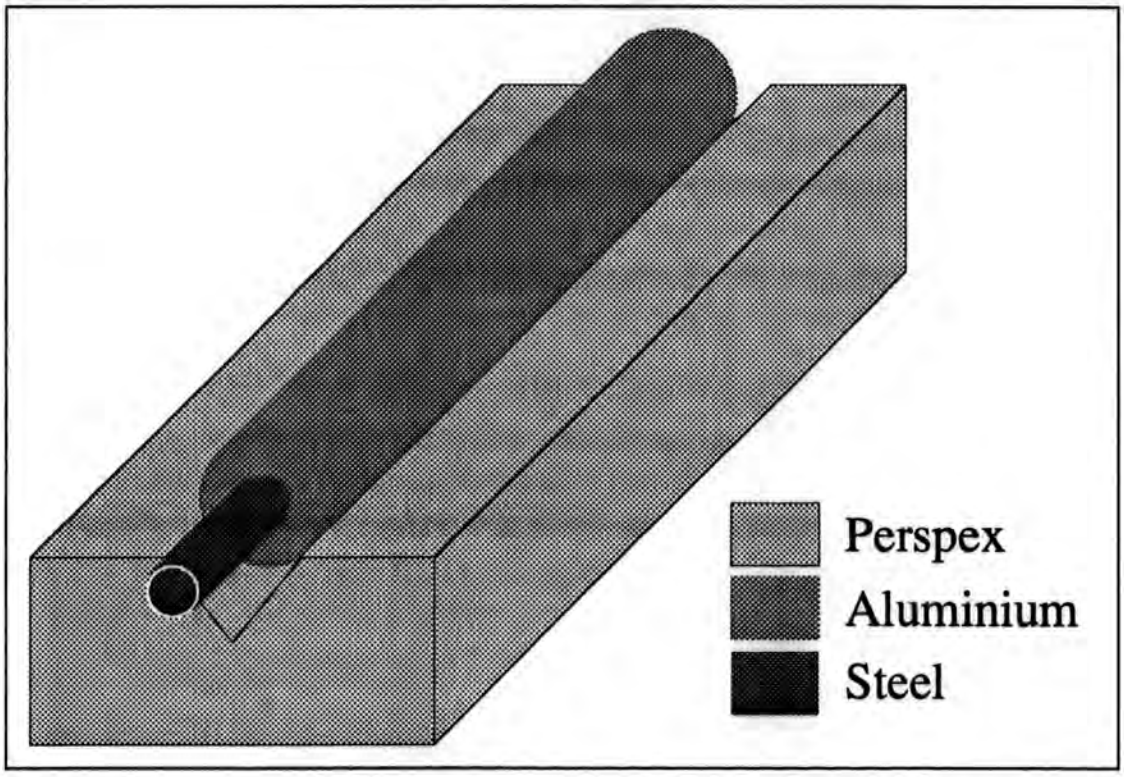

Figure 3.7 The fourth series of phantom tests used a more realistic geometry. An Al tube on a perspex base was scanned with and without a close-fitting steel rod inside Not to scale.

Six scans of the aluminium tube were performed, three with and three without the steel rod in position, and the resulting images analyzed. For each scan image, a grid of 25 ROI's was analyzed in the same way as was used for the scans of a square cross-section discussed above. ROI 1 was positioned 12 pixels in from the phantom's right edge and 40 pixels down from the top. Figure 3.8 outlines this technique (cf. Figure 3.5), and the BMD data obtained are given graphically in Figure 3.9.

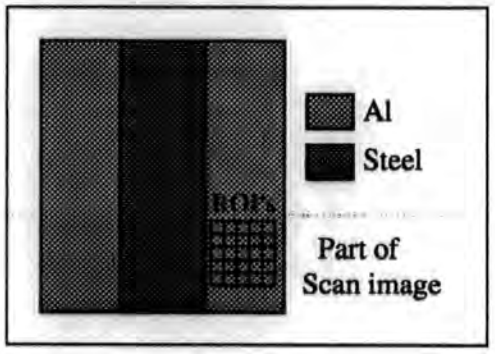

Figure 3.8 Analysis method adopted for the fourth series of phantom scans. A 5 by 5 grid of ROI's, each 1.2 by 2.4 mm, was analyzed and the results compared for scans with and without steel. Not to scale.

ANOVA was used once again to assess the effect of steel and/or columnar position on BMD results (Table 3.3). The plots in Figure 3.9 have the familiar form, although the dips are not equally visible on both curves, as the scan image pixelation has meant that

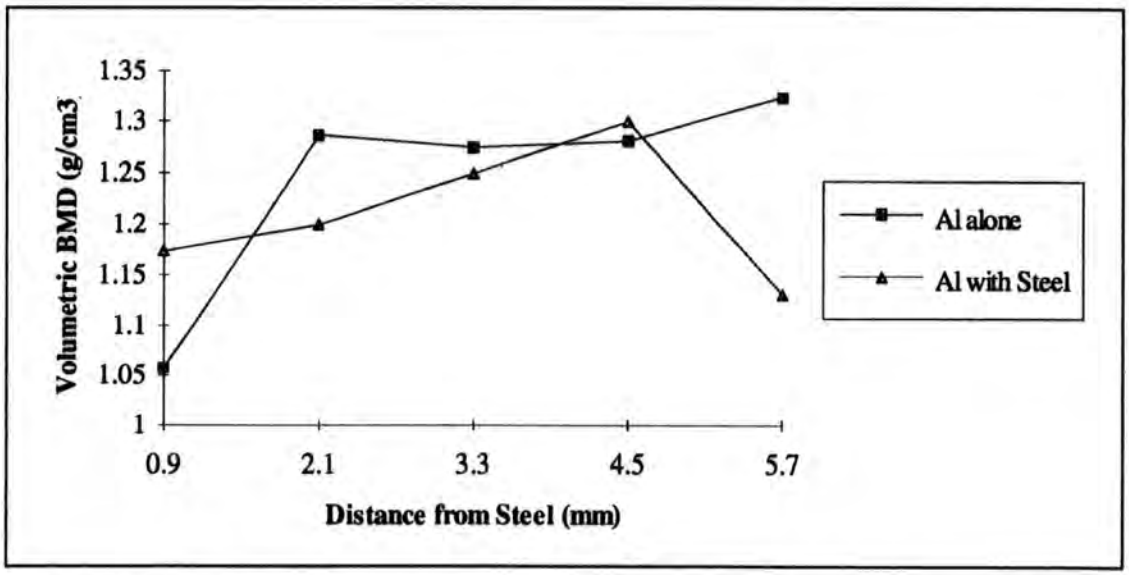

Figure 3.9 Graph showing the effect of the presence of a steel rod on values of BMD in a cylindrical aluminium phantom (cf. Figure 3.6).

the curves with and without steel do not tie up precisely. This has in turn meant that there is a significant column/steel interaction effect, but this disappears when the central portion only of the aluminium is examined. As above, removing the outermost columns removes any hint of a columnar or interaction effect from the analysis results. Since the width of aluminium either side of the steel in this phantom was 7.5 mm and not 8 mm as for the square cross-section, it was necessary to exclude both columns 1 and 5 from the second ANOVA model to give sufficient clearance at the outer edge. For this phantom model too, there was no statistical evidence of a steel effect at all.

Columns	Column	Steel	Column*Steel
1-5	0.000	0.111	0.000
2-4	0.382	0.267	0.302

Table 3.3 ANOVA results from BMD data from scans of the fourth Al phantom, with and without steel. P-values are to 3 significant figures.

3.3 Summary

The phantom tests described above demonstrated, first, that aluminium is a satisfactory radiological model of bone, on whose properties the Lunar DPX-L scanner bases it calculations of BMD. Having established this, further tests using three geometries of aluminium and steel on a perspex base were performed. The first geometry, consisting of aluminium and steel bars of varying thickness scanned side by side, suggested that the presence of steel had no effect on analysis reliability. On the other hand, the scanner appeared to be very sensitive to the changes in density at both edges of the aluminium bars. These findings were reinforced by analyses of scans of the other two phantoms, with square and round cross-sections respectively. The clinical significance of these results will be discussed in Section 4.4.2.1.

CHAPTER 4 - CLINICAL RESULTS

Patients were scanned using the Lunar DPX-L system in the Department of Rheumatology at South Cleveland Hospital, Middlesbrough. Within the time period of this study, 15 patients have been under monthly observation, of whom five were lost to follow-up having had three or fewer scans. In addition, five discharged patients have been recalled for scans up to two years after fracture.

The only requirement for inclusion in the study was that a patient should have a tibial shaft fracture treated by internal or external fixation. Cast bracing was not a suitable method of fixation as removal of the cast would have been necessary before scanning. Of the 10 patients who have been examined at monthly intervals with four or more scans, two were treated by intramedullary nailing (IMN) and nine by external skeletal fixation (ESF). The five recalled patients had all had their fixations removed by the time of the recall scan - two of their fractures had been stabilized by intramedullary nailing and three by external fixation.

4.1 Patients

Of the 10 patients who attended for scans on four or more occasions, seven were male and three female; of those recalled, two were male and three female. Two of the recalled patients (Patients 11 and 12) also had their original series of scans during the time of the study. The average age at first scan was 38.0 years, with a range between 19 and 71. The average time from fracture to the first DXA scan session was 13.6 days (Patients 10 to 19), the earliest scan being four days after fracture and the latest twenty-two. Full details of all patients, including those recalled, are given in Table 4.1. Patients 2, 8 and 10 are identical with Patients 2, 8 and 10 in Cook (1993); new patients are numbered from 11 onwards.

Patient	Sex	Age[1]	Fracture Type	Leg	Position	Fibula[2]	Fixation	Delay[3]	Recalled	Scans[4]
2	F	63	spiral	L	mid-shaft	✗	IMN	10	✓	5
8	M	25	spiral	L	mid-shaft	✗	IMN	25	✓	5
10	M	22	oblique	R	mid-shaft	✗	ESF	15	✓	6
11	F	34	spiral	L	distal third	✗	ESF	14	✓	6
12	F	38	oblique	L	mid-shaft	✓	ESF	15	✓	6
13	M	70	spiral	R	mid-shaft	✓	ESF	8	✗	5
14	M	38	spiral	R	distal third	✗	ESF	7	✗	5
15	M	29	spiral	R	distal third	✗	ESF	6	✗	5
16	M	19	transverse	L	distal third	✗	ESF	17	✗	5
17	F	33	spiral	L	distal third	✓	ESF	12	✗	6
18	M	47	spiral	L	distal third	✓	ESF	6	✗	4
19	M	49	oblique	R	mid-shaft	✗	IMN	22	✗	†3

Table 4.1 Summary table of the twelve patients scanned during this study (excluding those lost to follow-up). †Ongoing. [1]Complete years at time of fracture. [2]✓ indicates the presence and ✗ the absence of a fibular fracture. [3]Number of days from fracture to first scan. [4]Includes recall scan where applicable.

4.2 Scans

After the first scan session, each patient was scanned at approximately monthly intervals. All scans were conducted using the Lunar DPX-L system and the Lunar Forearm software. As the name implies, this software was designed specifically for measuring forearm BMD, but it also works well when used for lower leg scans. Cook (1993) compared the clinical use of two Lunar software packages for this application and found that the Forearm package gave acceptable results whilst the Orthopaedic software tended to produce conflicting information on consecutive occasions. The Orthopaedic software is designed to take account of hip-joint replacements and the associated anatomical geometry, and so it was not altogether surprising that its behaviour in the present application was at best unreliable.

Before each scan, the patient was positioned supine on the scan table with the leg secured in a brace at the foot. The source and detector move from left to right in the

coronal plane, and from the proximal to the distal end of the tibia. Each left-right movement of the scanning arm across the leg translates into one horizontal pixel in the scan image, and in this way a two-dimensional view of the tibia is built up. The 'Fast' scan setting (which gives a pixel size of 0.6 mm by 0.6 mm) was used for all scans. Whenever a fractured leg was scanned, the unfractured contralateral tibia was also scanned immediately afterwards. The series of contralateral scans for each patient gave a stable control BMD level with which the fracture scans could be compared. In a few cases, however, problems were encountered when comparing contralateral scans - this difficulty was eventually resolved, and details are given in Appendix 2.

4.2.1 Long-term Repeatability

In order to assess the long-term repeatability of BMD measurements performed using the Lunar DPX-L scanner and Forearm software, monthly scans were taken of an aluminium block on a perspex base. Aluminium models the radiological behaviour of bone very closely and so it was preferable to use this invariant phantom material rather than relying entirely on the results obtained from scans of healthy contralateral tibiae. The block was 250 mm long by 25 mm wide by 10 mm thick and was aligned parallel to the edges of the perspex base. On each occasion, BMD was analyzed by placing twenty identical adjacent ROI's along the length of the phantom, starting two pixels from the top edge, at a magnification of 80. Each ROI was 18.0 mm wide by 4.8 mm deep. The results of the eight scans are summarized in Table 4.2 and analysis of variance (ANOVA) shows that there was negligible change over time ($p = 0.311$).

Date	09-Apr	21-May	18-Jun	23-Jul	17-Sep	08-Oct	09-Nov	30-Nov
BMD(gcm^{-2})	1.227	1.218	1.221	1.226	1.218	1.224	1.214	1.221
cv(%)	1.210	1.471	1.667	1.382	1.382	1.841	1.249	1.546

Table 4.2 Scans of a 10 mm thick aluminium block were conducted at approximately monthly intervals. A mean BMD from twenty ROI's, positioned in the same way for each scan, shows minimal variation both between ROI's and from scan to scan.

4.3 Analysis

The Forearm software has two analysis modes, automatic and manual. The automatic mode is useful only for scans of the forearm, as it involves the automated definition of a number of specific regions of interest which are analyzed and the BMD values compared with a reference population. The scans in this study were analyzed in manual mode, which allows the user to select up to twenty regions of interest for simultaneous analysis. A schematic diagram of the analysis method is given in Appendix 3. Two exclusion ROI's were used in all cases to eliminate the associated soft tissue and fibula from analysis. The remaining eighteen ROI's were positioned adjacent to each other along the length of the tibia, each of length 4.8 mm and the same width as the tibia. When the available scanned length exceeded the length of the 18 ROI's, the required number of ROI's was moved into the remaining space and a second analysis conducted. This analysis procedure has been established as providing the best compromise between speed of analysis and reproducibility of results (Cook 1993).

Internally fixated fractures had previously been analyzed using three exclusion ROI's, the third over the intramedullary nail, but it was found by observation and comparison that the results were indistinguishable with and without the nail excluded. This is explained because the software automatically excludes from the analysis highly attenuating areas. It should be stressed that this observation is independent of the significance of the investigations described in Chapter 3. These demonstrated that highly attenuating metal has no effect on the scanning phase, whereas this comment relates solely to the analysis of the results.

4.4 External Fixation

Nine of the new patients scanned since September 1993 were treated by external fixation. Most of these scans were analyzed without any problems - a particular advantage of external fixation in this respect is that the bulk of the metalwork is kept out of the area of the scan. In one case alone (Patient 12) a complicated fixator did obtrude into a scan and unfortunately the only course of action open was to abandon the analysis. A further benefit encountered with external fixators was that the pins could be used as accurate datum points for each analysis. Apart from Patient 12, who was treated with a unilateral Hoffmann frame, all other patients had their fractures stabilized by a unilateral Orthofix device.

4.4.1 Patients

Patient 10: This patient had his first scan on 21st June 1993, fifteen days after suffering an oblique mid-shaft fracture of the right tibia. He had five pairs of scans initially, the last being about 24 weeks after fracture, and was additionally recalled for a scan a year or so after fracture. The complete set of six tibial BMD profiles is given in Figure 4.1. For comparison with these scans, a seventh profile is included of the unfractured contralateral tibia. This is an average calculated from six scans taken on the same occasions as those of the fractured tibia. As a demonstration of the relative lack of variability in the BMD of the contralateral bone, a separate graph (Figure 4.2) shows all of these profiles. In these and all following graphs, the proximal direction is to the left and the distal to the right.

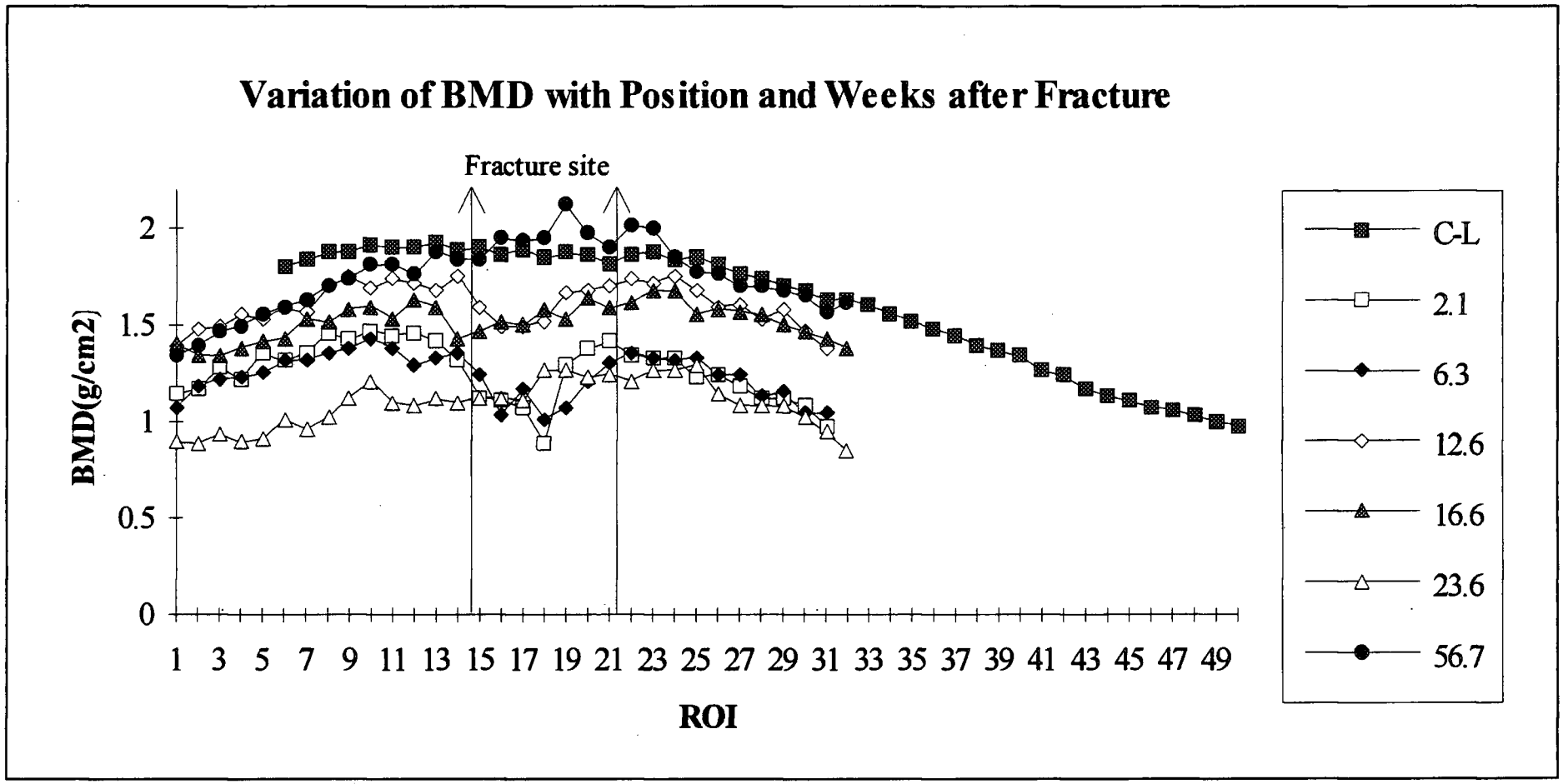

Figure 4.1 BMD profiles for Patient 10 with an oblique mid-shaft fracture of the right tibia. Fracture date was 06-Jun-93.

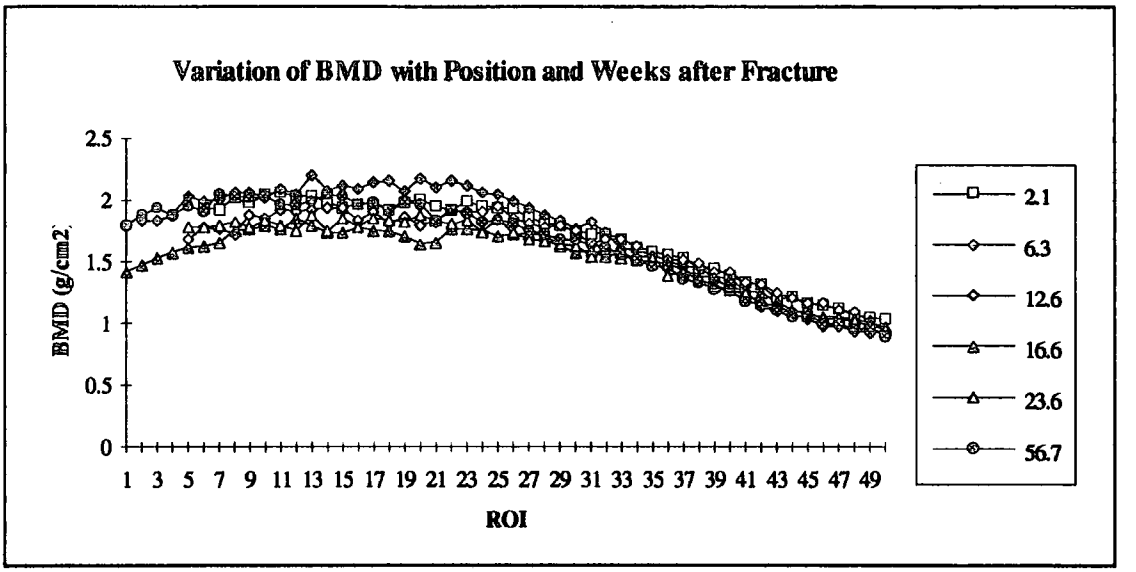

Figure 4.2 BMD profiles for the unfractured contralateral tibia of Patient 10.

At fifteen days post-fracture, the BMD level for the whole of the fractured tibia is considerably lower than that for the contralateral, and there is a pronounced dip in the plot at the fracture site due to necrosis and resorption, or maybe simply to the presence of a gap, as noted by Cook and Cunningham (1995). There is little change evident on the date of the second scan, but by 12½ weeks post-fracture there has been a fairly uniform increase in BMD throughout the length of the tibia. Again, in the next month, there is no marked change, except for a slight increase in the proximal portion of the tibia.

When it comes to the fifth scan, five months after fracture, an unforeseen fall in BMD has occurred. There are two effects at work here: firstly, the dense callus has begun to be resorbed in the remodelling phase of the healing process, and secondly, there will be an element of disuse osteoporosis, probably affecting the whole leg. By scan 6, thirteen months after fracture, there is no longer conclusive evidence of a fracture and overall both tibiae have very similar BMD profiles.

Patient 11: Patient 11 suffered a spiral fracture of the distal third of the left tibia on 2nd November 1993, and this was fixed with an Orthofix frame. The first scans were taken a fortnight after fracture, and were followed by five further pairs, the last being eight months after fracture. The spiral nature of the fracture means that both the scan image and the BMD profiles (in Figure 4.3) give ambiguous information - the fracture is not restricted to one plane and so is not visible as a clean gap or dip. Moreover, the fracture was near to the distal end of the diaphysis and so Figure 4.3 shows only that part proximal to the break.

Scan 1 is mostly at a lower level than the contralateral mean profile, although they seem to be convergent at some distance from the fracture. Were it not more obvious from the scan image where the break was, it would be very difficult to judge this from the profile alone. The decrease in the next month is marginal, particularly in the fracture zone, but there is then a sharp fall, more pronounced in the distal portion than elsewhere, followed in scan 4 by a recovery along the scanned section. By the time of scan 5, 19 weeks post-fracture, the level has dropped once more; qualitatively this is similar behaviour to that observed in Patient 10, and can be explained in a comparable way.

On recall, eight months after fracture, the BMD level in the fractured area approximates to that existing in the contralateral tibia although the profile is less uniform, probably indicating that remodelling is not complete. Away from the fracture there is plainly some disuse osteoporosis, suggesting that there has been reluctance on the part of the patient to weight-bear.

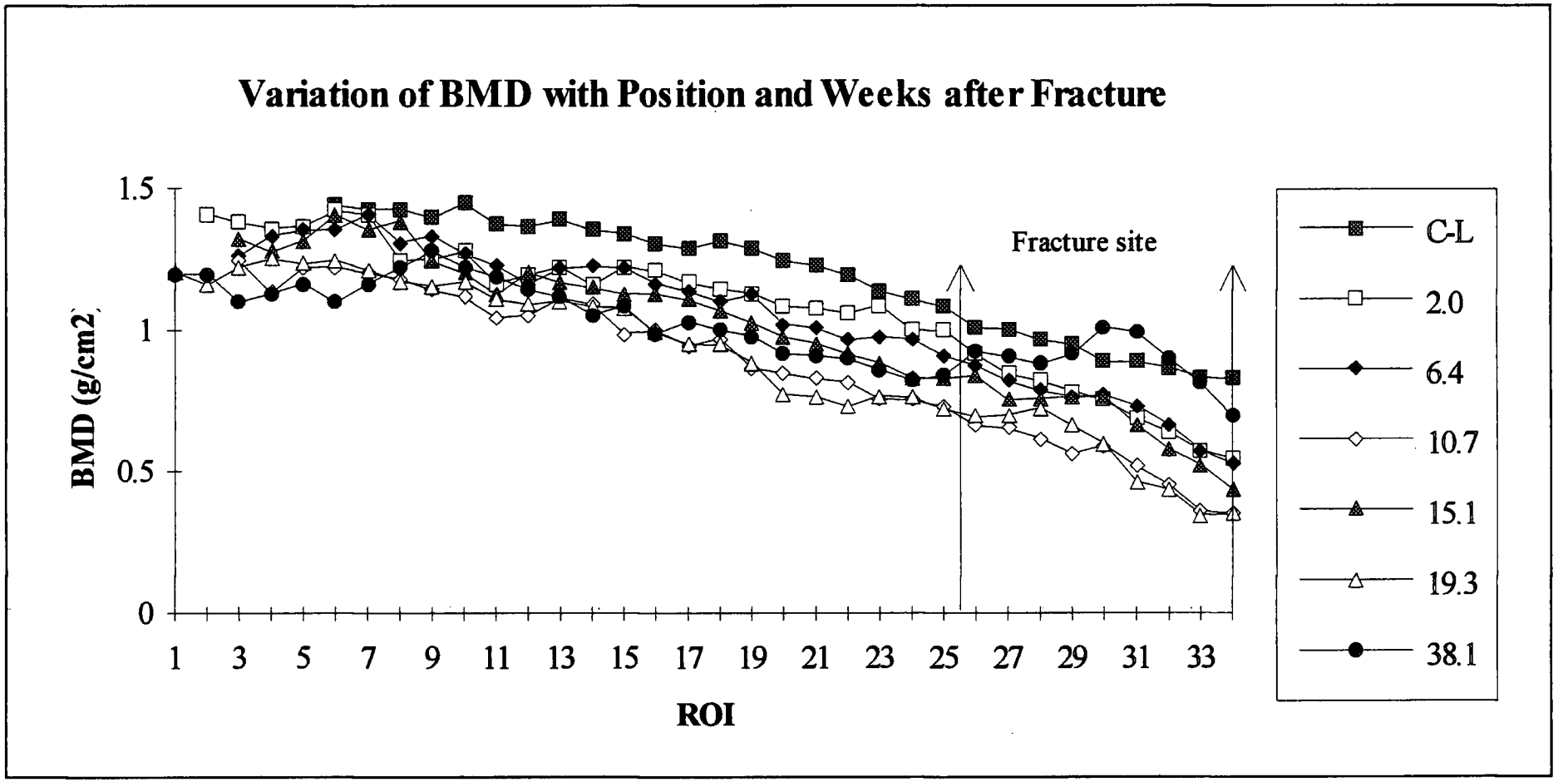

Figure 4.3 BMD profiles for Patient 11 with a spiral fracture of the distal third of the left tibia. Fracture date was 02-Nov-93.

Patient 12: This patient was alone amongst those treated by external fixation in having a Hoffmann fixator applied to her fracture. She sustained an oblique mid-shaft fracture of the left tibia, with an accompanying segmental fracture of the fibula. The first scan of this patient, on 17th November 1993, was unfortunately of no use as the fixator frame obscured most of the tibia. The first analyzable scan therefore was at 44 days post-fracture. Profiles for both the fractured and contralateral tibiae are given below in Figures 4.4 and 4.5 respectively. Again because of the more complicated fixation, not so much of the fractured tibia was available for analysis in this case. This is clear from Figure 4.4. Patient 12 is notable compared with most of the others scanned for the very limited change in BMD over the 4½ months covered by the first four (usable) scans. That is not to say that a healing trend is not apparent, as this patient in fact presents one of the most straightforward progressions of all.

At 44 days after injury, the BMD level in the fractured tibia is at a very low level compared to the contralateral bone, and there is a well-defined dip indicating the presence of the fracture. After another month the level has fallen slightly more, and then in the two remaining months there is a slow but perceptible rise over the scanned length of the tibia. The BMD away from the fracture (to the left in Figure 4.4) has returned to about the same level as in the first scan and the fracture itself is much less obvious. By the time of the last scan, 11 months after injury, outside the fracture zone the tibia has recovered a similar level of BMD to that in the contralateral, and in the region of the fracture the mineralization is significantly greater than in the unfractured bone. This bulge in the profile is most probably due to incomplete remodelling of the tibia - in time, the bone will regain its original shape, and the BMD profile in the fracture zone will fall to the level of the contralateral.

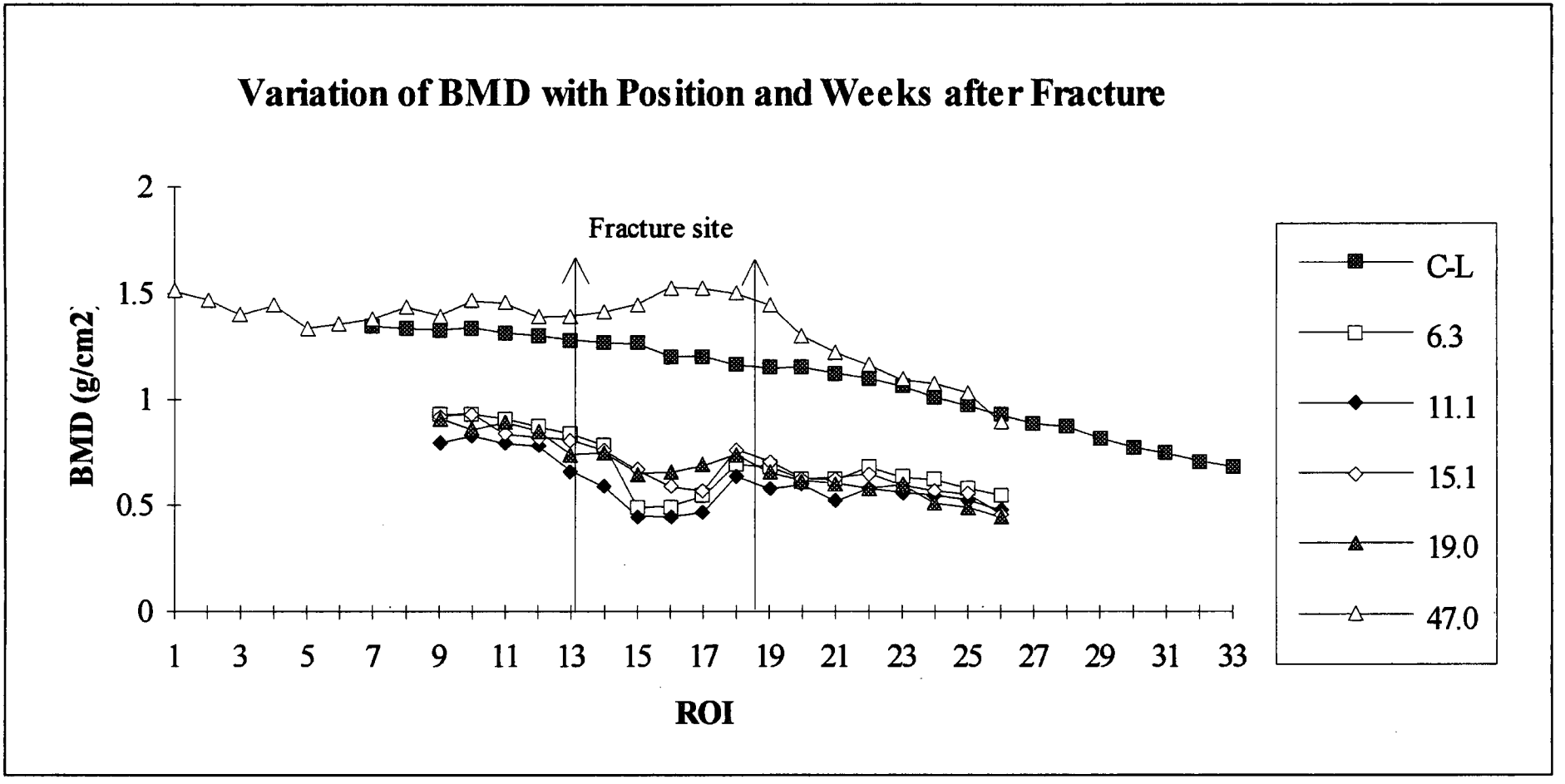

Figure 4.4 BMD profiles for Patient 12 with an oblique mid-shaft fracture of the right tibia and a segmental fibular fracture. Fracture date was 02-Nov-93.

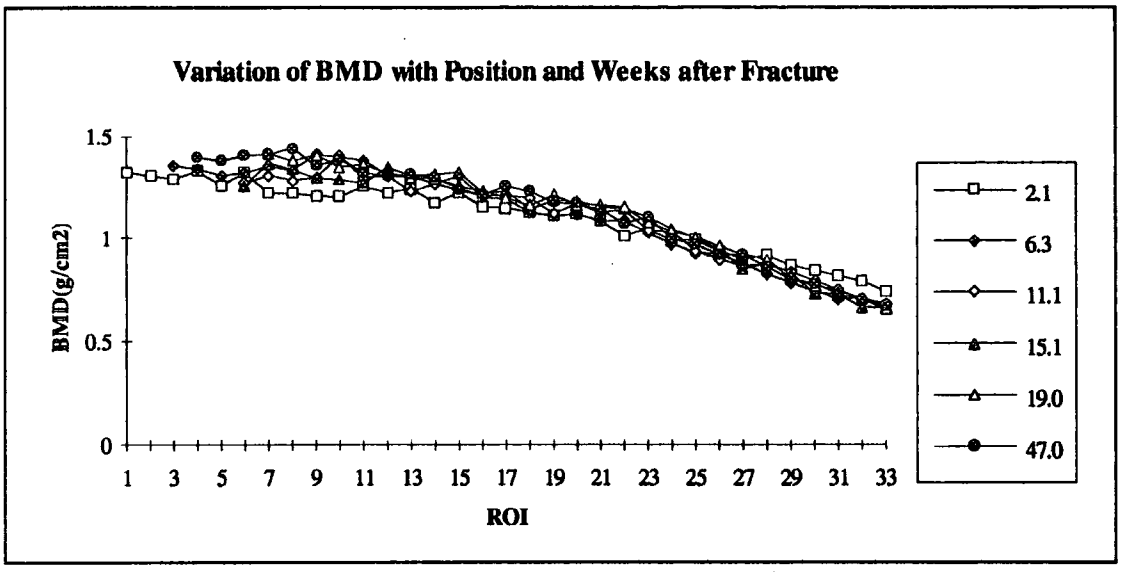

Figure 4.5 BMD profiles for the unfractured contralateral tibia of Patient 12.

Patient 13: This patient had a spiral mid-shaft fracture of the right tibia with a detached wedge, and a simple fibular fracture. The break was fixed with an Orthofix frame and scanned first eight days post-trauma on 24th January 1994. The profiles in Figure 4.6 show a clear healing trend at the fracture site, the location of which is obvious in every scan. Up to scan 3, at 11.3 weeks post-fracture, there is a steady decrease in BMD from the region of the fracture down; proximal to this zone there is little ordered change after the initial drop visible immediately in January.

By the fourth scan, the BMD in the fracture gap itself has begun to rise, although distal to it there is a continuing decrease in mineralization, the effect of which remains apparent in the last scan. There is still a pronounced fracture site by the fifth scan, however there has now been a reversion to the BMD level of the contralateral in the proximal third of the tibia.

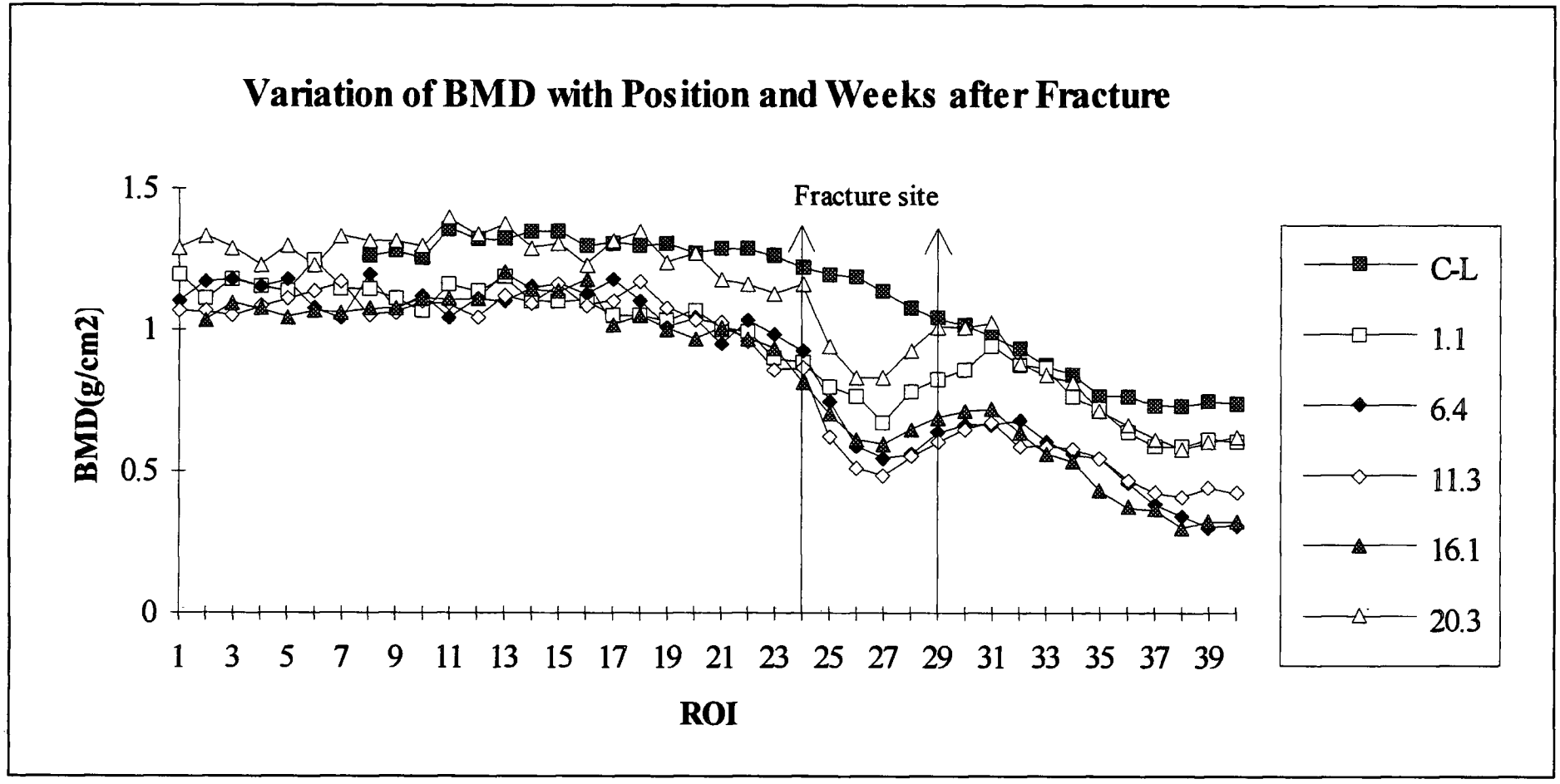

Figure 4.6 BMD profiles for Patient 13 with a spiral wedge fracture of the mid-shaft of the right tibia and a simple fibular fracture. Fracture date was 16-Jan-94.

Patient 14: As with Patient 11, this was another spiral fracture, of the distal third of the right tibia, and so there is no deep fracture trough in Figure 4.7. The first pair of scans was taken on 2nd March 1994, a week after the break - unusually, outside the fracture zone there has not yet been a noticeable fall in BMD when compared with the contralateral profile. In the next month, however, there is a dramatic fall in density along the whole scanned length and this low range is maintained in the third scan. At Scan 4 a recovery in BMD has started, but by 20 weeks post-fracture the now familiar remodelling behaviour can be seen. In this patient the area proximal to the fracture returns to the level of scans 2 and 3 whereas the fracture zone itself drops less far.

Patient 15: Patient 15 had a spiral wedge fracture of the lower third of his right tibia on 2nd March 1994. Fixation was with an Orthofix frame, and the first scans were taken six days after injury. The fracture as a whole and the wedge in particular were long, and the profiles in Figure 4.8 are consequently composed mostly of the fracture site. The oblique break in the shaft extends from ROI 17 to ROI 22; the wedge, which was on the medial side of the tibia, from arrow to arrow.

At the first scan, only six days after fracture, there had already been a considerable fall in the BMD of the fractured tibia, and a further loss of mineralization had occurred by scan 2 at five weeks after fracture. In the next four months there was then no significant recovery along most of the scanned length, the proximal quarter of the fracture being an exception. This lack of change suggested that healing might not be progressing normally, but unfortunately it was not possible to contact this patient for further investigation.

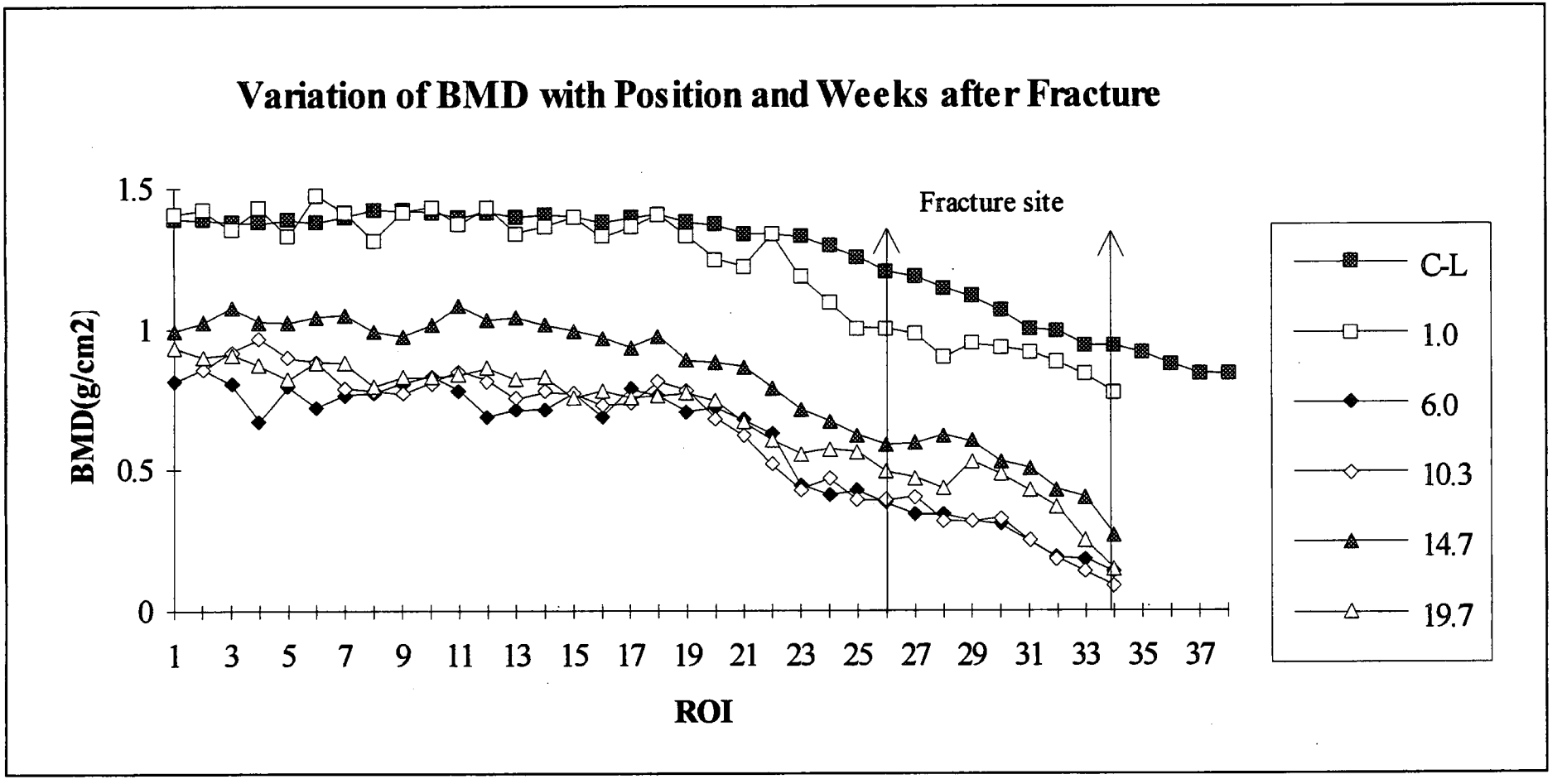

Figure 4.7 BMD profiles for Patient 14 with a spiral fracture of the distal third of the right tibia. Fracture date was 23-Feb-94.

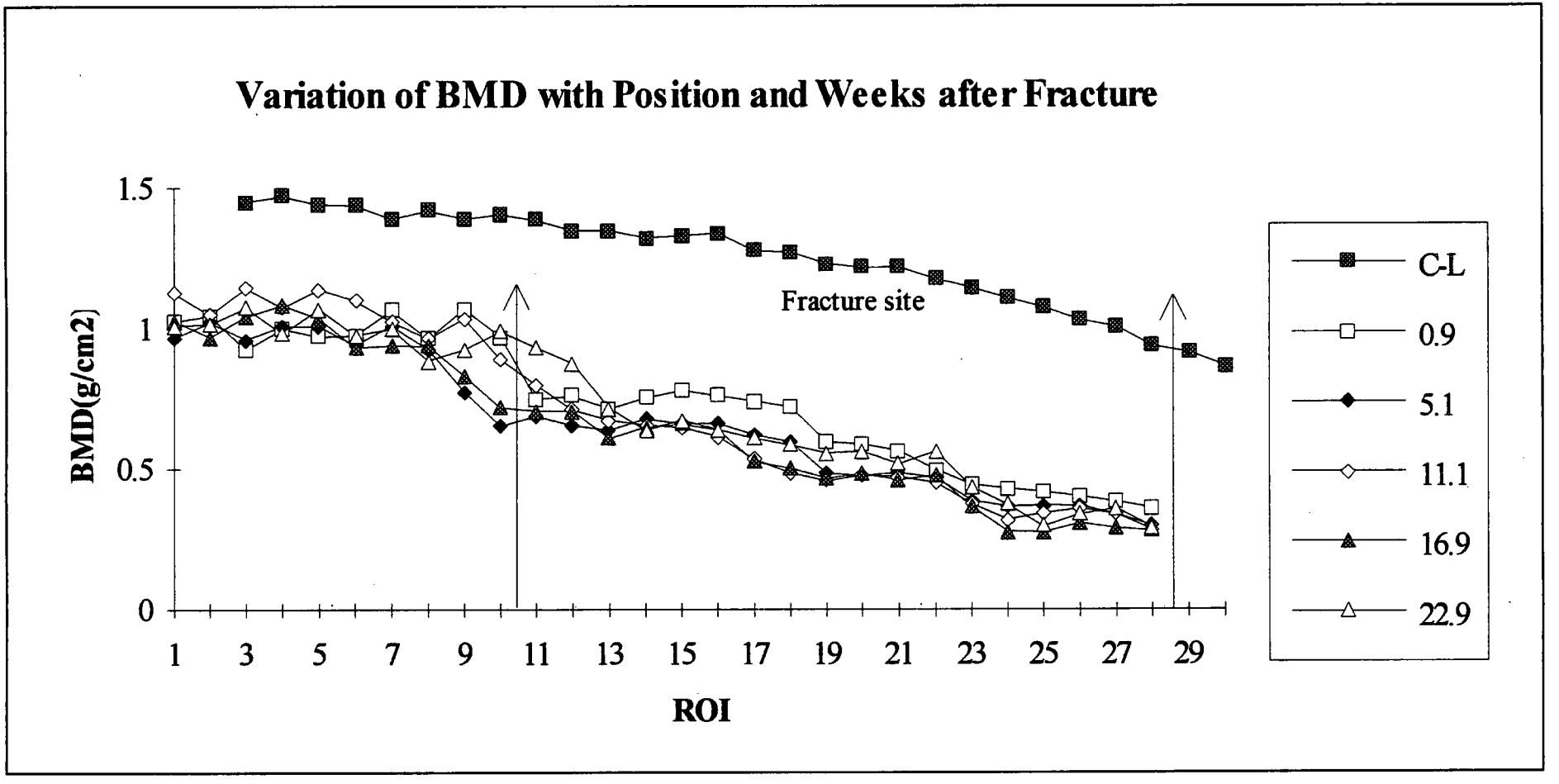

Figure 4.8 BMD profiles for Patient 15 with a spiral wedge fracture of the distal third of the right tibia. Fracture date was 02-Mar-94.

Patient 16: Patient 16's transverse wedge fracture of the distal third of the tibia was sustained on 20th March 1994, and fixed by the usual Orthofix frame. Scans were taken first seventeen days afterwards, by which time a large difference existed in BMD between the fractured and contralateral legs. The fracture gap was not wide and so the depression visible in Figure 4.9 is not deep. Little development had taken place by the second scan, but by the scan at 12½ weeks post-fracture there had been another, smaller fall in BMD along the whole scanned portion. The fourth scan sees an increase in the area of the fracture, and by scan 5 there is little question that the fracture itself has almost healed, although above the break there is still post-traumatic/disuse osteoporosis evident.

Patient 17: Patient 17 had a spiral wedge fracture of the distal third of her left tibia, as well as a fibular fracture. Fixation was again by an Orthofix frame. This patient's healing was singular in that there was very little change in BMD over the whole seven months of scanning. This was also the only patient diagnosed with delayed healing, and these two facts may be related. The first scan (see Figure 4.10) is especially unusual because the profile produced is at the same level as the contralateral, even though the scan is from twelve days after the break. This is very different to all of the patients discussed previously.

At the second scan there has been no significant change in BMD, but then at scan 3, 11½ weeks after fracture, the only noticeable drop takes place. Still there has been very little movement in BMD either side of the fracture, however the fall in the distal half of the fracture gap is rather dramatic, suggesting that considerable resorption is occurring. The break has a complex geometry, with an unattached medial wedge and a large gap distally, so healing has perhaps not been progressing well. By scan 5 there is a hint of osteoporosis proximal to the fracture, but the BMD profile in the gap is now level again.

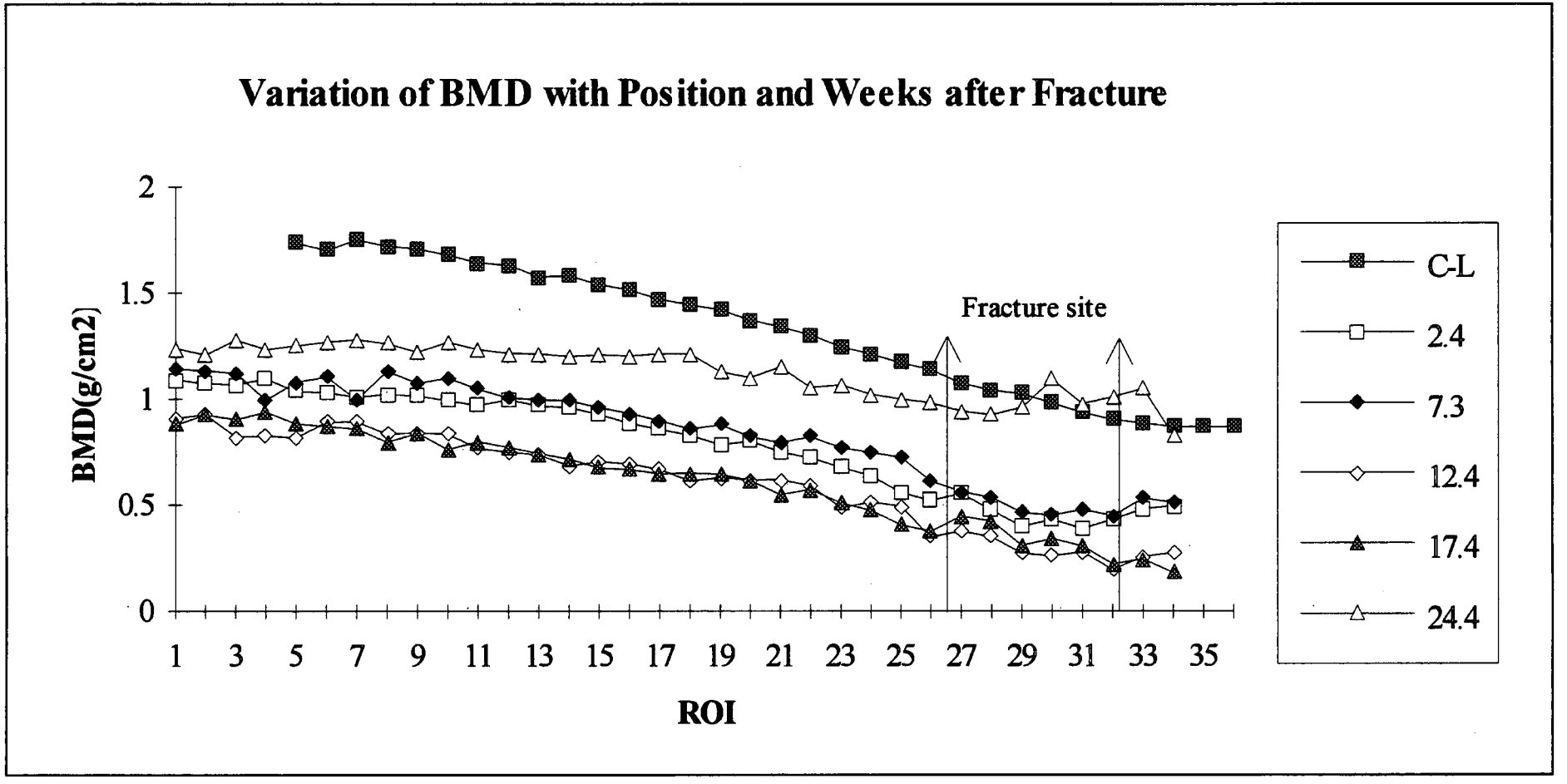

Figure 4.9 BMD profiles for Patient 16 with a transverse wedge fracture of the distal third of the left tibia. Fracture date was 20-Mar-94.

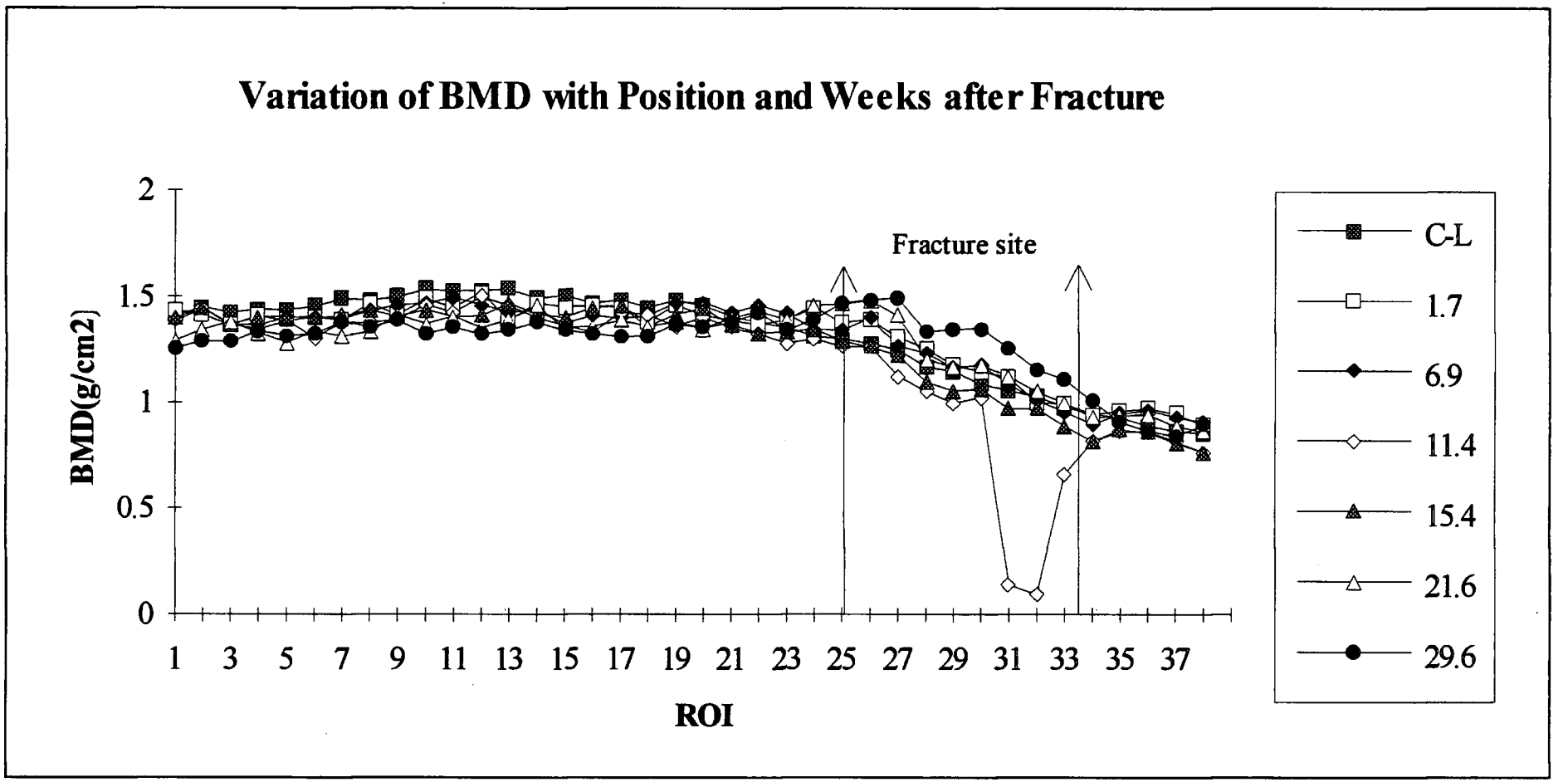

Figure 4.10 BMD profiles for Patient 17 with a spiral wedge fracture of the distal third of the left tibia and a fibular fracture. Fracture date was 09-Apr-94.

Scan 5, 21½ weeks after injury, finds a remineralized fracture gap, although the osteoporosis proximal and now possibly distal to this region remains. By the last scan, about 7 months post-fracture, there are definite signs of disuse osteoporosis persisting in the proximal shaft. In the fracture region the BMD is now markedly higher than in the contralateral tibia, and distally there is little difference.

Patient 18: Patient 18 had a spiral fracture of the distal third of their left tibia as well as a fibular fracture. The date of fracture was 14th May 1994, fixation was with an Orthofix frame, and the first pair of scans was taken six days after injury (see Figure 4.10). At this early stage, there has been a significant decrease in BMD in and around the fracture site, but the rest of the tibia is still at the level of the contralateral. In the month to the next scan the whole tibia fell in mineral density, leaving the fracture area very low in mineralization. By the next scan, at 10½ weeks, there has been some recovery in BMD in the zone of the fracture, although away from the fracture there has again been a fall in BMD.

Unfortunately the fourth scan is also the last, as this patient was latterly lost to follow-up. By this last scan, 102 days after fracture, the proximal scanned portion has reached a plateau, remaining at much the same level as a month earlier. Nearer to the fracture, and at the site itself, there has been a drop in BMD since the previous scan, which again could be put down to the greater resorptive activity at the beginning of the remodelling phase of healing. As with other patients, it appears that there is noticeable post-traumatic/disuse osteoporosis distal to the fracture although it is hard to judge in this case due to the shortage of data. Despite there being only four scans, a recognizable pattern of healing emerges, and there is nothing to suggest delayed healing.

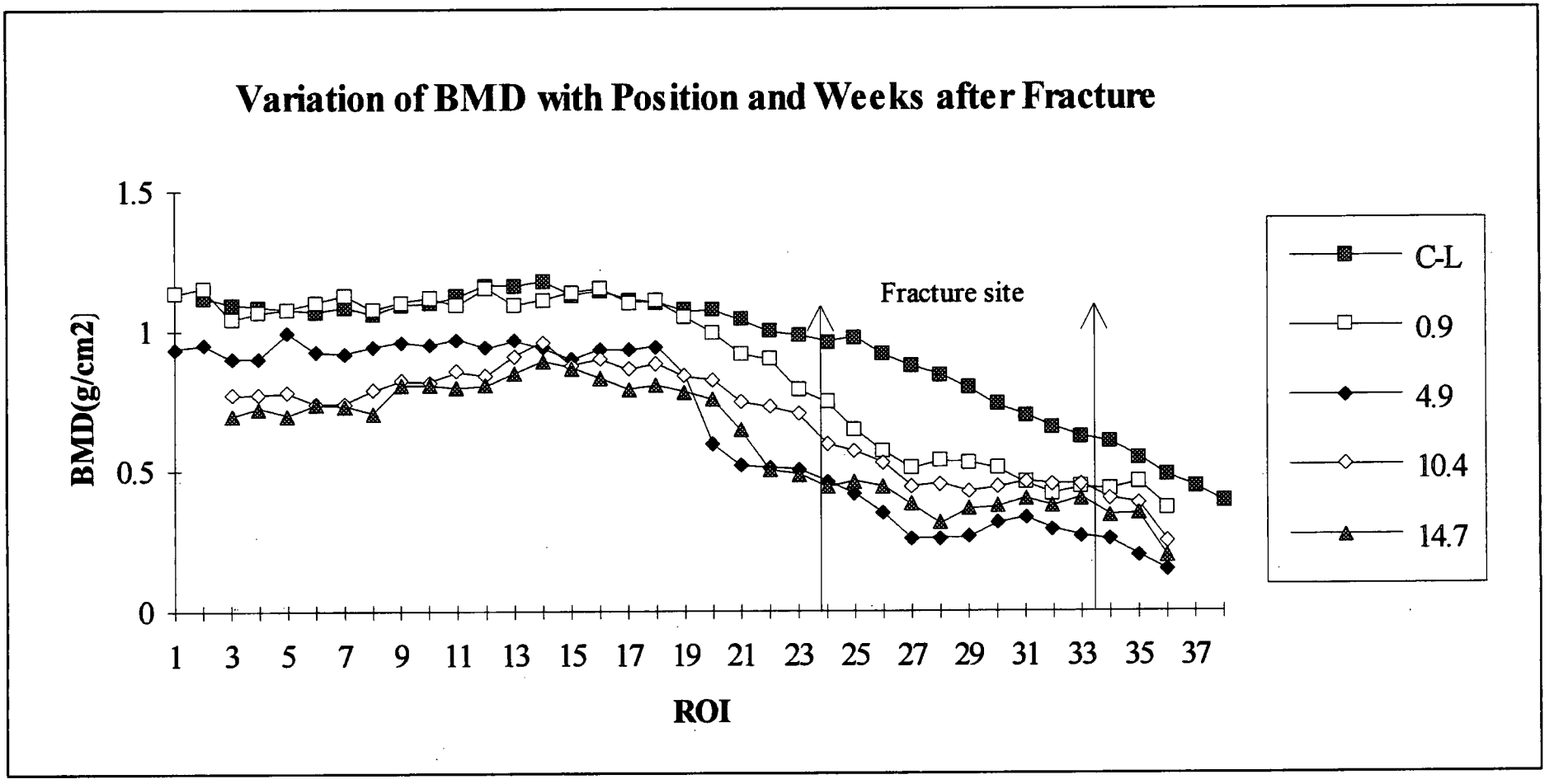

Figure 4.11 BMD profiles for Patient 18 with a spiral fracture of the distal third of the left tibia and a fibular break. Fracture date was 14-May-94.

4.4.2 Healing Trends

An overall picture of the progression of healing in all patients treated by unilateral external fixation is given by Figure 4.12, which contains one point for every scan of a fractured tibia performed during this study and thus acts as a neat summary. Each point represents the state of healing (y-axis) of a particular patient's fracture (legend) at some time post-fracture (x-axis). The healing state is expressed in terms of BMD averaged over the length of the fracture as a percentage of the average BMD along an equivalent length of the contralateral tibial shaft (mean of all contralateral scans). The use of contralateral data for control purposes is widespread in fracture healing studies (Oni *et al.* 1989, Ulivieri *et al.* 1990, Cunningham and Kershaw 1991b, Van der Wiel *et al.* 1994) - it is otherwise impossible to gauge the true extent of remineralization of the fracture, since prospective data are unlikely to be available. Figure 4.15 contains information complementary to Figure 4.12, this time summarizing the mineralization in five ROI's at a distance of ten ROI lengths from the fracture site in the proximal direction. These summaries could not be extended to cover those fractures stabilized by intramedullary nailing, because of the dissimilarity of BMD data from the fractured and contralateral legs in these cases (see Section 4.5).

Comment on the summary graphs can only be very general as the population is quite restricted. Overall, Figure 4.12 shows an initial trend downwards in BMD from the first scan immediately after fracture, followed by a slight plateau and a gradual increase in mineralization. Although the data between 25 and 60 weeks after fracture are very sparse, and so conclusions here need even greater care, none of these four points is at a level lower than 100%, so it is probably fair to say that in uncomplicated healing the fracture site BMD can be expected to regain its original level by around 6 months post-fracture. The discussions of individual patients in the pages preceding suggest that these generalizations may not be entirely appropriate, so next two rather more homogeneous trends will be identified.

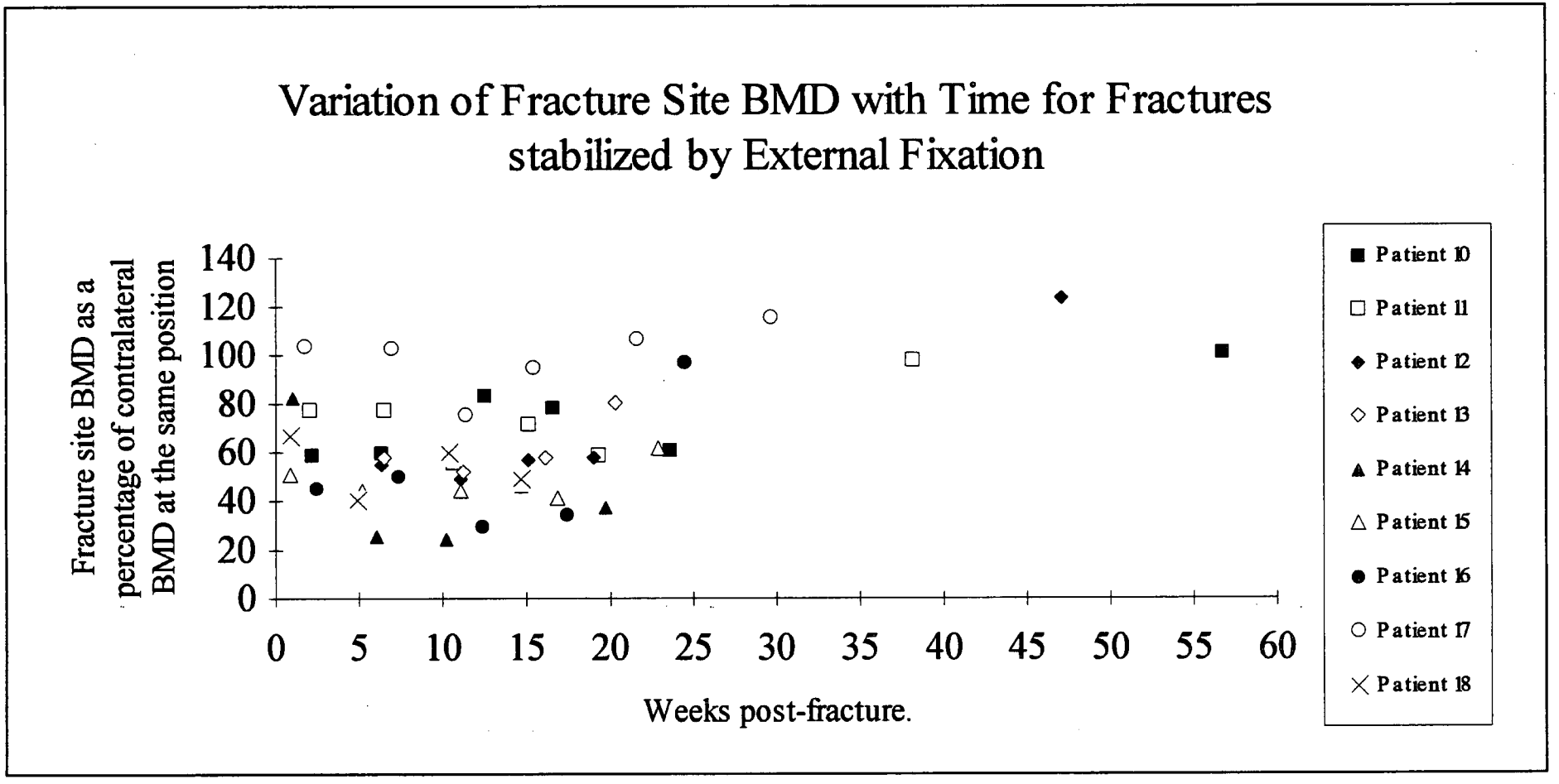

Figure 4.12 Graph showing the changes in fracture site BMD with time for all patients treated by unilateral external fixation. The state of healing in the fractured bone is expressed in terms of mineralization at the fracture site as a percentage of that at an equivalent location in the contralateral tibia.

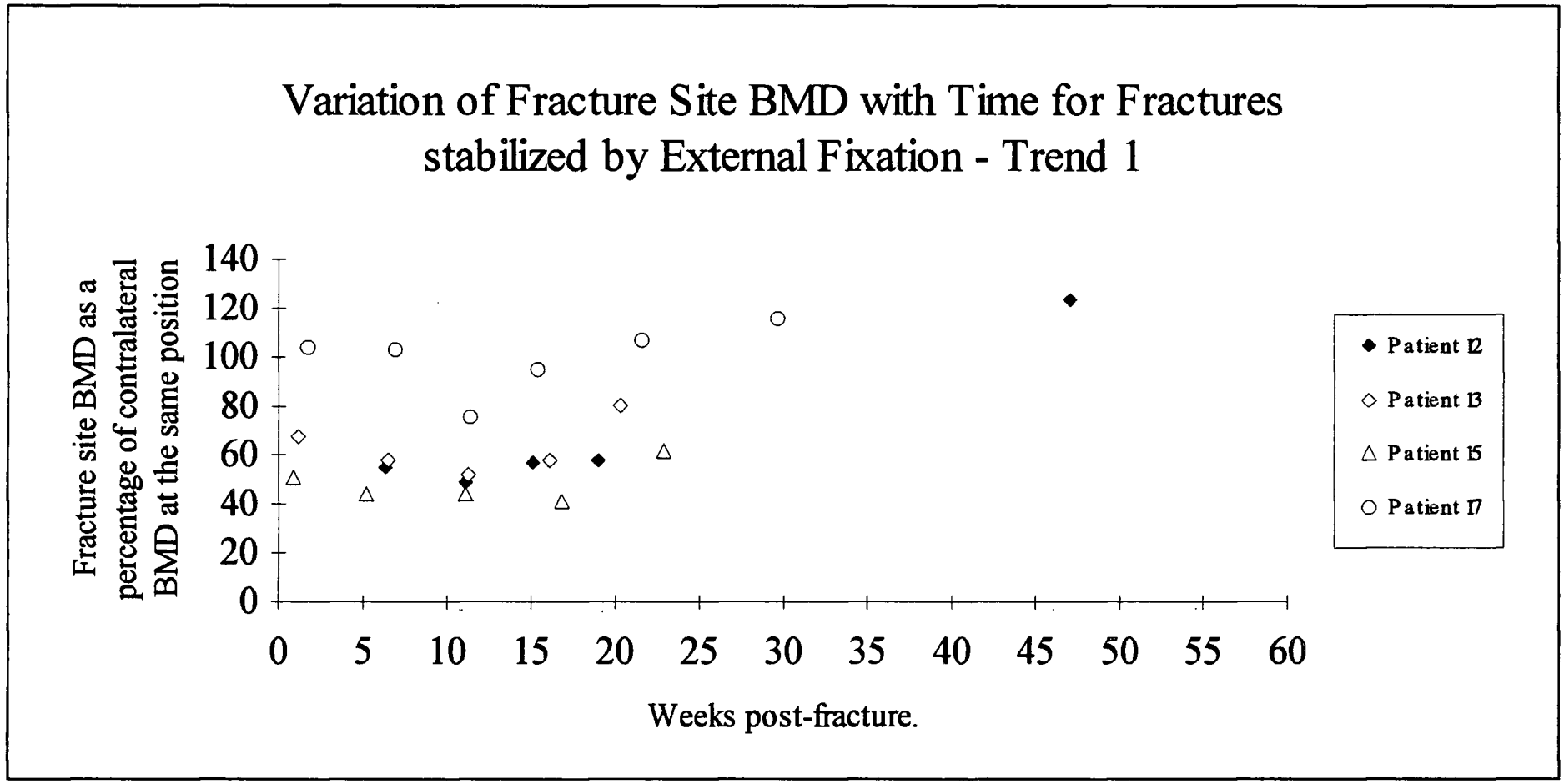

Figure 4.13 Graph showing the changes in fracture site BMD with time for Patients 12, 13, 15 and 17 (Trend 1 healing).

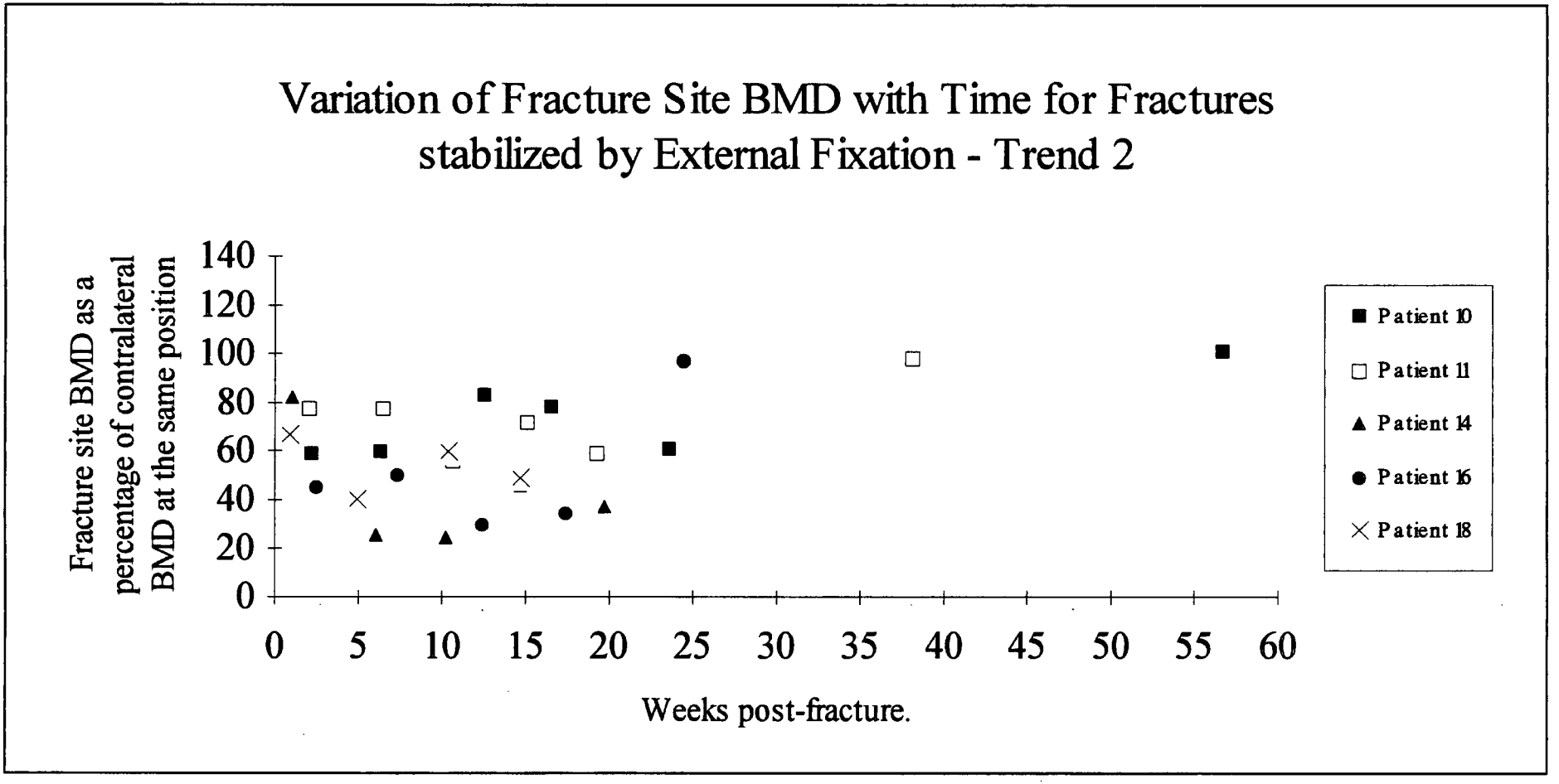

Figure 4.14 Graph showing the changes in fracture site BMD with time for Patients 10, 11, 14, 16 and 18 (Trend 2 healing).

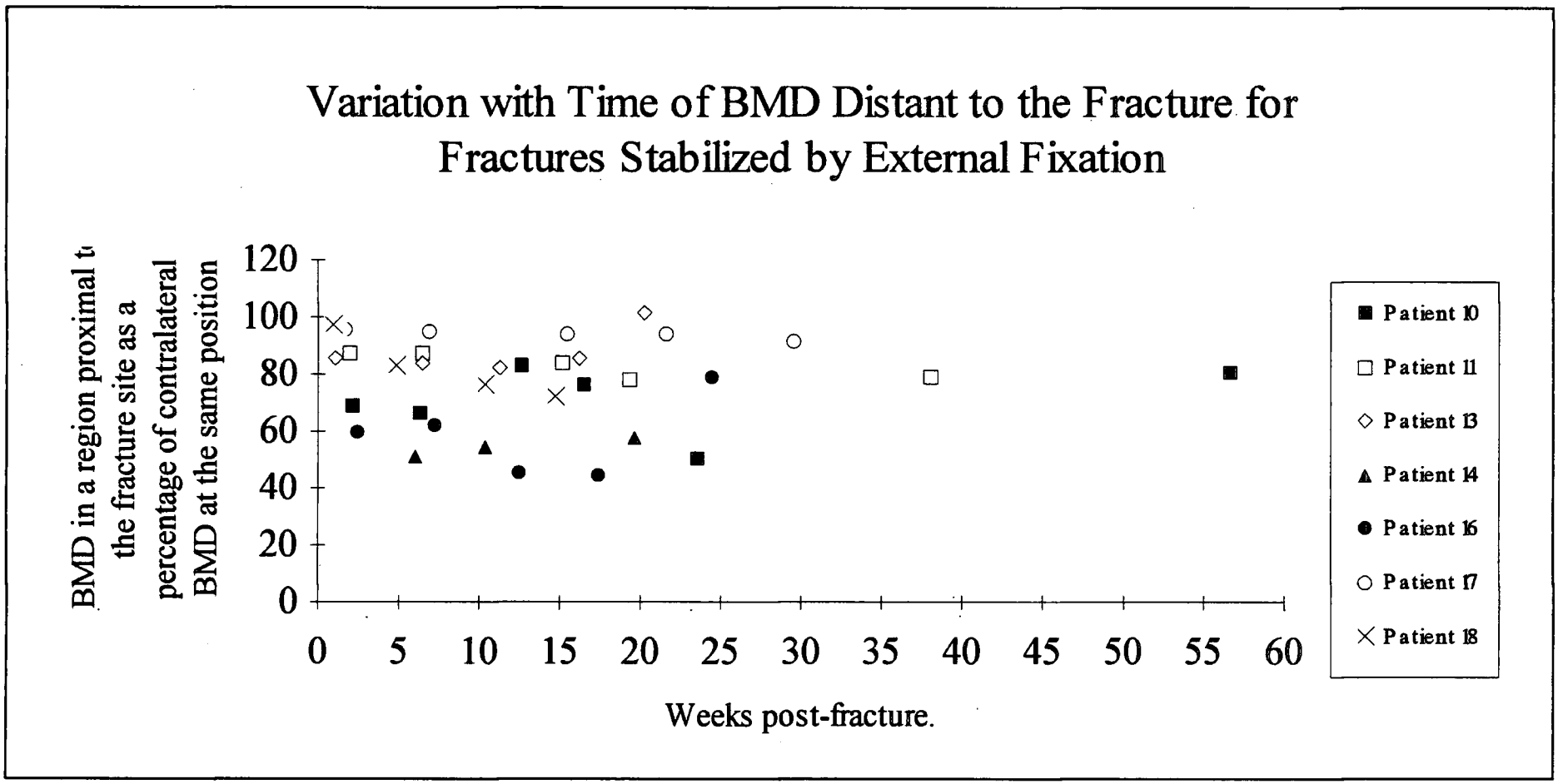

Figure 4.15 Graph showing the temporal variation of BMD in a region of five ROI's, distant by ten ROI lengths proximally from the fracture site, for patients treated by unilateral external fixation. Mineralization is expressed in terms of BMD in this region as a percentage of that at an equivalent location in the contralateral tibia.

These trends are descriptive of the mineralization behaviour in the fracture zone, and do not relate to the tibia as a whole. The first trend (Figure 4.13) includes those patients whose fractures healed with a smooth accompanying change in BMD, *i.e.* BMD fell to a minimum before rising again towards the contralateral level. Patients in this category are 12, 13, 15 and 17, and their healing could perhaps be called 'direct'. Trend 2 (Figure 4.14) includes Patients 10, 11, 14, 16 and 18, and is characterized by an initial fall and rise in BMD which is then followed by a second drop, from which point the bone mineral density approaches a healthy value again. This type of healing could analogously be called 'indirect'. The terms 'direct' and 'indirect' are appropriate for two reasons. Firstly, the progression of healing was uninterrupted in the former group of patients and interrupted in the latter. Secondly, the interruption in Trend 2, which was interpreted in Section 4.4.1 as being indicative of increasing resorptive activity as fracture callus is consumed and remodelled, suggests that healing was in these cases indirect in the usual sense (*i.e.* with an external callus), whereas the uninterrupted progression to union in Trend 1 suggests direct healing with little callus.

In terms of minimum mineral densities attained at the fracture site relative to the contralateral tibia, in Trend 1, BMD touched bottom at 20-50% from 2-11 weeks after injury. Trend 2 patients tended to have a slightly higher minimum BMD of 30-60%, which was first reached 2-5 weeks into healing and subsequently at any time from 13 to 24 weeks post-fracture, the two minima usually being at around the same level. Exact values for both the time to the minimum and its percentage level are of course impossible to derive, since scans were taken at most every four weeks - the above figures are meant as broad settings only. The only patient whose minimum BMD fell outside the above ranges was Patient 17, whose fractured tibia stayed at much the same level as the contralateral throughout the seven months to their last scan. The minimum reached in this case was around 75% after 12 weeks. Here is a potentially significant result, as this was the only patient to be clinically diagnosed with delayed union, but it would not be productive to make a generalization from just one patient.

Trend 2 behaviour has not been distinguished explicitly by other authors. Aro *et al.* (1988), however, in a histomorphometric and microradiographic study of osteotomy healing in rat tibiae and fibulae, observed two peaks of osteoid production at 14 and 35-42 days, the latter associated with maximal resorptive activity during the remodelling phase. The healing timescale is shortened in rats, but the second maximum could well correspond to the second BMD minimum in Trend 2, interpreted above as extensive remodelling resorption. The first BMD trough might then occur immediately before the first osteogenetic peak. Proportionately, the timings of both Trend 2 events fit in reasonably well with the osteogenetic maxima. Such accurate temporal data on the succession of healing phases in humans are not (and are never likely to be) available, because of the inconvenience involved in subjecting patients to the necessarily intensive observation. Richardson (1989) has, however, proposed that remodelling starts at around 20 weeks after fracture in man, which is in rough agreement with Trend 2 behaviour. Only one of the two trends would have been observed by Aro *et al.* because of the standardized osteotomy and stabilization used.

At some distance proximal to the fracture site (10 ROI lengths, equivalent to 48 mm), Figure 4.15 demonstrates that there was far less variation in BMD over time. This summary omits Patients 12 and 15, as an insufficient length of tibia proximal to the fracture was scanned in these cases. Again Patient 17 stands out, with no significant change in BMD evident during the 30 weeks of observation. Otherwise, there was obvious variation in all patients, but in a narrower band than at the fracture site. One interesting feature of this graph is that none of the points (including those for the two long-term follow-up scans) is at a level greater than 100% with respect to the contralateral tibia, suggesting that post-traumatic osteoporosis may be more of a problem away from the zone of the fracture.

4.5 Intramedullary Nailing

The potential difficulty with intramedullary nails was that such a significant volume of highly attenuating material in the very middle of scans might adversely affect the reliability of scanning. For this reason, the phantom tests detailed in the previous chapter were conducted. Three of the patients scanned since Autumn 1993 had their fractures managed by intramedullary nailing - two of these were lost to follow-up after only three scans, which unfortunately provides insufficient information for a healing trend to be identified unless repair is exceptionally quick. Moreover, the third attended appointments erratically and as yet just the first three scans of his series are available. In consequence, it will regrettably not be possible to review specific healing progressions in any of these cases. Two of the five patients recalled had also been treated by this technique, but neither of these was new during the time of the study and they will be discussed separately in Section 4.5.3.

4.5.1 Relevance of the Phantom Tests

In summary, the presence of steel in *in vivo* scans was simulated by scanning perspex, aluminium and steel phantoms, which modelled the behaviour of the soft tissue, bone and implant respectively. By statistical comparison of scans with and without steel, it was established that there were no significant differences between them in any of the three geometries used. From this it was inferred that steel fixation implants would have no effect on the reliability or accuracy of the scan procedure, and that DXA is therefore an acceptable method to use for monitoring fracture healing when internal fixation (by intramedullary nailing or plating) is the fracture management technique. An investigation by Markel and Bogdanske (1994) into the effect of fracture fixation type on BMD measurement by DXA appears to disagree with this finding, by reporting a decrease in calculated BMD with nailed fractures. However, the scanner used in this study was a Hologic QDR 1000 in conjunction with software which

automatically subtracts metal from the ROI's that are analyzed. The Lunar Forearm software does not have this facility, and so the above result is not relevant.

A positive effect that the phantom tests did bring to light was due to step changes in BMD. The DXA scanner does not pick up edges exactly, and so either side of a sudden change in density there are narrow corridors of material where the BMD is recorded as being at a lower level than in reality exists. This has more to do with the sensitivity of the scanner to very small gaps than with its insensitivity to density changes. Phantom tests on a cylindrical aluminium fracture model (Cook and Cunningham 1995) revealed that even with the two identically dimensioned cylinders touching, scanning implied the existence of a gap. The extent of this effect is restricted to less than the minimum width of an ROI (1.2 mm), judging from the third and fourth series of phantom tests described in Chapter 3.

In terms of the analysis method, the edge effect will affect each patient scan in the same way, by underestimating the bone mineral content and therefore BMD immediately adjacent to the implant. There are a number of reasons why it is on balance productive to include this slightly distorted area in analyses. Firstly, the area in the scan covered by the intramedullary nail represents a considerable loss of bone mineral information and so excluding corridors of bone, however narrow, on either side of the implant (and indeed at the outer edges of the tibia) discards data which is proportionately more valuable than in the scans of externally fixated fractures. Secondly, excluding precise widths of bone accurately would be a very time-consuming process because of the manual method by which regions of interest are defined. Thirdly, exclusion of the edges is not particularly valuable when the important feature of the BMD profiles is in the relative changes between scans as healing progresses. In the absence of powerful arguments in favour of exclusion, analysis of scans containing intramedullary nails therefore did not attempt to avoid the affected areas.

4.5.2 Patients

Despite having insufficient clinical data on fractures stabilized by nailing to consider individual healing trends, taking all patients together an adequate number of scans has been analyzed for an optimum procedure to have emerged. This procedure was founded on the method given in Cook (1993), which used three ROI's to exclude the nail itself and the regions to each side of the tibia (see Appendix 3). As stated in Section 4.3, it was plain from a comparison of analyses with and without the central exclusion ROI in place that it in fact made no difference to the BMD readings, since the Forearm software automatically excludes areas with densities above a certain threshold from the analysis. In order to speed the process all subsequent analyses were performed with just the same two ROI's, excluding the soft tissue on either side of the tibia, as have been used for all externally stabilized fractures.

The second distinction in analysis for internally fixated fractures was the independent consideration of medial and lateral sides of the tibia. This measure followed from the unavoidable division imposed on scans of nailed tibiae by the central obscuration caused by the nail. If there were advantage in this style of analysis it would be that splitting the area into two might provide more information than lumping both blocks of unobscured bone together. However, because the tibia has such an irregular cross-section, the (areal) BMD's from these two sections are unlikely to be strictly comparable, and whatever changes are made to the analysis, BMD values from the fractured and contralateral bones will not be compatible. The other reservation over bipartite analysis is that any division of a fracture into two from the two-dimensional DXA image will be somewhat contrived for all but the simplest geometries, and a straightforward geometry would not provide more helpful information whether divided in two or not. This is not to say that separate medial/lateral analysis provides misleading information, simply that this information is not likely to be more valuable than that derived from a unified approach. So for the externally stabilized fractures

there is certainly no point in dividing the image, and for scan images with an intramedullary nail down the centre, the choice between the two routines may be arbitrary.

As an example of the differences between and possible advantages of the two types of analysis described above, Figure 4.16 shows the three lateral profiles from one of the patients lost to follow-up - profiles from the medial side are given in Figure 4.17. The alternative presentation is shown in Figure 4.18, which contains three profiles for the medial and lateral sides of the bone combined, with a mean profile from the three contralateral scans for reference, although contrary to appearances this is not numerically comparable with the profiles of the fractured leg. It is tempting to assume that because the medial and lateral profiles have distinct appearances this is a more helpful way to present the data. Beyond the obvious quantitative differences, however, the qualitative healing behaviour is the same in all three graphs. So unless the division into medial and lateral halves in the plane imposed by the scan orientation says something unique about the geometry of the fracture, the quantitative differences could be purely artefactual. In future, it may therefore be worthwhile to use the presentation of Figure 4.18 for nailed fractures, if only to minimize analysis time.

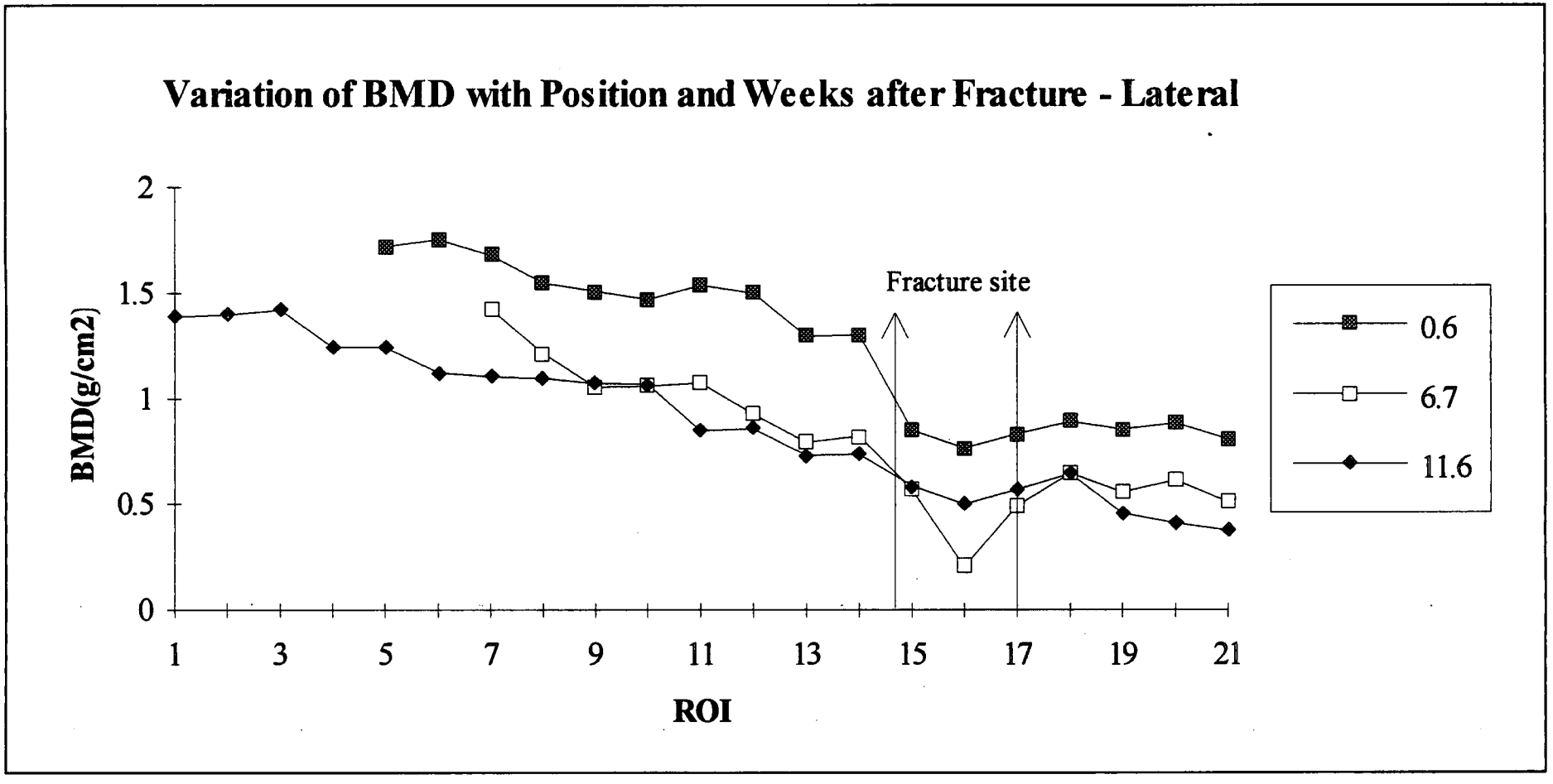

Figure 4.16 BMD profiles for the lateral side of an oblique mid-shaft fracture of the tibia stabilized by an intramedullary nail. Fracture date was 25-Sep-94.

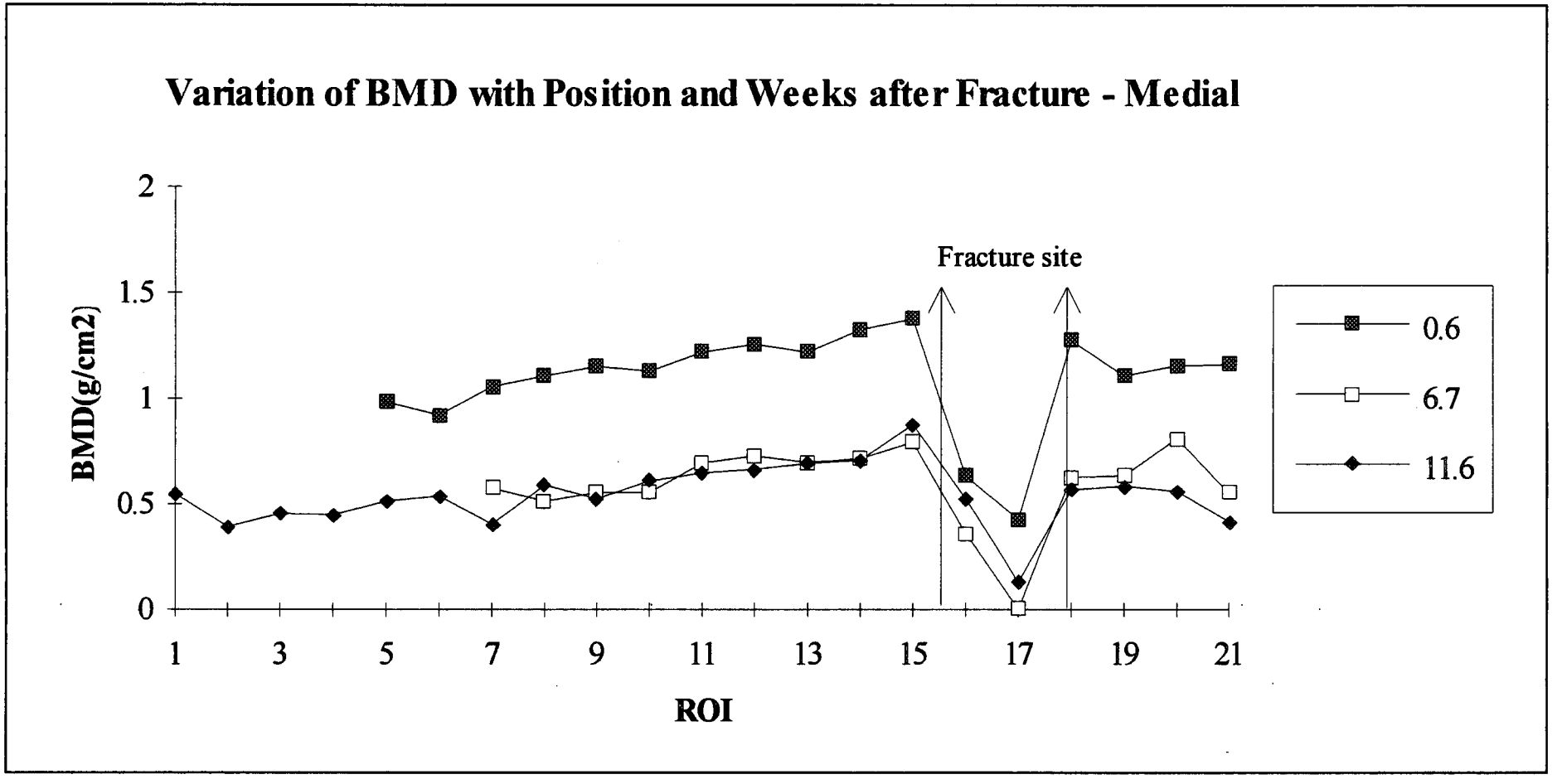

Figure 4.17 BMD profiles for the medial side of an oblique mid-shaft fracture of the tibia stabilized by an intramedullary nail. Fracture date was 25-Sep-94.

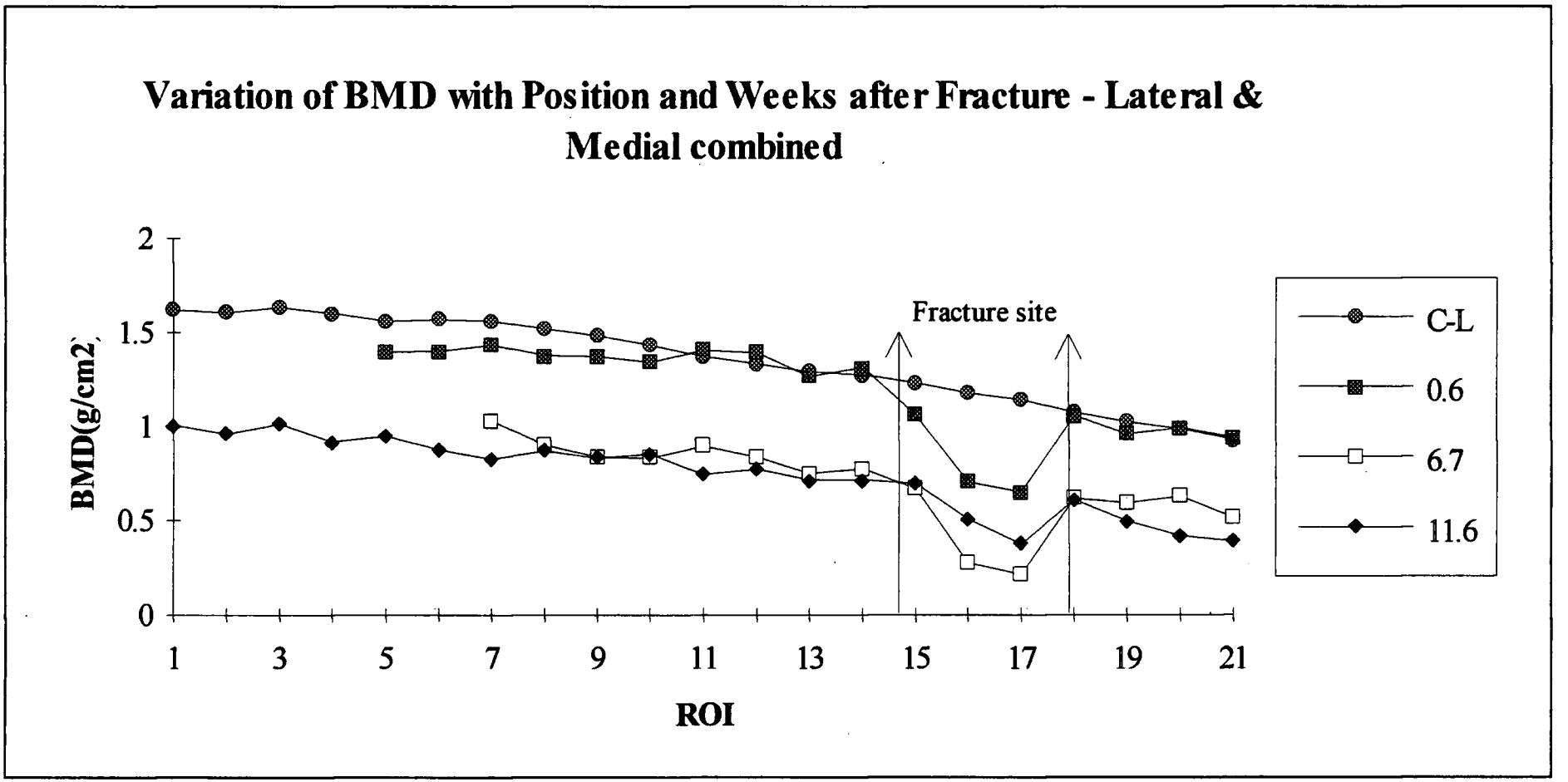

Figure 4.18 BMD profiles for an oblique mid-shaft fracture of the tibia stabilized by an intramedullary nail. Lateral and medial sides have been combined.

4.5.3 Long-term Follow-up: Patients 2 & 8

Patients 2 and 8 were not new during this study but were recalled for long-term follow-up scans at around two years after fracture. Ideally all subjects would be recalled at this stage and at intermediate six-monthly intervals, but it is often troublesome enough attempting to ensure regular attendance at the initial sessions, so this may be a rather optimistic aim. Both patients had had their fractures stabilized with intramedullary nails, which had been removed well before these scans. As the healing of their fractures has already been described (Cook 1993), it will suffice here to summarize what can be gleaned from Figures 4.19 and 4.20 which compare the BMD profiles in the originally fractured tibia with that in the unfractured contralateral bone for each patient.

There is little to say individually about Patient 2's two profiles, as it appears that healing has been complete and effective - if anything, the contralateral tibia is at a lower BMD level. Without the legend, there would be no way of telling the legs apart, and both curves could equally well have come from an intact tibia *in vitro*. The only remarkable thing about these curves is the overall BMD level. The highest point on each line gives a mineral density of around 0.85 gcm^{-2}, which is a very low absolute reading. The reason for this must be the onset of postmenopausal osteoporosis, which at the age of 63 seems already to have taken a heavy toll on this patient's skeleton.

Conversely, the BMD level in Patient 8's legs is far morewithin the normal range, whereas the fractured leg is still unmistakable over two years after fracture. A concern with intramedullary nailing is that the nail may shield the stabilized bone from mechanical stresses which it would otherwise absorb, leading to loss of strength, so that when the fixation is removed the bone is osteoporotic. The danger of refracture is then amplified and full recovery from the injury is delayed. The existence of this fixation-derived osteoporosis would accord with the difference in

density between the legs along most of the scanned length. The mineralization is not however at a dangerously low level and so there is probably no specific danger of refracture in this case. Given time, the bone will regain the level of mineral density in the contralateral, since the stress shielding effect of the nail has been removed and so the tibia will remodel to take account of the need for greater strength.

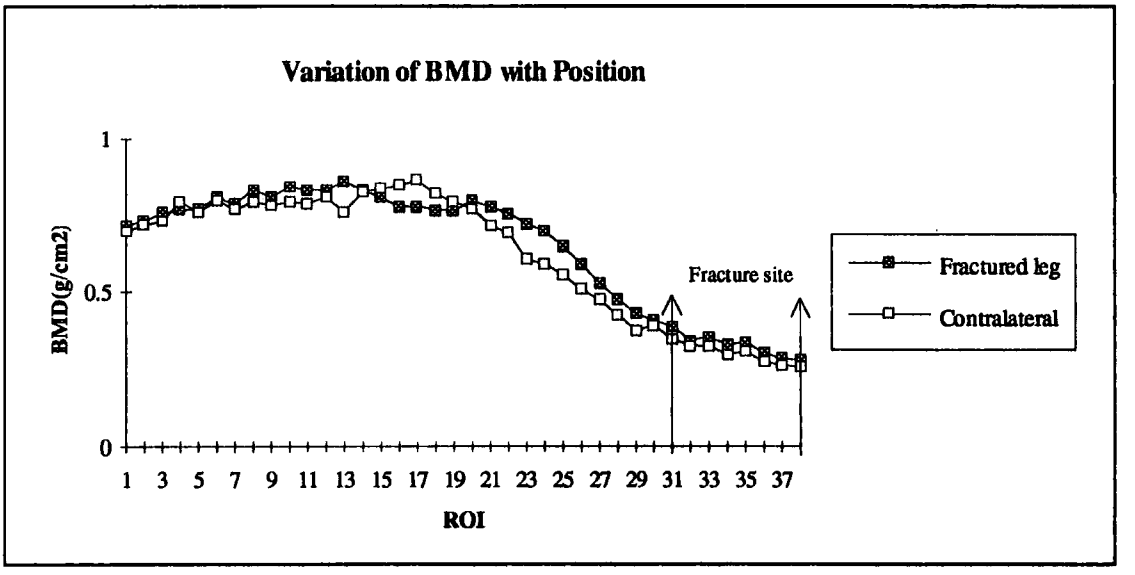

Figure 4.19 Comparison of BMD levels in the fractured and unfractured legs of Patient 2 two years after injury. Fracture date was 08-Nov-92. Date of this scan was 23-Nov-94.

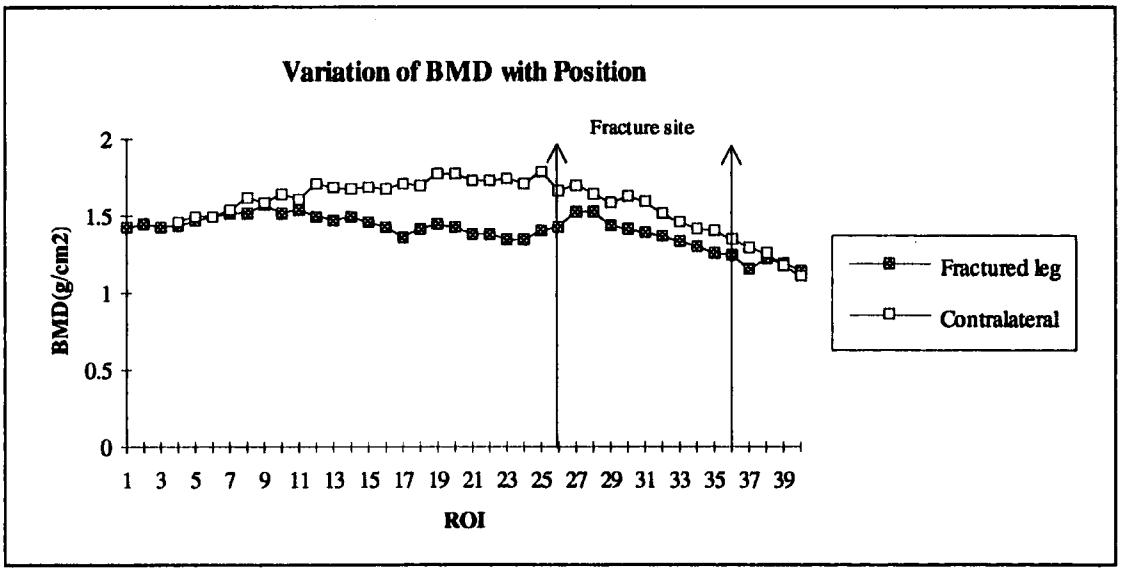

Figure 4.20 Comparison of BMD levels in the fractured and unfractured legs of Patient 8 two years after injury. Fracture date was 15-Oct-92. Date of this scan was 24-Nov-94.

CHAPTER 5 - CONCLUSIONS & FURTHER WORK

The validity of using DXA as a method for monitoring healing in tibial shaft fractures stabilized by intramedullary nailing has now been verified. This was demonstrated in Chapter 3 by three series of phantom scans of simple aluminium and steel geometries on a perspex base. There were found to be no statistically significant differences at the 5% level between BMD readings from scans with and without steel. Analyses of clinical scans from several patients have been carried out on this basis without any problems of consistency.

An expanding population of clinical data has been built up, mostly of patients treated by external fixation. Two healing trends were identified, and all but one of the subjects fell readily into one or the other category. The remaining patient was atypical in that she was diagnosed as having a delayed union, despite having a high value of BMD at the fracture site. In the first trend - referred to as 'direct' - the progression of healing was smooth, with a fall to a plateau value in the fracture zone (reached at 2-11 weeks post-fracture) followed by a steady rise back towards the contralateral value. Trend 2 - 'indirect' - was characterized by an initial fall in BMD at the fracture site (at 2-5 weeks) and then a small increase, followed by another drop (at 13-24 weeks) and a final rise towards the intact range. This second BMD decrease is interpreted as being due to resorption and remodelling of the dense fracture callus. Whether these two trends do correspond to two different progressions of healing is not certain, but some agreement was noted between Trend 2 behaviour and findings of Aro *et al.* (1988) with rat osteotomies.

The observations on healing trends are still based on a small number of patients, and in order for monitoring of fracture healing by DXA to be useful diagnostically for predicting delayed or non-union, a much greater population of results would have to be established. The present scan procedure could be retained, with scans of fractured

and unfractured tibiae performed at monthly intervals until union had been clinically diagnosed. Ideally more regular scans would be recommended during the early stages of healing, at least until remodelling of the callus had begun, however a number of the patients involved in this study proved to be unreliable at attending appointments. Five patients were lost from the study, having had three or fewer scans, and a handful of those who did undergo the complete set of four or more scans failed to turn up for a fifth or sixth, or were unwilling to come back for a longer-term follow-up scan. It would therefore be an unrepresentative body of subjects who turned up on a regular basis at fortnightly intervals for any length of time.

It would be valuable to extend the follow-up period so that patients were recalled where possible at six-monthly intervals after the initial set of monthly sessions, say at 12, 18, 24, 30 and 36 months after fracture, or until it became obvious that the BMD in the fractured leg was stable at a level similar to that in the contralateral. The long-term effects of immobilization on mineralization could then be investigated - specifically, various studies have shown that osteoporosis due to disuse can be a seriously prolonged condition (Andersson and Nilsson 1979, Young *et al.* 1983, Sarangi *et al.* 1993). It is consequently important to be able to understand the best mechanical environment for minimization of such bone loss, because regions remote from a fracture can be affected (Ulivieri *et al.* 1990, Van der Wiel *et al.* 1994), as was seen in Figure 4.13, raising the risk of fractures through a different site in the same bone, and in other bones altogether. As already noted, a special concern with intramedullary nailing is that if the fixation remains *in situ* for a protracted period of time the bone may be weakened by stress-shielding - this was seen in Patient 8 well over two years after fracture. This effect could easily be studied by rescanning at six-monthly intervals for some years post-trauma. Indeed, as Van der Wiel *et al.* (1994) propose, it would be illuminating to test the utility of antiresorptive agents such as calcitonin in preventing disuse osteoporosis, and this too could be simply achieved with DXA.

One of the disadvantages with nailed fractures is that the BMD profiles are not of the same form as those obtained from externally fixated fractures, because of the division imposed on scans by the presence of the nail (see Section 4.5.2). A second drawback is that a direct reference cannot be made to the contralateral limb. There might be some benefit to be gained in this case by cutting out from the analysis of contralateral scans an area identical (or as near as possible) in dimensions to the region obscured by the nail in the fractured tibia. Then medial and lateral measurements of BMD from the former could be compared with medial and lateral measurements from the latter, although because of the edge effect identified in Chapter 2, the comparison would still not be strictly valid. Also, the cost in time required to map the shape of the nail onto the contralateral image might outweigh the gain in ease of interpretation of results.

One ultimate goal for fracture healing studies would be to tie together mechanical and radiographic quantifications of repair with the accepted clinical markers of union. On the radiographic side this enterprise has been initiated, as many studies exist which demonstrate correlations between BMD readings from DXA and other imaging modalities (Markel *et al.* 1990, Overgaard *et al.* 1992, Harrison *et al.* 1993, Stewart *et al.* 1993). Another link in the chain exists in the form of work which has related changes in mechanical properties of bone to porosity and mineral content (Currey 1969, Schaffler and Burr 1988, Ashman and Rho 1988, Currey 1990). Currey (1988), for example, showed that over 80% of the variation in Young's modulus of compact bone was explained by variations in calcium content and volume fraction (or 1 – porosity). So there is a definite connection between BMD and localized mechanical properties. If gross mechanical properties, as measured by some of the techniques described in Chapter 1, could be correlated with local properties of the healing callus then an endpoint to healing could be defined in terms of BMD as well as whole bone properties such as stiffness. Alternatively, a more qualitative approach would involve the identification of corresponding patterns in the healing trends described by clinical, mechanical and quantitative radiographic assessments of healing.

APPENDIX 1 - VARIATION OF TIBIAL BMD WITH ROTATION

A small number of patient scans had produced BMD results which were significantly different in magnitude to the majority of scans of the tibia concerned. One straightforward reason for these discrepancies could have been that the limb was not secured in exactly the same orientation for each of the scans. The tibia has an irregular cross section and so any change in its position between scans might be expected to affect the BMD values, which measure not a true volumetric density but an areal density. In order to test this hypothesis, a series of phantom tests was performed using an intact dry tibia in water to model the *in vivo* situation.

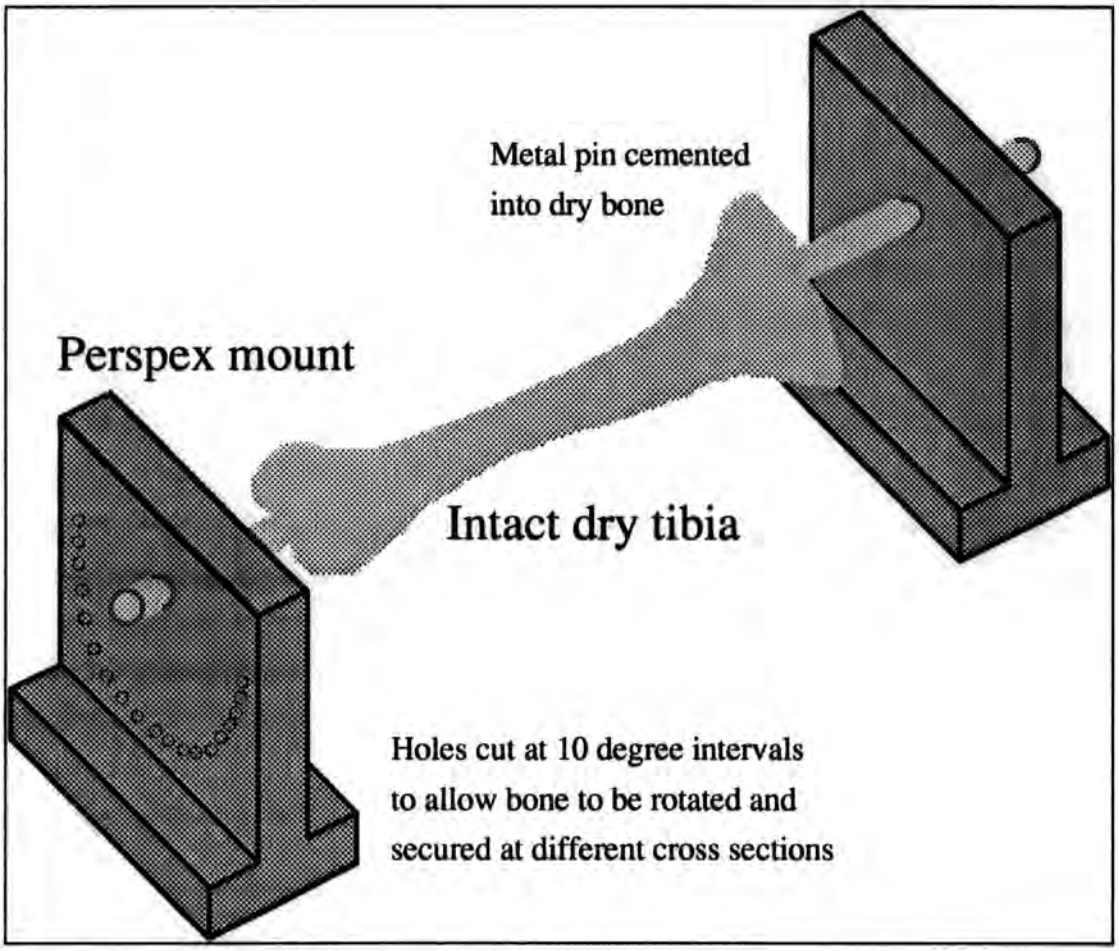

Figure A1.1 In order to assess the effect on bone mineral density measurements of scanning a leg at different orientations in consecutive scans, an intact dry tibia was mounted so that it could be rotated to different angles, secured and scanned. Not to scale.

A mount was designed to allow the intact tibia to be rotated through known angles and then secured so that scans could be taken through different cross-sections of the bone. This is sketched in Figure A1.1. Light aluminium rods, which could be inserted into the two perspex mounts, were cemented into each end of the tibia. One of the mounts was drilled with holes at 10° intervals so that a metal plate could be fastened between the end of the mounting rod and a small pin protruding from one of the holes. During scans the whole of this apparatus was immersed in water, which is an effective radiological soft tissue substitute (Hubbell 1993). Scans were conducted with water just covering the upper surface of the bone (a depth of 110 mm) and at angles of rotation of 0° and ± 10°, 20° and 30° from the anatomical lateral plane of the tibia.

BMC measures the mass of bone mineral in a given volume and so rotation produced very little effect on the readings of bone mineral content derived from analysis of the intact tibia. It would have been worrying if this were not so, as the orientation of the tibia under the scanning arm would then somehow have been affecting the measurement of the mass of mineral present. Figure A1.2 shows the BMC data from all seven analyses, with the proximal end of the tibia on the lefthand side of the plots.

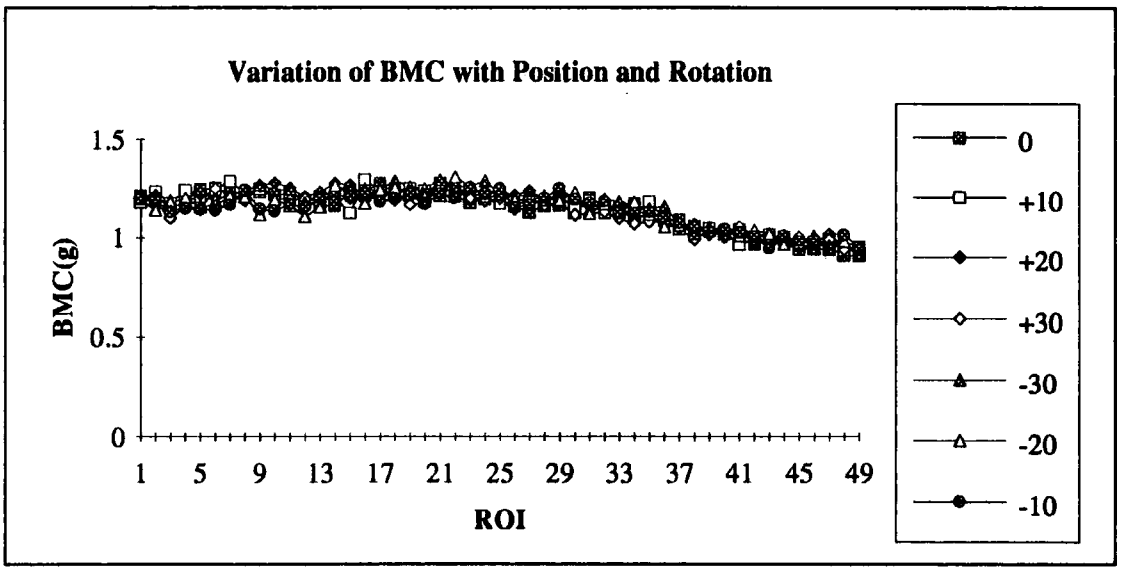

Figure A1.2 Graph showing the effect of varying the angular orientation of the tibia on readings of BMC produced by the Lunar Forearm software. Each ROI was 25.2 mm wide by 4.8 mm deep.

On the other hand, the values of BMD derived from each of the seven scans demonstrated obvious differences between each orientation of the bone. These departures of the BMD readings from those for the correctly orientated bone became more noticeable away from the epiphyses in the shaft of the bone, where the cross-section is rather more irregular. It is these differences which might have been important, because of the use made of BMD as the measure of bone-healing in this study. The graph in Figure A1.3 of all seven complete sets of readings clearly illustrates the effect of the rotation.

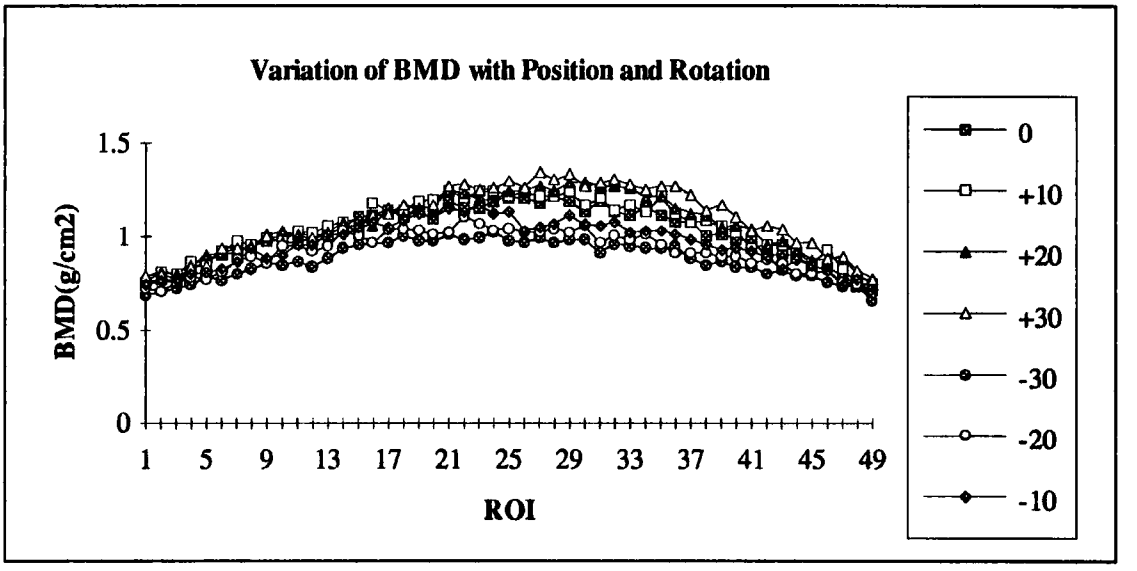

Figure A1.3 Graph showing the effect of varying the angular orientation of the tibia on readings of BMD produced by the Lunar Forearm software. Each ROI was 25.2 mm wide by 4.8 mm deep.

The scans of the intact tibia were taken from a mark below the knee where the diaphysis begins to straighten out, and were continued for two hundred passes of the scanning arm, a distance of 240 mm (one pass translating into one vertical pixel). Disregarding the obvious differences between scan results, the overall shape of each of the seven curves of BMD readings is qualitatively similar to the shapes produced by scanning fractured and unfractured tibiae *in vivo* (an example of the latter is given in Figure A1.4). There is usually not such a pronounced peak in the *in vivo* measurements, but this is due to most of these scans being conducted over a more

restricted length of the leg - typically around 150 mm (or 125 pixels) - and often over the central portion of the tibial shaft. The curve obtained from *in vivo* measurements is therefore usually shorter and flatter

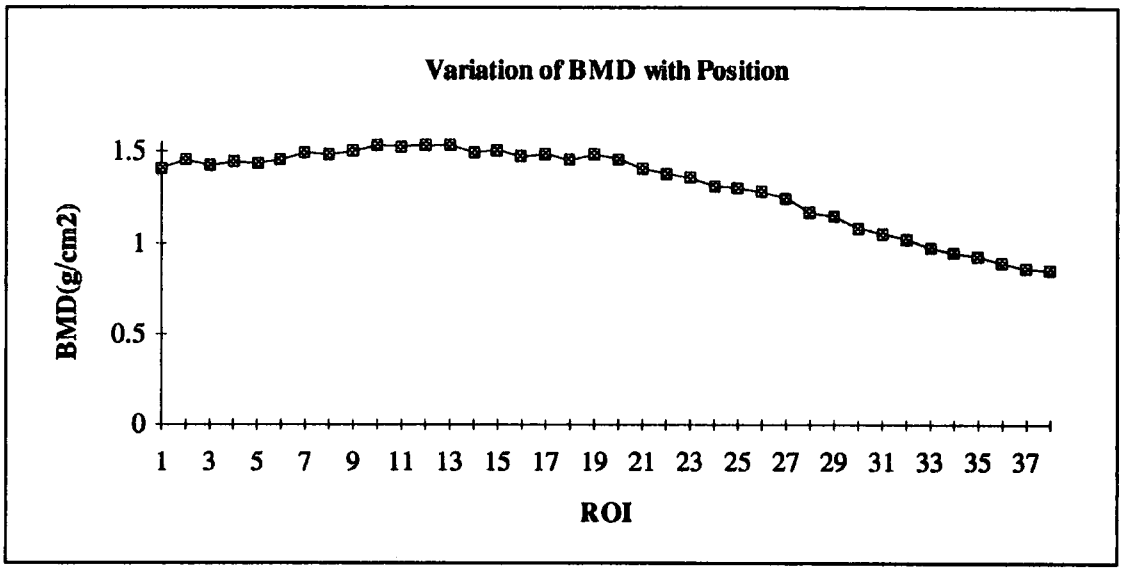

Figure A1.4 BMD profile for a typical unfractured tibia.

ANOVA on the full data sets for BMC and BMD confirmed what Figures A1.2 and A1.3 suggested. There was no evidence of a rotation effect on values of BMC (one way ANOVA gives p = 0.831), but there is strong evidence for such an effect on BMD measurements (p = 0.000 to three s.f.). In order to assess this latter effect more specifically, six further ANOVA tests were used to compare each of the ± 10°, 20° and 30° sets with the 0° set. The results are given in Table A1.1. At a 5% significance level, the angles that show significant divergence in BMD from the scan of the straight leg are −20° and ±30°. In practice these findings suggest that precisely repeatable alignment of the tibia is not critical for comparable BMD results

Angles compared	p-value
0°, +10°	0.308
0°, +20°	0.131
0°, +30°	0.033
0°, −30°	0.000
0°, −20°	0.001
0°, −10°	0.060

Table A1.1 Results of ANOVA tests conducted to quantify the effect of leg rotation on DXA BMD measurements.

to be produced from scan to scan - if the leg is out by up to 10° either way, this should not make much difference to accuracy. This is a reassuring result, as it gives some latitude for error in the clinical situation, but also it seems unlikely that a misalignment of more than 10° would go unnoticed by the radiographers, and so this is an improbable source of the disagreement between contralateral profiles. Indeed, the eventual explanation of the occasionally inconsistent clinical results was unrelated to tibial misalignment (see Appendix 2).

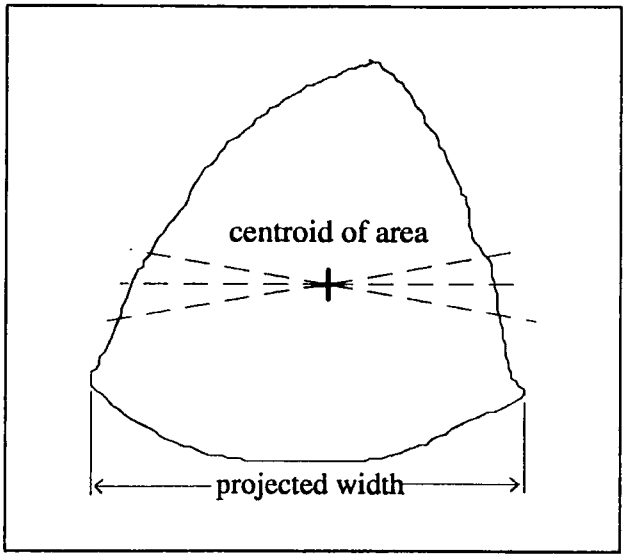

Figure A1.5 A typical cross-section of the tibial diaphysis. Angles are ±10° from the horizontal.

The form of the relationship between BMD and tibial rotation seen in Figure A1.3 is worth explaining as it seems superficially rather curious. Since the diaphyseal portion of the tibia has such an irregular cross-section, asymmetry in the rotational results would be expected. The actual form of the variation, with increasing BMD in one direction of rotation and decreasing in the other, is accounted for by considering a typical cross-section of the tibial shaft (Figure A1.5).

At any given orientation, the calculated areal BMD of the bone is proportional to the inverse of the projected area, or:

$$\text{Areal BMD} \propto 1/(\text{projected area})$$

$$\propto 1/(\text{projected width})$$

So for the neutral orientation shown, BMD is proportional to the inverse of the width indicated. By rotating 10° clockwise, the projected width will be increased (hence BMD will fall), whereas a 10° rotation anticlockwise will cause a slight decrease in this dimension (and a resultant increase in BMD) because of the irregularity of the cross-section. This respective increase and decrease in projected width will continue for several further rotations of 10° until the maximum or minimum width has been reached. The appearance of Figure A1.3 is therefore in line with what would have been expected.

APPENDIX 2 - AN INTERMITTENT PROBLEM

The examination of each of the patients in this study left to one side a problem which affected several sets of results, and mostly scans of unfractured contralateral tibias. In general, each series of contralateral scans has presented a very stable picture, with negligible change in BMD over time at a given position along the tibia (Figure A2.1). In Patients 11 and 13 and in one of those lost to follow-up, however, a number of analyzed scans stood at a distinct BMD level to the remainder (Figure A2.2). A handful of other scans were also affected. This difficulty threatened to be intractable, as the rogue results occurred with no predictability, with only contralaterals on the whole being affected even though scans of both legs are always performed consecutively on the same occasion. So certainly the error was not procedural. Appendix 1 described one attempt at an explanation, but it was found that rotational misalignment of the tibia was not the root of the problem.

It was eventually established that in the scans concerned, the Forearm software was setting its reference base-line at the wrong level. The explanation for these occasional failings in the software is as yet obscure. Base-lines are set from a comparison of the soft-tissue and bone attenuation coefficient averages for each scan - if problems had arisen in scans containing significant areas of highly attenuating metal, they would have been immediately understandable. As it stands, most of the scans with incorrectly set base-lines were of unfractured contralaterals where there was no question of metal confusing the calculations. Also, the vast majority of scans of fractured tibiae, which all contained some metal, were not problematic. Fortunately, an incorrectly set base-line can be remedied manually (see Figure A2.3) - from experience, a contralateral scan with a base-line value outside the range 2.24-2.30 should be reset to 2.27. The base-lines in scans of fractured bones move with healing anyway, and so it is virtually impossible to judge an erroneous setting. Without knowing why the software lapses arise, this slightly unsatisfactory position remains.

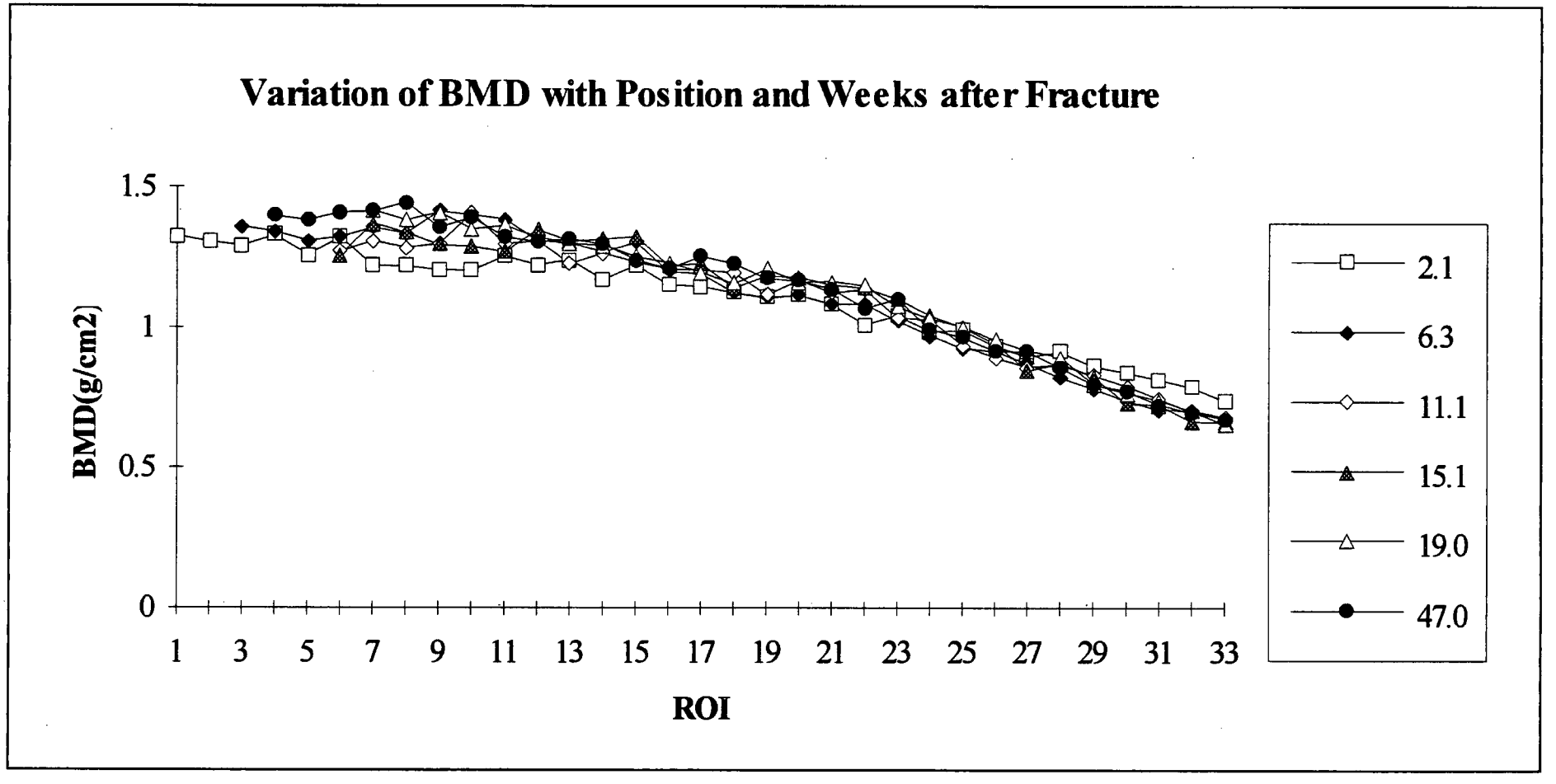

Figure A2.1 The BMD profiles for the unfractured contralateral tibia of Patient 12 exhibit little variation over time.

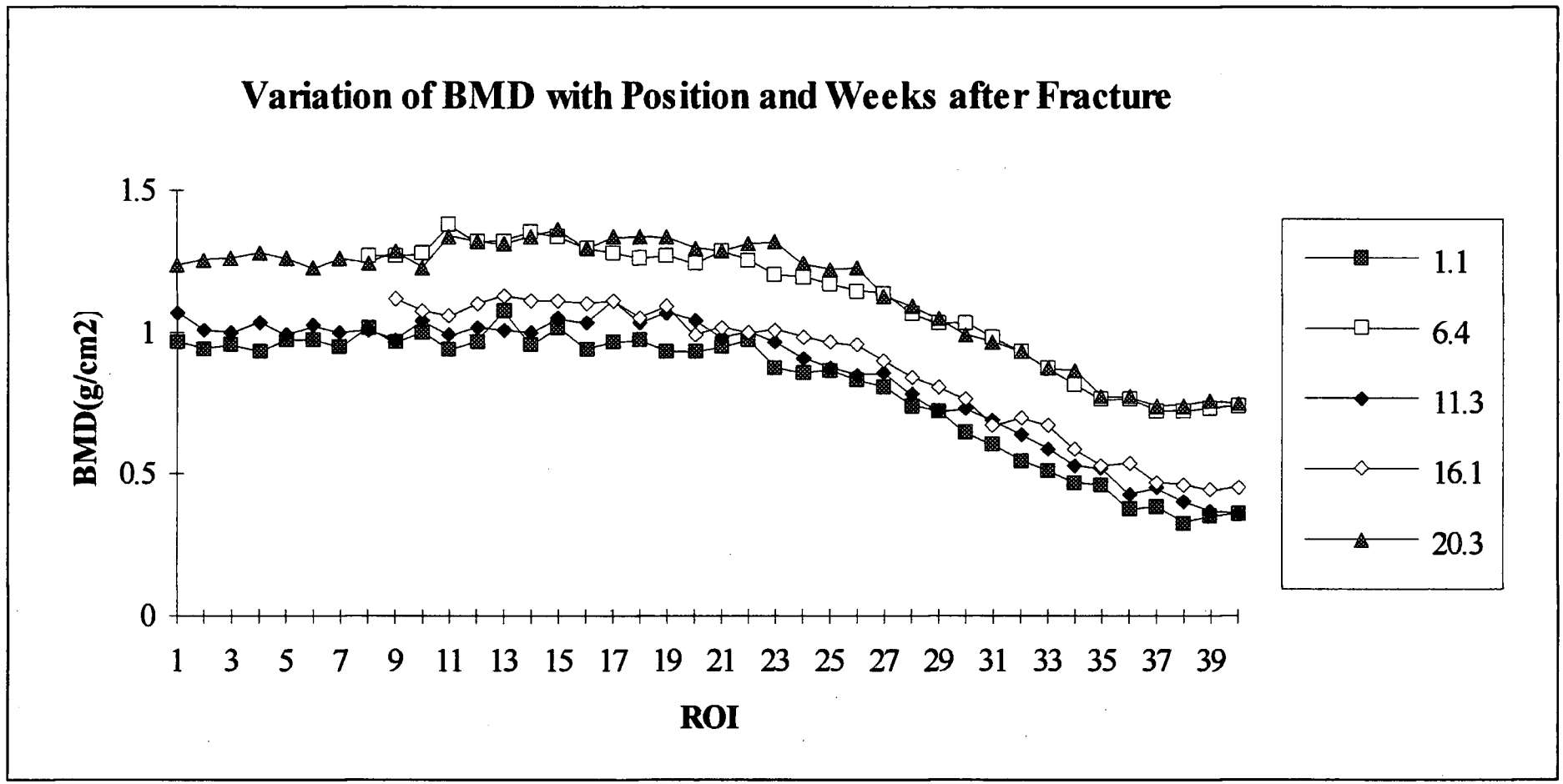

Figure A2.2 BMD profiles for the unfractured tibia of Patient 13 before correction of base-lines. There appears to be significant variation with time.

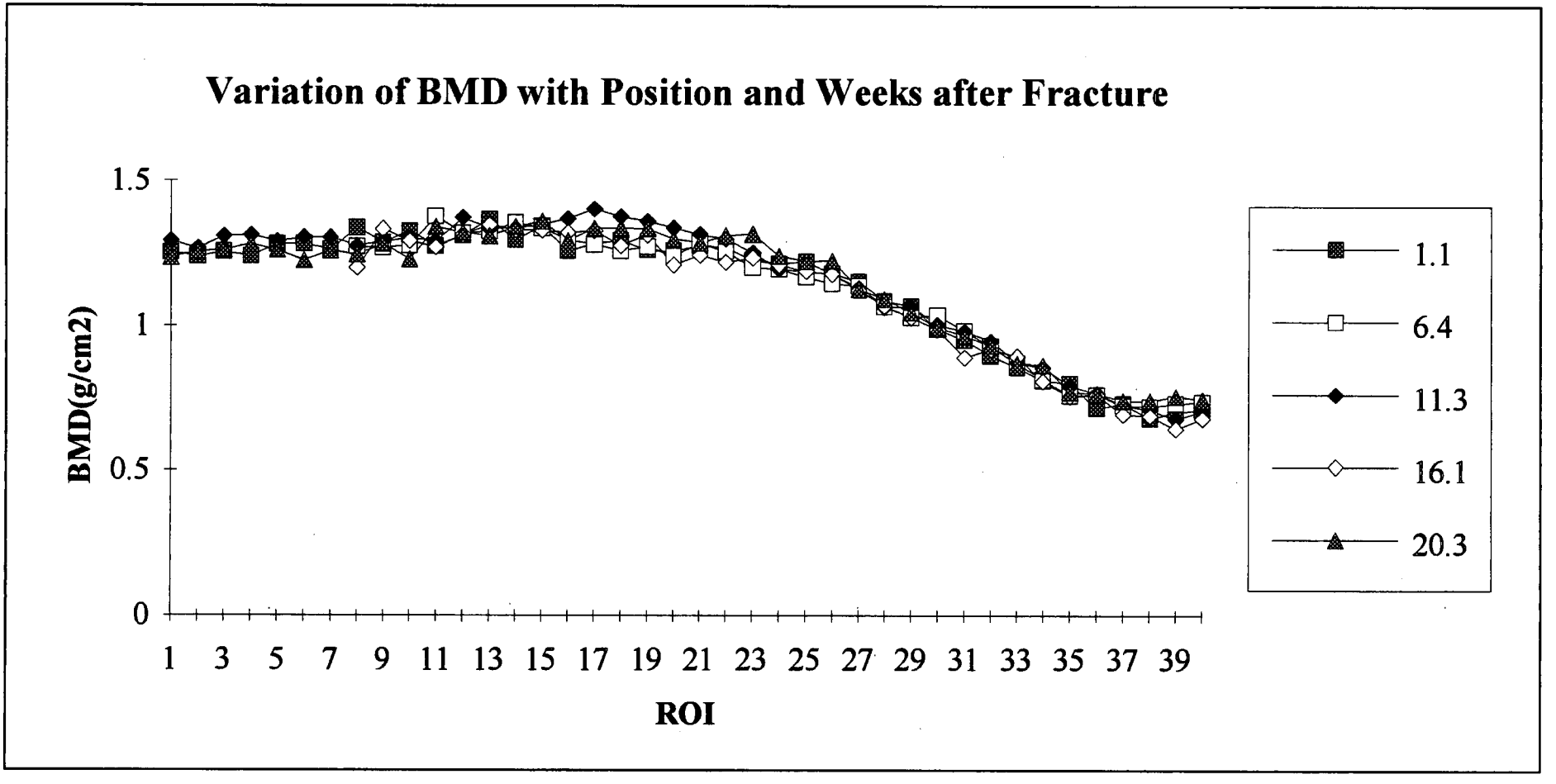

Figure A2.3 BMD profiles for the unfractured tibia of Patient 13 after base-line correction. There is now insignificant inter-scan variation.

APPENDIX 3 - POSITIONING OF ROI'S IN CLINICAL SCANS

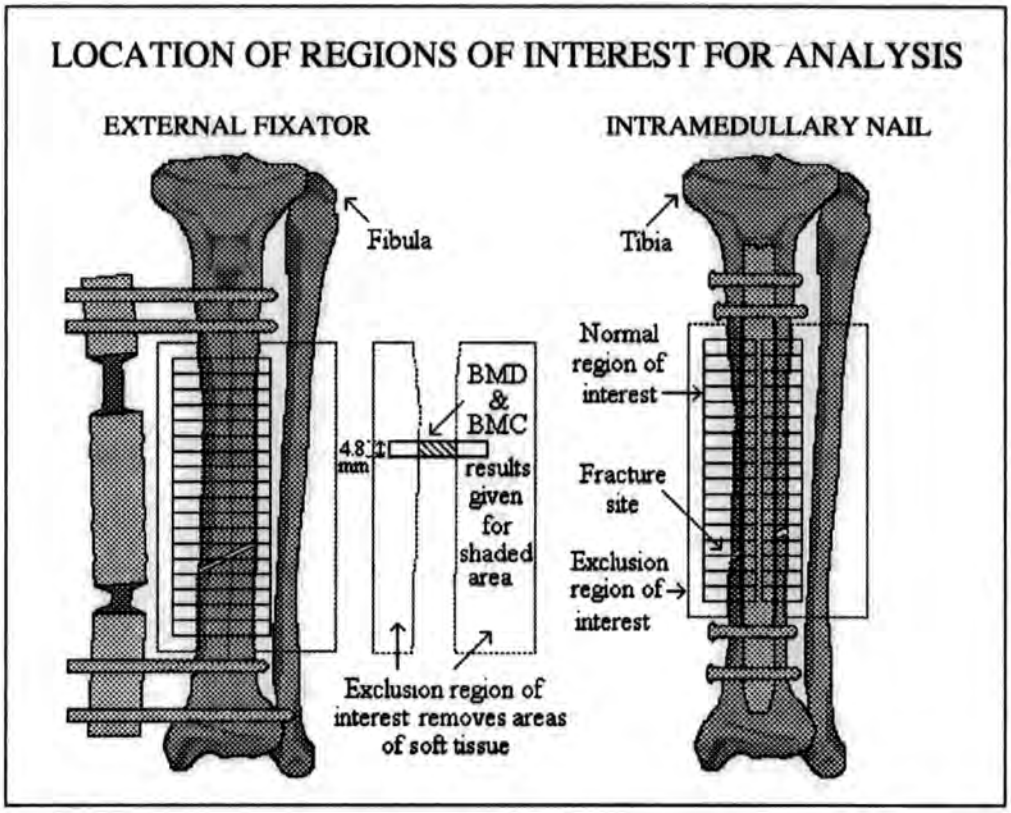

Figure A3.1 Schematic diagram of tibiae stabilized by external and internal fixation. The positioning of exclusion and inclusion regions of interest for analysis is shown. (Adapted, with permission, from a drawing by Juliette Cook of the University of Exeter.)

REFERENCES

Alhava EM (1991). Bone Density Measurements. *Calcified Tissue International*, **S49**, 21-23.

An HS, Xu RM, Lim TH, McGrady L, Wilson C (1994). Prediction of Bone Graft Strength Using Dual Energy Radiographic Absorptiometry. *Spine*, **19**, 2358-2363.

An K-A, Kasman RA, Chao EYS (1988). Theoretical Analysis of Fracture Healing Monitoring with External Fixators. *Engineering in Medicine*, **17**, 11-15.

Andersson SM, Nilsson BE (1979). Changes in Bone Mineral Content Following Tibia Shaft Fractures. *Clinical Orthopaedics and Related Research*, **144**, 226-229.

Apley AG, Solomon L (1982). *Apley's System of Orthopaedics and Fractures* (6th edn), 333-368. Butterworths, UK.

Aro HT, Wippermann BW, Hodgson SF, Wahner HW, Lewallen D, Chao E (1988). Noninvasive Monitoring of Fracture Callus Mineralization Using High-resolution SPA. *Transactions of the 34th Annual Meeting of the Orthopaedic Research Society*, 415. Orthopaedic Research Society, USA.

Ashman RB, Rho JY (1988). Elastic Modulus of Trabecular Bone Material. *Journal of Biomechanics*, **21**, 177-181.

Beaupré GS, Hayes WC, Jofe MH, White AA (1983). Monitoring Fracture Site Properties with External Fixation. *Journal of Biomechanical Engineering*, **105**, 120-126.

Bentzen SM, Hvid I, Jørgensen J (1987). Mechanical Strength of Tibial Trabecular Bone Evaluated by X-ray Computed Tomography. *Journal of Biomechanics*, **20**, 743-752.

Börner W, Schneider P (1992). DEXA. *Journal of the American Medical Association*, **268**, 474-475.

Bowker P, Pratt DJ, McLauchlan J, Wardlaw D (1978). Early Weight-bearing Treatment of Femoral Shaft Fractures Using a Cast-brace: A Preliminary Biomechanical Study. *Journal of Bioengineering*, **2**, 463-467.

Brand RA, Rubin CT (1987). Fracture Healing. In *The Scientific Basis of Orthopaedics* (2nd edn) (ed. Albright JA, Brand RA), 325-345. Appleton & Lange.

Burny F, Donkerwolcke M, Bourgois R, Hinsenkamp M (1985). Twenty Years Experience of Clinical Measurement of Bone Implants Deformation with Strain Gauges. In *Monitoring of Fracture Healing by Vibration Analysis and Other Mechanical Methods* (ed. Van der Perre G, Borgwardt-Christensen A), 145-162. Acco, Leuven.

Burny F, Donckerwolcke M, Moulart F (1990). Monitoring of Orthopedic Implants. In *Implantable Telemetry in Orthopaedics* (ed. Bergmann G, Graichen F, Rohlmann A), 11-22. Freie Universität Berlin.

Cameron JR, Skofronick JG (1978). *Medical Physics*, 38-63. Wiley, USA.

Carter DR, Bouxsein ML, Marcus R (1992). New Approaches for Interpreting Bone Density Data. *Journal of Bone and Mineral Research*, **7**, 137-145.

Chakkalakal DA, Lippiello L, Wilson RF, Shindell R, Connolly JF (1990). Mineral and Matrix Contributions to Rigidity in Fracture Healing. *Journal of Biomechanics*, **23**, 425-434.

Choi K, Kuhn JL, Ciarelli MJ, Goldstein SA (1990). The Elastic Moduli of Human Subchondral, Trabecular and Cortical Bone Tissue and the Size-dependency of Cortical Bone Modulus. *Journal of Biomechanics*, **23**, 1103-1113.

Cohen B, Rushton N (1994). A Comparative Study of Peri-Prosthetic Bone Mineral Density Measurement using Two Different Dual-Energy X-Ray Absorptiometry Systems. *The British Journal of Radiology*, **67**, 852-855.

Collier RJ, Donarski RJ, Worley AJ, Lay A (1993). The Use of Externally Applied Mechanical Vibrations to Assess Both Fractures and Hip Prostheses. In *Micromovement in Orthopaedics* (ed. Turner-Smith AR), 151-163. Clarendon Press, Oxford.

Cook JE (1993). *Assessment of Tibial Fracture Healing Using Dual Energy X-Ray Absorptiometry*. MSc Thesis, University of Durham.

Cook JE, Cunningham JL (1995). The Assessment of Fracture Healing using Dual X-Ray Absorptiometry: A Feasibility Study using Phantoms. *Physics in Medicine and Biology*, **40**, 119-136.

Cunningham JL, Evans M, Harris JD, Kenwright J (1987). The Measurement of Stiffness of Fractures Treated with External Fixation. *Engineering in Medicine*, **16**, 229-232.

Cunningham JL, Kershaw CJ (1991). Measurement of Fracture Healing Using an Ultrasound Technique. In *In Vivo Assessment of Bone Quality by Vibration and Wave Propagation Techniques* (ed. Van der Perre G, Lowet G, Borgwardt-Christensen A), 93-100. KU Leuven.

Currey JD (1962). Strength of Bone. *Nature*, **04-Aug**, 513-514.

Currey JD (1969). The Mechanical Consequences of Variation in the Mineral Content of Bone. *Journal of Biomechanics*, **2**, 1-11.

Currey JD (1975). The Effects of Strain Rate, Reconstruction and Mineral Content on Some Mechanical Properties of Bovine Bone. *Journal of Biomechanics*, **8**, 81-86.

Currey JD (1988). The Effect of Porosity and Mineral Content on the Young's Modulus of Compact Bone. *Journal of Biomechanics*, **21**, 131-139.

Currey JD (1990). Physical Characteristics Affecting the Tensile Failure Properties of Compact Bone. *Journal of Biomechanics*, **23**, 837-844.

Dickson K, Katzman S, Delgado E, Contreras D (1994). Delayed Unions and Non-unions of Open Tibial Fractures - Correlation with Arteriography Results. *Clinical Orthopaedics and Related Research*, **302**, 189-193.

Dolder E (1992). External Tibial Fixation with Immediate Weightbearing. *Helvetica Chirurgica Acta*, **58**, 959-962.

Eyres KS, Bell MJ, Kanis JA (1993). New Bone Formation During Leg Lengthening Evaluated by DEXA. *Journal of Bone and Joint Surgery* **75-B**, 96-106.

Fenner JAK, Wilkinson R, Stother IG, Craigen MAC (1993). Quantification of Bone Mineral Density Changes in the Proximal Femur following Total Hip Replacement.

In *Micromovement in Orthopaedics* (ed. Turner-Smith AR), 169-178. Clarendon Press, Oxford.

Figueiredo UM, Watkins PE, Goodship AE (1993). The Influence of Micromovement in Experimental Leg-Lengthening. In *Micromovement in Orthopaedics* (ed. Turner-Smith AR), 32-39. Clarendon Press, Oxford.

Gautier E, Perren SM, Ganz R (1992). Principles of Internal Fixation. *Current Orthopaedics*, **6**, 220-232.

Genant HK, Faulkner KG, Gluer CC (1991). Measurement of Bone Mineral Density: Current Status. *American Journal of Medicine*, **91**, 49-53.

Goodship AE, Kenwright J (1985). The Influence of Induced Micromovement upon the Healing of Experimental Tibial Fractures. *Journal of Bone and Joint Surgery*, **67-B**, 650-655.

Goodship AE, Norrdin R, Francis M (1993a). The Stimulation of Prostaglandin Synthesis by Micromovement in Fracture Healing. In *Micromovement in Orthopaedics* (ed. Turner-Smith AR), 291-295. Clarendon Press, Oxford.

Goodship AE, Watkins PE, Rigby HS, Kenwright J (1993b). The Role of Fixator Frame Stiffness in the Control of Fracture Healing: An Experimental Study. *Journal of Biomechanics*, **26**, 1027-1035.

Halstead LB (1974). *Vertebrate Hard Tissues*, 159-169. Wykeham Publications, London.

Hamanishi C, Yoshii T, Totani Y, Tanaka S (1994). Bone Mineral Density of Lengthened Rabbit Tibia is Enhanced by Transplantation of Fresh Autologous Bone Marrow Cells - An Experiment Study Using Dual Energy X-Ray Absorptiometry. *Clinical Orthopaedics and Related Research*, **303**, 250-255.

Hammer RR, Hammerby S, Lindholm B (1985). Accuracy of Radiologic Assessment of Tibial Shaft Fracture Healing in Humans. *Clinical Orthopaedics and Related Research*, **199**, 233-238.

Harris JD, Kenwright J, Evans M (1985). Fracture Stiffness Monitoring with External Fixation Using Strain Gauge Transducers and Forceplate. In *Monitoring*

of Fracture Healing by Vibration Analysis and Other Mechanical Methods (ed. Van der Perre G, Borgwardt-Christensen A), 177-186. Acco, Leuven.

Harrison JE, Krishnan SS, Muller C, Strauss A, Mukherjee S, Sturtridge WC (1993). How Well Does DPA Predict Osteoporosis - A Comparison between Neutron-Activation Analysis and DEXA. *Journal of Radioanalytical and Nuclear Chemistry*, **169**, 301-305.

Heymsfield SB, Wang Z, Wang J, Allison D, Pierson RN, Yasamura S (1994). Theoretical Foundation of Dual Energy X-Ray Absorptiometry (DEXA) Soft Tissue Estimates - Validation In Situ and In Vivo. *FASEB Journal*, **8(04)**, 278.

Hubbell JH (1982). Photon Mass Attenuation and Energy Absorption Coefficients from 1 keV to 20 MeV. *International Journal of Applied Radiation and Isotopes*, **33**, 1269-1290.

Joerring S, Krogsgaard M, Wilbek H, Jensen LT (1994). Collagen Turnover after Tibial Fractures. *Archives of Orthopaedic Trauma Surgery*, **113**, 334-336.

Johnson J, Dawson-Hughs B (1991). Precision and Stability of DEXA Measurements. *Calcified Tissue International*, **49**, 174-178.

Johnston CC, Slemenda CW, Melton LJ (1991). Clinical Use of Bone Densitometry. *New England Journal of Medicine*, **324**, 1105-1109.

Kellie SE (1992). Measurement of Bone Density with DEXA. *Journal of the American Medical Association*, **267**, 286-294.

Kellie SE (1992). DEXA - Reply. *Journal of the American Medical Association*, **268**, 475.

Kenwright J (1992). The Principles of Use of External Fixation. *Current Orthopaedics*, **6**, 214-219.

Kenwright J, Goodship AE, Kelly DJ, Newman JH, Harris JD, Richardson JB, Evans M, Spriggins AJ, Burrough SJ, Rowley DI (1986). Effect of Controlled Micromovement on Healing of Tibial Fractures - Preliminary Communication. *Lancet*, **22-Nov**, 1185-1187.

Kershaw CJ , Cunningham JL, Kenwright J (1993). Tibial External Fixation, Weight Bearing and Fracture Movement. *Clinical Orthopaedics and Related Research*, **293**, 28-36.

Latta LL, Zych GA (1991). The Mechanics of Fracture Fixation. *Current Orthopaedics*, **5**, 92-98.

Lewallen DG, Aro HT, Chao EYS, Berquist TH, Kelly PJ (1988). Noninvasive Evaluation of Bone Healing Using Quantitative MRI Imaging. *Transactions of the 34th Annual Meeting of the Orthopaedic Research Society*, 409. Orthopaedic Research Society, USA.

Lindsay R R, Aitken JM, Anderson JB, Hart DM, MacDonald EB, Clarke AC (1976). Long-term Prevention of Postmenopausal Osteoporosis by Oestrogen. *Lancet*, **15-May**, 1038-1041.

Lowet G, Lammens J, De Clerck P, Desmet P, Van der Perre G (1991). Ultrasound Detection of Fracture Healing. In *In Vivo Assessment of Bone Quality by Vibration and Other Mechanical Methods* (ed. Van der Perre G, Borgwardt-Christensen A), 111-114. Acco, Leuven.

Mabuchi K, Fujie H, Yamatoku Y, Yamamoto M, Sasada T (1992). A New Methodology with an Application of Robotics to Control the Mechanical Environment around Experimentally Fractured Bone. In *Biomechanics in Orthopedics* (ed. Niwa S, Perren SM, Hattori T), 183-193. Springer-Verlag, Tokyo.

Markel MD, Bogdanske JJ (1994a). The Effect of Increasing Gap Width on Localized Densitometric Changes within Tibial Ostectomies in a Canine Model. *Calcified Tissue International*, **54**, 155-159.

Markel MD, Bogdanske JJ (1994b). Dual Energy X-Ray Absorptiometry of Canine Femurs with and without Fracture Fixation Devices. *American Journal of Veterinary Research*, **55**, 862-866.

Markel MD, Gottsauner-Wolf F, Bogdanske JJ, Wahner HW, Chao EYS (1993). Dual Energy X-Ray Absorptiometry of Implanted Femora after Cemented and

Press-Fit Total Hip Arthroplasty in a Canine Model. *Journal of Orthopaedic Research*, **11**, 452-456.

Markel MD, Wikenheiser MA, Morin RL, Lewallen DG, Chao EYS (1990). Quantification of Bone Healing - Comparison of QCT, SPA, MRI and DEXA. *Acta Orthopaedica Scandinavica*, **61**, 487-498.

Martin RB, Burr DB (1989). *Structure, Function and Adaptation of Cortical Bone*. Raven Press, New York.

May PC (1989). Controlling the Fracture Environment by Applying External Fixator Biomechanics. *Proceedings of the Institute of Mechanical Engineers*, **5**, 139-147.

Mazess RB, Sorenson JA, Hanson JA, Collick BD (1988). Dual Photon X-ray Absorptiometry (DEXA). *Clinical Physics and Physiological Measurement*, **9**, 178.

Mooney MD (1982). Major Fractures. In *Orthopedic Rehabilitation* (ed. Nickel VL), 331-343. Churchill Livingstone, New York.

Mosheiff R, Klein BY, Leichter I, Chaimsky G, Nyska A, Peyser A, Segal D (1992). Use of Dual-Energy X-Ray Absorptiometry (DEXA) to follow Mineral Content Changes in Small Ceramic Implants in Rats. *Biomaterials*, **13**, 462-466.

Müller ME, Allgöwer M, Schneider R, Willenegger H (1991). *Manual of Internal Fixation* (3rd edn). Springer-Verlag, Berlin.

National Osteoporosis Society (1993). *The National Osteoporosis Society Annual Report 1992/3*. NOS, Bath.

Oni OOA, Graebe A, Pearse M, Gregg PJ (1989). Prediction of the Healing Potential of Closed Adult Tibial Shaft Fractures by Bone Scintigraphy. *Skeletal Radiology*, **245**, 239.

Overgaard K, Hansen MA, Riis BJ, Christiansen C (1992). Discriminatory Ability of Bone Mass Measurements (SPA and DEXA) for Fractures in Elderly Postmenopausal Women. *Calcified Tissue International*, **50**, 30-35.

Pan WT, Einhorn TA (1992). The Biochemistry of Fracture Healing. *Current Orthopaedics*, **6**, 207-213.

Perren SM (1992). Stability and Bone Healing. In *Biomechanics in Orthopedics* (ed. Niwa S, Perren SM, Hattori T), 3-12. Springer-Verlag, Tokyo.

Rhinelander FW (1974). Tibial Blood Supply in Relation to Fracture Healing. *Clinical Orthopaedics and Related Research*, **105**, 34-81.

Richardson JB (1989). *The Mechanics of Fracture Healing*. MD Thesis, University of Aberdeen.

Richardson JB, Cunningham JL, Kenwright J, O'Connor B (1993). Fracture Stiffness as a Measure of Fracture Healing. In *Micromovement in Orthopaedics* (ed. Turner-Smith AR), 3-10. Clarendon Press, Oxford.

Richardson JB, Kenwright J, Cunningham JL (1992). Fracture Stiffness Measurement in the Assessment and Management of Tibial Fractures. *Clinical Biomechanics*, **7**, 75-79.

Riggins RS, Simanonok C, Lewis DW, Smith AH (1985). Weight-bearing: Its Lack of Effect on Fracture Healing. *International Orthopaedics*, **9**, 199-203.

Rockwood CA, Green DP (ed.) (1984). *Fractures in Adults* (2nd edn). J.B.Lippincott Company, Philadelphia

Rubin CT, McLeod KJ, Bain SD (1990). Functional Strains and Cortical Bone Adaptation: Epigenetic Assurance of Skeletal Integrity. *Journal of Biomechanics*, **23S1**, 43-54.

Sarangi PP, Ward AJ, Smith EJ, Staddon GE et al (1993). Algodystrophy and Osteoporosis after Tibial Fractures. *Journal of Bone and Joint Surgery*, **75-B**, 450-452.

Sartoris DJ, Moscona A, Resnick D (1990). Progress in Radiology: Dual-Energy Radiographic Absorptiometry for Bone Densitometry. *Annals of the New York Academy of Sciences*, **592**, 307-325.

Schaffler MB, Burr DB (1988). Stiffness of Compact Bone: Effects of Porosity and Density. *Journal of Biomechanics*, **21**, 13-16.

Schneider E, Michel MC, Genge M, Perren SM (1990). Loads Acting on an Intramedullary Femoral Nail. In *Implantable Telemetry in Orthopaedics* (ed. Bergmann G, Graichen F, Rohlmann A), 221- 227. Freie Universität Berlin.

Shen W-J, Shen Y-S (1993). Fibular Non-union after Fixation of the Tibia in Lower Leg Fractures. *Clinical Orthopaedics and Related Research*, **287**, 231-232.

Shipman P, Walker A, Bichell D (1985). *The Human Skeleton.* Harvard University Press, Massachusetts.

Simpson AHRW, Kenwright J (1993). The Response of Peripheral Nervous Tissue to Limb Lengthening. In *Micromovement in Orthopaedics* (ed. Turner-Smith AR), 221-226. Clarendon Press, Oxford.

Simon SR, Riggins RS, Wirth CR, Fox ML (eds) (1986). *Orthopaedic Science. A Resource and Self-Study Guide for the Practitioner.* American Academy of Orthopaedic Surgeons, Illinois.

Smith EJ, Ward AJ, Watt I (1993). Posttraumatic Osteoporosis and Algodystrophy after External Fixation of Tibial Fractures. *Injury - International Journal of the Care of the Injured*, **24**, 411-415.

Stewart SP, Bramley PN, Heighton R, Green JH, Horsman A, Losowsky MS, Smith MA (1993). Estimation of Body-composition from Bioelectrical Impedance of Body Segments - Comparison with DEXA. *British Journal of Nutrition*, **69**, 645-655.

Taktak AFG, Edwards J, Kay P, Laycock DC (1993). Improvement in the Monitoring of Fracture Repair by Noninvasive Mechanical Techniques. In *Micromovement in Orthopaedics* (ed. Turner-Smith AR), 140-150. Clarendon Press, Oxford.

Tiedeman JJ, Lippiello L, Connolly J, Strates BS (1990). Quantitative Roentgenographic Densitometry for Assessing Fracture Healing. *Clinical Orthopaedics and Related Research*, **253**, 279-286.

Tosteson ANA, Rosenthal DI, Melton LJ, Weinstein MC (1990). Cost Effectiveness of Screening Perimenopausal White Women for Osteoporosis: Bone Densitometry and Hormone Replacement Therapy. *Annals of Internal Medicine*, **113**, 594-603.

Tothill P (1989). Methods of Bone Mineral Measurement. *Physics in Medicine and Biology*, **34**, 543-572.

Trémollieres F, Vidal H, Pouilles JM, Cahuzac JP, Ribot C (1993). Monitoring of Bone Mineralization after Limb Lengthening - A New Application for DEXA in Orthopaedic Surgery. *Journal of Bone and Mineral Research*, **8S1**, 239.

Trueta J (1963). The Role of the Vessels in Osteogenesis. *Journal of Bone and Joint Surgery*, **45-B**, 402.

Ulivieri FM, Bossi E, Azzoni R, Ronzani C, Trevisan C, Montesano A, Ortolani S (1990). Quantification by Dual Photonabsorptiometry of Local Bone Loss After Fracture. *Clinical Orthopaedics and Related Research*, **250**, 291-296.

Van der Perre G (1993). Noninvasive Monitoring of Fracture Healing. *KU Leuven internal report.*

Van der Perre G, Van Audekercke R, Martens M, Muller JC (1983). Identification of In Vivo Vibration Modes of Human Tibiae by Modal Analysis. *Journal of Biomechanical Engineering*, **105**, 244-248.

Van der Wiel HE, Lips P, Nauta J, Patka P, Haarman HJThM, Teule GJJ (1994). Loss of Bone in the Proximal Part of the Femur following Unstable Fractures of the Leg. *Journal of Bone and Joint Surgery*, **76-A**, 230-236.

Wallace AL, Draper ERC, Strachan RK, McCarthy ID, Hughes SPF (1993). The Vascular Response to Micromovement in Experimental Fractures. In *Micromovement in Orthopaedics* (ed. Turner-Smith AR), 11-22. Clarendon Press, Oxford.

Wallace AL, Draper ERC, Strachan RK, McCarthy ID, Hughes SPF (1994). The Vascular Response to Fracture Micromovement. *Clinical Orthopaedics and Related Research*, **302**, 189-193.

Wallace AL, Strachan RK, Blane A, Best JJK, Hughes SPF (1992). Quantitative Early Phase Scintigraphy in the Prediction of Healing of Tibial Fractures. *Skeletal Radiology*, **21**, 241-245.

Webster JG (ed.) (1988). *Encyclopedia of Medical Devices and Instrumentation* (vol. 2), 837-839. Wiley Interscience, New York.

White AA, Panjabi MM, Southwick WO (1977). Effects of Compression and Cyclical Loading on Fracture Healing - A Quantitative Biomechanical Study. *Journal of Biomechanics*, **10**, 233-239.

Williams JL, Lewis JL (1982). Properties and an Anisotropic Model of Cancellous Bone from the Proximal Tibial Epiphysis. *Journal of Biomechanical Engineering*, **104**, 50-56.

Young DR, Niklowitz WJ, Steele CR (1983). Tibial Changes in Experimental Disuse Osteoporosis in the Monkey. *Calcified Tissue International*, **35**, 304-308.